2020

Application of Immobilized Palladium Monolithic Catalysts in Suzuki-Miyaura and Tsuji-Wacker Redox Reactions

Sajjad Ghobadi
Virginia Commonwealth University

Application of Immobilized Palladium Monolithic Catalysts in Suzuki-Miyaura and Tsuji-Wacker Redox Reactions

A Dissertation Submitted in Partial Fulfillment of the Requirements for the Degree of Doctor of Philosophy in Chemical Engineering at Virginia Commonwealth University

By

Sajjad Ghobadi

Director: B. Frank Gupton, PH.D.

Floyd D. Gottwald Jr. Endowed Chair, Department of Chemical and Life Science Engineering

Virginia Commonwealth University, Richmond, Virginia

Co-Advisor: Carlos E. Castano, PH.D.

Assistant Professor, Department of Mechanical and Nuclear Engineering

Virginia Commonwealth University, Richmond, Virginia

July 2020

Dissertation defense committee members

1. Prof. B. Frank Gupton, PH.D. (VCU CLSE)
2. Assist. Prof. Carlos E. Castano, PH.D. (VCU MNE)
3. Prof. Ram Gupta, PH.D. (VCU CLSE)
4. Assist. Prof. Christina Tang, PH.D. (VCU CLSE)
5. Assist. Prof. Benjamin H. Meekins, PH.D. (USC CEC)
6. Dr. Anton A. Toutov, PH.D. (VCU CLSE)

Contents

List of Figures

Acknowledgements and dedication

I would like sincerely thank my adivsor Dr. B. Frank Gupton, & my co-advisor Dr. Carlos E. Castano whom their supervision and guidance were crucial for this work to be successfully accomplished. I would like to express my appreciation for the instructions and help by my committee members during my Ph.D. candidacy. I wanted to appreciate the financial and intellectual support from the VCU College of Engineering, the Medicines for All Institute, and the NSF Center for Rational Catalyst synthesis.

My thanks next go to my undergraduate interns and fellow graduate students at Virginia Commonwealth University, College of Engineering. Special thanks to Michael Burkholder, Santiago Vargas, Diana Osorio, and Dylan Rodene.

Last but not the least, I wanted to thank and dedicate my dissertation to my family, especially my fiancé Ms. Parastoo Rajabzadeh for their uninterrupted support and invaluable words of encouragement that I have always felt despite the thousands of miles distance between us.

Sajjad Ghobadi

July 2020

Abstraction

APPLICATION OF IMMOBILIZED PALLADIUM MONOLITHIC CATALYSTS IN SUZUKI-MIYAURA AND TSUJI-WACKER REDOX REACTIONS

By Sajjad Ghobadi, Ph.D.

A Dissertation Submitted in Partial Fulfillment of the Requirements for the Degree of Doctor of Philosophy in Chemical Engineering at Virginia Commonwealth University

Virginia Commonwealth University, 2020

Major Director: B. Frank Gupton, PH.D.

Floyd D. Gottwald Jr. Endowed Chair, Department of Chemical and Life Science Engineering

Virginia Commonwealth University, Richmond, Virginia

Fine chemicals and pharmaceutical industries are among the most strategic fields for any country. Redox reactions are among the processes that have been actively used as the critical route to obtain desired organic products. Metal catalysis is one of the major approaches to improve the efficiency and rate of such reactions. Suzuki-Miyaura cross-coupling and Tsuji-Wacker oxidation are among the most common reactions in the field. Both of these reactions are catalyzed using metal species, with palladium (Pd) being the most common one. Although these two reactions have similar catalytic cycles, they use different metal species. Particularly, while Suzuki reactions use metallic (Pd^0), whereas ionic species (Pd^{II}) are the actively utilized catalytic species.

Additionally, two of the synthetic settings with the highest potential in future improvement in industrial synthesis are flow and electrochemical frameworks. Solid-supported catalyst production

Both of these settings require specific design considerations for catalyst synthesis. Preparing metal-decorated monolithic catalysts, where the support structure is a macroscopic highly porous with enhanced mechanical and electrical properties, is projected as the approach for preparing the next generation of high-performance solid-supported catalysts.

Herein, a wholistic analysis of the viability of monolithic catalysts for redox reactions is presented. The interdisciplinary approach taken in this systematic study included preparation and investigation on Pd-on-carbon monoliths as catalysts in a flow and electrochemical settings.

The Suzuki-Miyaura reaction-focused study led to rational design, preparation, and successful application of Pd^0-on-graphene oxide (GO) monolithic catalysts in flow conditions. In this study a combination of chemical reduction, freeze-casting, and vapor-phase reduction processes was applied to Pd-GO structures leading to the preparation of these monoliths. The Suzuki flow synthesis reactions revealed that the monolithic structure led to significantly improved catalytic longevity compared to 2D solid-supported catalysts. Nonetheless, the turnover frequency and product metal contamination (leaching-off) analysis indicated superior performance for monolithic catalysts.

Electrochemical Wacker-type oxidations are among the most common reactions in the industry. However, in order to prepare a rationally designed monolithic catalyst for this reaction, further catalyst studies were required. Therefore, a comprehensive study on 2-dimensional Pd-on-graphene nanoplatelets was conducted, leading to a proposed industrial design space for oxidation catalyst manufacturing. Afterwards, as a proof of concept viability of Pd^{II}-on glassy carbon (GC) monoliths were used as catalytic electrodes for Wacker-type oxidation in the electrochemical setting.

Via this approach, a comprehensive investigation and validation of monolithic catalyst preparation and applications in industrially feasible synthetic processes, including catalytically different redox reactions in flow and electrochemical settings, were successfully attained.

1. Introduction to Recent Advances in Solid-Supported Catalysis

1.1. Solid-Supported Catalysis in Organic Synthetic Processes

Organic reactions have been identified as one of the main possible routes through which life was first created. To the day, they have not lost their level of importance in influencing human lives. [1] The ever-growing demand for fine and pharmaceutical chemicals since the second half of the 20th century has been the driving force for the development of more efficient organic synthetic processes (OSPs). [2] One of the significant strategies towards these process improvements is the utilization of reaction-promoting non-consumable species. [3] Catalysts are among this category of materials, a set of species that kinetically enhance the rate of reactions.

Many OSPs are catalyzed via transition and rare-earth metallic particles. [4] These catalytic systems have revolutionized many industrial processes and enabled crucial discoveries in the field of fine chemicals and active pharmaceutical ingredients (APIs) synthesis. [5]

While the importance and positive role of metallic catalysts are undeniable, there are multiple process-focused as well as mechanism-oriented difficulties associated with them. [6] This cross-disciplinary set of issues has resulted in the emergence of catalysis research among chemical engineers and process chemists.

Transition metal catalysts, one of the most common groups of OSP catalysts, are often irreversibly dissolved in the reaction media.[7] Considering the high costs of these metallic particles and strict mandates enforced by regulatory agencies (e.g., FDA regulation for the allowed amount of transition metal content in pharmaceutical products [8]) this criterion must be met by any process pursuing commercialization.

The amount of soluble catalyst (known as a homogeneous catalyst) used in these reactions is very high (sometimes up to 50 mol% of reagents).[9] Hence, rendering this approach commercially and technically inapplicable in industrial settings.

In order to address these issues while benefiting the most from metal catalysis, solid-supported catalysis was adopted and advised in the second half of the 20th century. [10] During this process catalyzing species (metallic, [11] organometallic, [12] etc.) are immobilized on a solid substrate, known as the support. This support structure is often chosen from materials with high electrical and thermal conductivity while possessing mechanical strength (e.g. graphene, [13] carbon black, [14] and carbon nanotubes [15]).

A variety of difficulties associated with homogeneous catalysts are addressed through solid-supported catalyst synthesis. In a desired solid-supported catalyst system, the catalyst particles are strongly immobilized on the high surface area solid support's accessible surfaces. This high surface area provides catalyst particles with the possibility of effectively interacting with reagents without the need for their dissolution in the reaction media. Therefore, the catalyst leaching off into the product mixture is minimized.

In many organic syntheses, the catalyst is oxidized or reduced and then regenerated through its catalytic cycle (Figure 1.1). Solid supports often provide the system with a pool of excess delocalized electrons, which can effectively promote a faster catalyst redox process, regenerating the catalyzing species. Consequently, the amount of catalyst required for fast reaction completion is reduced, thus significantly improving the catalyst system's potency.

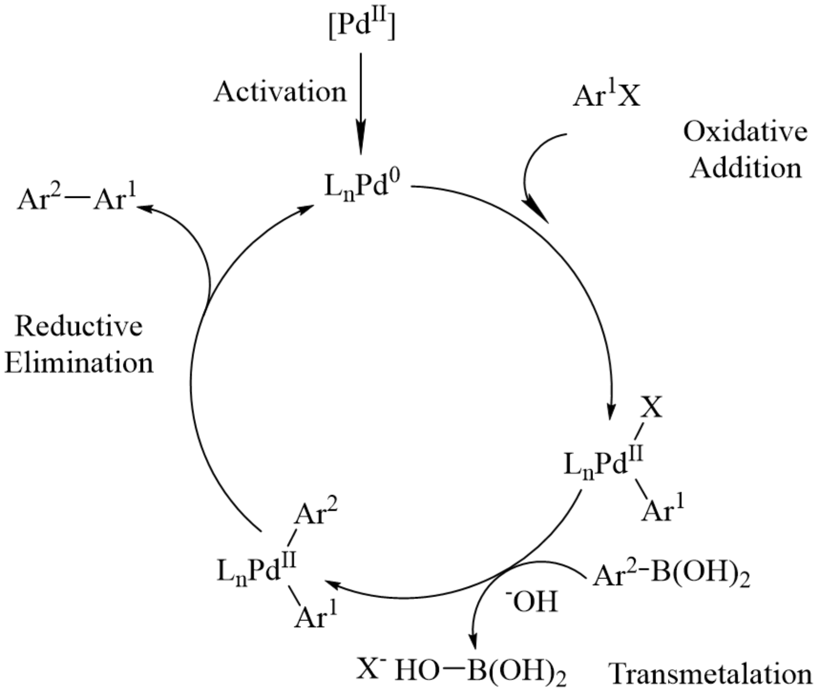

Figure 1.1. Catalyst redox cycle for Suzuki cross-coupling reactions

Solid-supported catalysis has made some reactions possible that they were previously deemed practically impossible or industrially infeasible. Pericàs et al. [16] showed that the enantioselectivity required for various fine chemicals and pharmaceutical ingredients is heavily dependent upon the quality of chiral catalysts used. In some cases, the only way to control the catalyst chirality is to utilize solid-supported catalysts where the support dictates the deposited particle properties.

In another investigation by Leitner and co-workers, [17] one the key intermediates for Janus kinase 2 (JAK2) inhibitor was prepared via solid-supported ruthenium catalysts with significantly higher selectivity while satisfying the green chemistry conditions.

Although these improvements and novel process discoveries were achieved, the true API synthesis potential of catalysis was yet to be discovered as a viable route for industrial-scale manufacturing.

1.2. Assemblies of Monolithic Structures for Catalytic Applications

One of the major advances in API synthesis was translating the conventionally performed batch reactions into synthesis in flow. [18] During this approach, the reaction is completed whilst its mixture is conveyed in a stream. This method yields significant improvements in the synthetic process efficiency.

Tosso et al. [19] showed an improved industrial-scale synthesis route for ciprofloxacin with improved isolated yields of 83% compared to commercially practiced routes. The reduction in number of synthesis steps while increasing the process throughput achieved in that study were the direct results of the successful implementation of synthesis in flow approach.

Usually, during the flow synthesis, catalysis is involved at various stages of the process. The catalysts in flow are often utilized via packed bed settings. [20] The catalyst packed beds allow the reaction stream to pass through them while keeping the bed in place, which allows the control of reagents residence time, and bed's pressure and temperature control with desirable accuracy. Solid-supported catalysts, which provide advantageous properties for catalysis of such reactions, have been found to be the most suitable candidates for packed bed applications. [21] However, there are two major drawbacks associated with then in packed bed settings.

Firstly, the backpressure of the stream is often dramatically increased when using a conventional heterogeneous catalyst packed bed. [22] This phenomenon happens due to catalyst overpacking (pressing against each other) (Figure 1.2-a). This results in dramatically lowered reaction throughout and in extreme cases, clogging in the system which can further inflict noticeable financial damage in industrial settings and requires intensive cleaning and overhaul procedures.

Secondly, as the reaction stream is flown through the 2-dimensional solid-supported catalyst packed beds, flow paths of least resistance can form within the packed bed bulk. This process is called microchanneling (Figure 1.2-b) which prevents the reagents from interacting with catalyst particles in the bulk of the bed (especially those away from microchannels). [23] Therefore, the true fraction of reacting catalyst becomes significantly lower than the intended amount (e.g. stoichiometric catalyst amount). There have been numerous reports of experimental and theoretical studies concerning these two issues from bench to industrial scales of production.

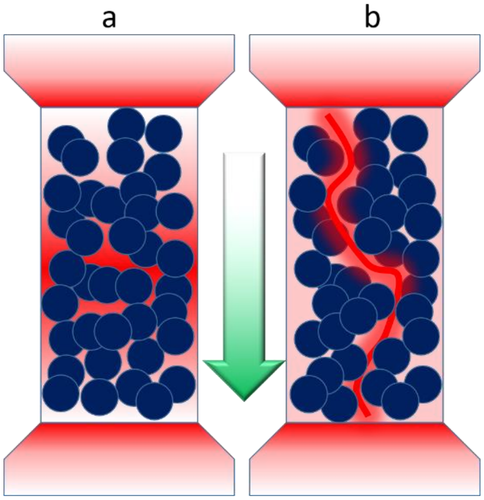

Figure 1.2. Illustration of a) high backpressure and clogging, and b) microchanneling in 2D catalyst packed beds. (the green arrow, dark blue particles, and red gradients, represent the flow direction, solid-supported catalysts, and high pressure regions, respectively.)

One of the most successful solutions proposed for these issues associated with 2D solid-supported catalyst packed beds has always been to prepare a macroscopic assembly of catalytically active species. These structures then act as plug-and-play cartridges for catalyst packed beds. These structures are called monolithic catalysts. The highly porous, and at the same time, mechanically robust structure of monolithic catalysts allow the uninterrupted flow of reaction stream while maintaining its originally designed shape. Thus, preventing the microchannel formation in the packed beds.

Electrochemical organic synthetic processes (EOSs) are another type of synthesis approach with extremely high potential in profitability as well as in scientific discoveries. [24] The EOS methodology has been extensively utilized in the field of eco-friendly and renewable energy production. Similarly, there are several industrial EOS processes actively used for commodity [25] (e.g. acetone, ammonia, and chlorine gas) as well as specialty chemicals (such as APIs [26], and ultrapure polymers, [27]) in industrial scale. The improvements in equipment enabling electrochemical production led to the rapid growth of EOS adoption by industry and academia. Currently, there are over 1500 commercial products synthesized through EOS approach. [25]

Despite the mentioned successful applications of EOS, the true potential of this approach has not been utilized to its utmost capacity. The EOS is a surface process that is heavily reliant upon the interaction between reagents and electrode(s). [28] This characteristic is a governing factor in preventing many EOS processes to be commercialized as almost all the completed reaction cycles (especially those require catalysts) happen at a less than 100µm distance from the electrode surface, rendering the process unscalable. Thus, there have been two major catalysis-oriented approached to address this drawback.

I) As shown in Figure 1.3., during EOS, the reagents are oxidized or reduced (at the anode or cathode, respectively). This process often requires catalytic species. However, until recently, only homogeneous catalysts that can be dissolved and effectively interact with reagents at the electrode surface, were used. [29] This approach was successful in improving the chances of responding to difficulties associated with this method of catalysis in electrochemical settings. Firstly, the catalytic species in a one-pot (known as an undivided cell) electrochemical cell, could promote an undesired reaction as the counter electrode is also present and could cause unwanted oxidation/reductions. Utilization of two half-cells connected via an ion bridge or a semi-permeable membrane (completing the electrical circuit) addressed this issue. [30] However, this design approach decreased the electrochemical regeneration rate due to the significantly lowered charge transfer rate in such configurations.

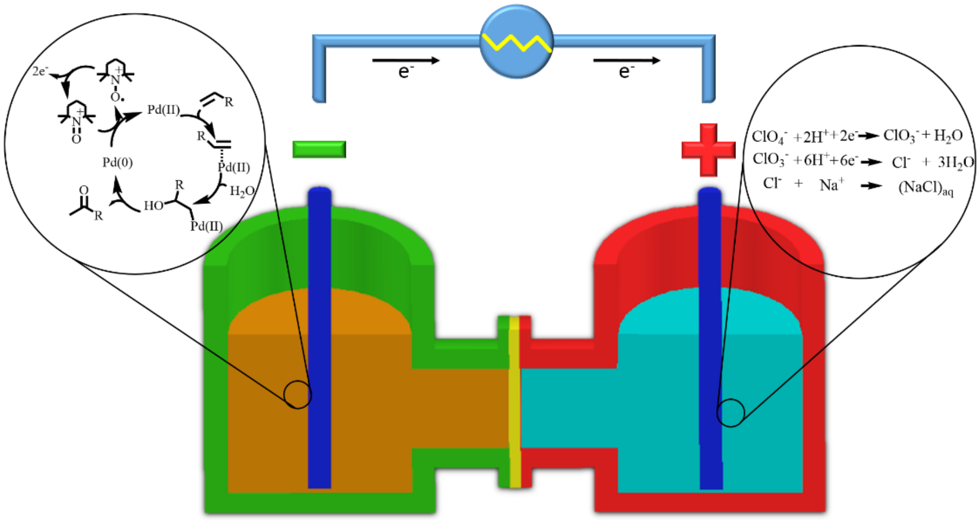

Figure 1.3. Electrochemical Wacker oxidation of alkenes (left: oxidation of alkene to ketone at anode and right: reduction of electrolyte salt to sodium chloride(aq))

Secondly, similar to conventional OSPs, the filtration and recycling of dissolved homogeneous catalyst species (often rare-earth or transition metals) was extremely hard and virtually impossible in some cases. Hence, decreasing the product purity while increasing the cost by wasting the catalyst material. [31] Nonetheless, the potential clogging of a permeable membrane or ion-bridge input ports in case metallic salts crashing out and precipitation was another issue associated with this methodology. [32] The last difficulty can be exacerbated by using solid-supported catalysts.

II) Until recently, the utilization of retrievable high-activity solid-supported catalysts in EOS was deemed only available through immobilization of the catalyst on the electrode surface. [33] However, due to the limited electrode surface area, and design limitations for efforts in increasing it, the catalyst loading was drastically lower than the required amounts for high throughput reaction completion.

There has been a series of recent reports indicating that dispersion of solid-supported catalysts in the reaction electrolyte, while under rapid mixing, can be extremely beneficial to this approach. [33] During this process, the quick contact and detachment of catalyst particles from the electrode allow them to complete their redox cycle and be readily available again for catalysis. [34] Nonetheless, significantly higher amounts of catalyst allowed in this method increase the potential of EOS in performing hard-to-attain reactions.

This novel catalyst incorporation methodology is called fluidized electrochemical catalysis and has proven to be one of the most reliable approaches for catalyzed EOS. In order to improve upon fluidized electrochemical catalysis, two difficulties must be addressed. First of all, as this method is only in developing bench-scale stages, the procedure to define the proper criteria for the preparation of catalysts for such reactions must be devised. Hence, a systematic approach for catalyst design space generation supported by experimental results is required. [33]

Moreover, the mentioned precipitation of 2D solid-supported catalysts on the permeable membrane slows the charge transfer between two half cells, hindering completion of a fast, minimally energy-consuming reaction. [35] To address this difficulty, a catalytic monolith electrode which contains catalyst particles in its highly porous structure can potentially be active while still benefiting from the advantages of fluidized electrochemical catalysis.

In order to provide systematic solutions to the drawbacks of using solid-supported catalysis in flow OSPs as well as EOS processes, the following research, tailored towards palladium (Pd) catalysis, is presented. In chapter 2, a rationally designed and robust method for preparation of mechanically sturdy, and highly porous graphene oxide monoliths for model Suzuki cross-coupling reactions in flow is presented. Chapter 3 provides a comprehensive approach for the preparation of design space for specialty Pd-on-graphene nanoplatelets (Pd/GNP) solid-supported catalysts for fluidized electrochemical oxidation of electron-deficient olefins (Tsuji-Wacker reaction) is detailed. Chapter 4 depicts the design, manufacturing, and proof of concept performance of Pd on reticulated vitreous carbon (RVC) catalytic monolith electrodes for Wacker-type electrochemical oxidation terminal olefins.

Throughout these studies, in addition to the design and preparation of specialized solid-supported catalyst structures, their superiority over homogeneous catalysts as well as the depiction of the positive impact they introduce to their respective reaction settings (flow and electrochemical) is pursued.

2. Preparation and characterization of monolithic catalysts

2.1. Pd-decorated GO monolith Manufacturing: Synthesis, Characterization

2.1.1.Background and Motivation

Since the 19th century, catalysts have been actively utilized in a variety of processes [36]. These catalysts due to kinetic effects can accelerate the production of a certain product or efficiently generate energy by reducing the activation barrier of the reactions. The importance of catalyst development is highlighted by the tremendous amount of research being conducted to meet the rapidly growing demand for large quantities of synthetic products, improving reaction efficiency, and catalyzing more difficult reactions [37].

Traditionally, many petrochemical and fine chemical industries use metal particles as their catalysts of choice for most catalyzed processes. Specifically, cross-coupling processes in the pharmaceutical industry have utilized selective transition metal catalysts [38-39]. Homogeneous metal compounds [40-41] are favored for such applications due to their durability and high activity. These homogeneous catalysts are usually expensive, require high catalyst loading, and are difficult to separate from products [42]. It is noteworthy that the metal impurities in pharmaceutical products are highly regulated by agencies such as the Food and Drug Administration (FDA) (e.g. 10 ppm limit for Palladium in Q3D Elemental Impurity Guidance for Industry [8]) making the separation of the metallic species from products a crucial and often costly issue.

Heterogeneous catalysis is one of the most effective ways to address these drawbacks. For example, the utilization of solid-supported catalysts not only provides ease of separation, it also reduces or eliminates the amount of metal contamination of the products [43-46]. Nevertheless, additional improvements are sometimes required for a solid-supported catalyst to be technically and financially feasible on a commercial level.

Overcoming the costs associated with solid-supported catalysts can be achieved by increasing the catalytic activity through synthesizing smaller metal particles on solid-supports. This approach results in increased active surface area to volume ratio. Another improvement pursued in solid-supported catalysis is to utilize an electrically conducting support for fast and low activation energy redox cycle of metal particles during catalysis. This goal has been achieved by using conducting and cheap supports (e.g. graphene [47-49], activated charcoal [50] and carbon black [51]).

One challenge that recently has received interest is to effectively implement the use of solid-supported catalysts in continuous or flow syntheses (e.g., catalyst packed bed reactor configuration) in petrochemical catalysis [18] and particularly, active pharmaceutical ingredients (APIs) [52-53]. As stated by Buchwald et. al. has identified multiple difficulties to be addressed in flow synthesis, and importantly the implementation of solid-supported catalysts was listed as one of the top challenges in that framework [39]. Packed catalyst beds tend to have a high pressure-drop across the bed, flow channeling, or clogging, preventing their effective use and commercialization [54-55].

The high pressure-drop in flow synthesis can be a result of the solid-supported catalysts packing, which also reduces the available active sites and thus catalytic activity. Catalyst packing can also lead to accelerated deactivation [54]. Micro channeling of catalyst packed beds is another issue that prevents efficient catalysis as the reaction media can flow through these channels and interact less with the catalyst particles. In other words, the residence time as well as catalyst efficacy are both reduced [55].

Research efforts to address high pressure-drop and micro channeling of catalyst packed beds have been reported using various bottom-up assembly methods for large scale catalyst preparation. In Haswell and co-workers' study [56], sol-gel bottom-up assembly of silica nanoparticles led to formation of a robust macroscopic structure. A three-dimensional (3D) Pd/silica monolithic catalyst was synthesized by physically adsorbing palladium salt precursors on silica nanoparticles. The preparation process was then completed by calcination of the silica monoliths which ultimately resulted in improved catalyst performance in flow synthesis. However, the harsh and non-reproducible conditions of both sol-gel as well as calcination processes were among the main drawbacks of this approach.

In another study by Barbaro et. al. [57], it was shown that a Pd@sulfonated silica monolith was prepared as a catalyst for partial hydrogenation reactions. While the catalytic activity of the monolithic catalysts improved over four times in selectivity with respect to the two-dimensional Pd@silica, the catalyst preparation required the expensive commercial monolith and harsh functionalization treatment conditions thereof.

Modak et al, prepared Pd particles immobilized inside hollow n-doped carbon tubes with holes in their structure. These macroscopic 3D supports were obtained through a top-down manufacturing process, during which highly cross-linked polymer tubes were carbonized in presence of Pd (II) ions. They showed such high surface area macroscopic structures possess significantly improved catalytic activity over their conventional 2D solid-supported counterparts. Such structures' performance superiority was confirmed for Sonogashira and cyanation type C-C bond formation reactions as well as hydrogenation of nitrobenzene and compounds alike to their corresponding anilines [58]. To have a large scale map of Pd particles inside carbon tubes was among the main challenges of this study.

An optimized monolithic catalyst has been the main interest of the related research community. Achieving this will require a straightforward, efficient, and low-cost preparation method. Additionally, the catalyst sustainability and ultimate flow catalytic longevity of these engineered hybrid nanomaterials need to be systematically studied [59-62].

A rigorous study of 3D monolithic catalysts will require characterization of the pore structure on the macroscopic level. During multiple studies it was shown that the solvents and reagents are often entrapped within the nanoporous structure due to capillary conditions, making conventional porosity measurements ineffective. These problems have drawn the community's focus towards more facile nondestructive analytical techniques [63].

Recently there have been reports on using computer assisted tomography (CT-scan) scanning technique for evaluation of fillers and additive material orientations in polymer composites [64]. During these investigations, the contrast was obtained by the difference in the X-ray diffraction of fillers and polymer matrix layers. CT-scanning was then used to study the interior structure of the composites. However, since both the matrix and the additives are carbon-based, no elemental distinction could be obtained at larger than nanometer scales [65].

In Sheppard and co-workers' report, ceria-doped gold monolithic catalysts were also studied by micro-CT scan imaging giving micrometer scale resolution of the structure [62]. The study showed nanoporous gold/ceria monolith can be effectively used for catalysis and process intensification. However, the tomographic 3D mapping technique utilized, was not able to provide a ceria distribution map within the gold monolith structure. Large-scale structural alterations that occurred during the catalytic performance were not characterizable using micro-CT scan tomography.

The present study first investigates a multi-step, all aqueous-phase assembly approach for preparation of palladium-decorated graphene-based monolithic catalysts for improved catalytic performance. Afterwards, investigations on a new monolithic catalyst characterization technique using nondestructive micro CT-scan tomography for elemental and porosity mapping on the centimeter-scale is presented. The robustness of these monoliths to withstand synthesis in flow conditions was pursued via GO interlayer esterification; followed by a GO ethanol vapor partial reduction. The monolith structure was systematically analyzed and characterized by electron microscopy, X-ray photoelectron spectroscopy, and X-ray diffraction. The catalytic longevity of the monolithic catalysts in flow packed bed configuration was tested using a model Suzuki cross-coupling reaction and compared to the 2D catalyst. The feasibility and utility of the micro-CT mapping on the monolith structures was investigated with emphasis on microporosity alterations as well as Pd distribution throughout the entire monolithic structure.

2.1.2.Materials and Methods

2.1.2.1. Materials

Graphite flakes (>325 mesh size), 4-bromotoluene, and palladium chloride were purchased from Alfa-Aesar (Haverhill, MA, USA). Sulfuric acid, nitric acid, hydrogen peroxide, ethanol, polyvinyl alcohol (PVA) (99% hydrolyzed, MW. 8900-98000 g.mol^{-1}), and ascorbic acid were purchased from Sigma-Aldrich (Saint Louis, MO, USA). Phosphoric acid, and hydrochloric acid were purchased from Fisher Scientific (Hampton, NH, USA). Sucrose, and tetraaminepalladium(II) chloride (Alfa Aesar, 99.9%), were purchased from Caisson Labs (Smithfield, UT, USA), Fluka (Muskegon, MI, USA), and Science Labs (USA), respectively. All the chemicals were used without further purification.

2.1.2.2. GO monolith preparation

Graphene oxide was synthesized from graphite flakes via a green iteration of Hummer's modified method as described elsewhere [66]. Briefly, graphite nanosheets were oxidized by using $KMnO_4$, H_2SO_4, and H_3PO_4 for 24 hours, followed by dialysis in DI water until the GO mixture reached a pH of 5 and was then dried in a vacuum oven overnight. Once dried, the GO was dispersed in DI-water (5 mg/mL) by ultrasonication using an ultrasound bath (150 W, 100% amplitude, Branson® 1800) for 7 hours. Then, 2.5 mg sucrose and 0.25 mL of 1 wt/vol% aqueous solution of PVA (2.5 mg solid ca.) were added to 10 mL of the GO water dispersion under magnetic stirring at 500 rpm while kept at room temperature (25 °C) for two hours to yield the monolith precursor solution.

The monolith precursor mixture was then poured into molds of the desired shape, to fit the packed bed cartridge, and freeze-casted by exposing the mold's bottom surface to liquid nitrogen creating a temperature gradient (Figure 2.1.). The gradual growth of ice crystals is obtained in the monolith structure along the same axis. To achieve the maximum porosity, the approximate temperature gradient was about 2 $°C.min^{-1}$, measured by infrared temperature gun [67]. The freeze-casted monoliths were then lyophilized using a Labconco freeze dryer for 24 hours.

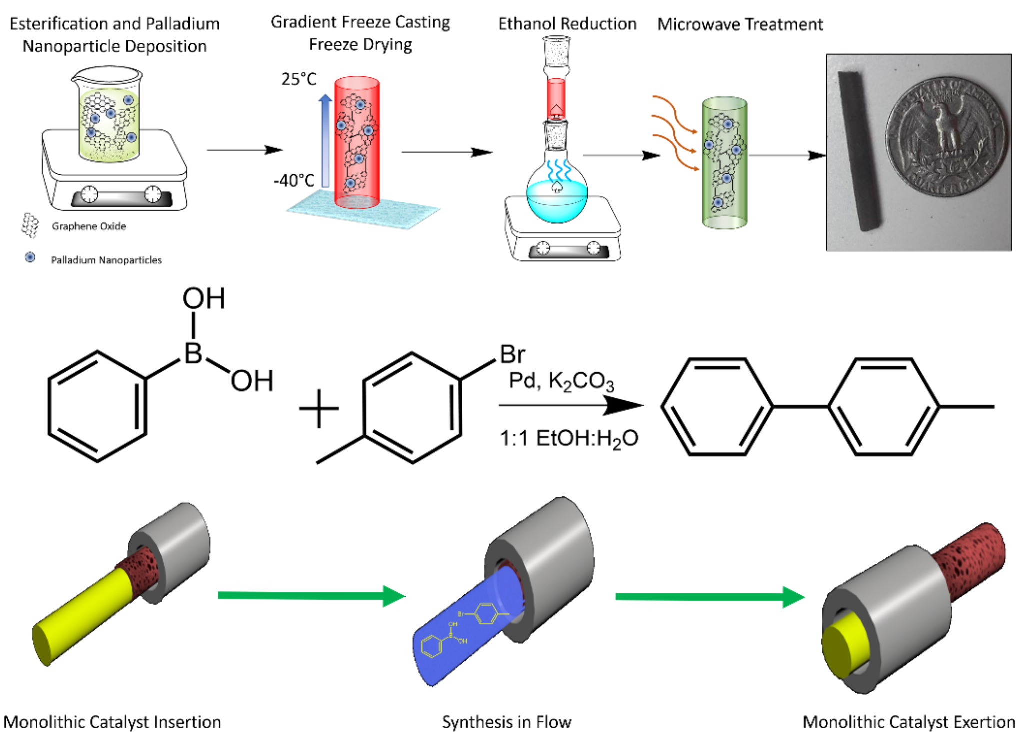

Figure 2.1. The schematic illustration of monolithic catalyst preparation, the model Suzuki cross-coupling reaction, and the flow synthesis using the monoliths

The samples were coded based on their support (e.g., Pd@M for monolith and Pd@GO for 2D catalyst). In addition, their specific post synthesis treatment was included in the naming scheme. For example, Pd@M-MW is a Pd on GO monolith catalyst which is microwave treated.

2.1.2.3. Pd@M monolithic catalyst preparation

The procedure for the Pd@M monolithic catalyst preparation followed the GO monolith precursor preparation, but with the addition of a Pd precursor salt ($PdCl_2$ as the cationic, $Pd(NH_3)_4Cl_2$ as the anionic salts) at 5 wt% metallic Pd with respect to GO, as well as ascorbic acid (2 molar equivalence with respect to metallic Pd) were added to monolith mixture prior to the 2-hours esterification period. The $Pd(NH_3)_4Cl_2$ and $PdCl_2$ were first dissolved in DI-water, and 0.1 M HCl aqueous solution, where $PdCl_4^{2-}$ species were formed before addition to the GO monolith precursor solution.

Partial reduction of the monolith (and monolithic catalysts) was performed using ethanol vapor as the reducing agent in a closed round bottom flask heated to 74 °C for 2 hours (Figure 2.1) located below the mold containing the monolith or monolith catalyst precursor solution. The treated monolith was then transferred to an autoclave reactor which was sealed and heated in an oven at 100°C for 24 hours.

For comparison, in addition to Pd on GO monolith model sample prepared via use of $PdCl_2$ precursor, a Pd on graphene oxide (GO) 2D catalyst was prepared via the identical reduction technique as the Pd@M monolithic catalysts. However, the freeze casting and lyophilization steps were not applied for 2D catalysts.

2.1.2.4. Microwave-treatment

A microwave treatment was implemented to further reduce the Pd nanoparticles, improving their interaction with GO by formation of Pd-graphene defects inside the support structure [45]. The treatment was performed via a CEM Discover S microwave reactor by treating the sample at 100°C for 1.5 minutes under varied power.

2.1.2.5. Micro CT-Scan imaging

The 3D micro CT scanning and imaging of the monoliths was performed using a Bruker Skyscan 1173 Micro-CT scanner. To obtain reliable maps, X-ray source potential was optimized at 130kV, and exposure time for each image was set at 4000 ms. During the imaging, 360° rotation of specimen at 5 mm canonical distance from the source was maintained while random movements were not included. CTVOX free reconstruction software was used to process images. For all samples, green color was specifically assigned to the Pd particles captured in the 3D map, and the carbon-based matrix was colored white.

2.1.2.6. Materials Characterization

Scanning electron microscopy (SEM), X-ray diffraction analysis (XRD), and X-ray photoelectron spectroscopy (XPS), were done via a Hitachi SU-70 FE-SEM at 5 KV, a X'pert Pro PANanalytical XRD diffractometer (Cu Kα, λ=1.54 Å, scanned from 5° to 85°) and a Thermo Fisher ESCALAB 250 X-ray spectrophotometer with 2 eV step for survey and 0.1 eV step for high resolution elemental scans, respectively. The XPS spectra were studied via CASAXPS 2.3 19PR software using NIST standard database 20 version 4.1 for detailed analysis.

The palladium metal uptake was determined by first dissolving the sample in 1 vol/vol % hydrochloric acid solution for 24 hours at 25°C. Afterwards, the mixture was filtered using a 0.2 µm syringe filter and ten times dilution with DI-water. Then the Pd concentration was measured using an inductively coupled plasma-optical emission spectroscopy (ICP-OES) (Agilent 5110 ICP-VCV-OES).

The average %Pd leached from the solid-supported catalysts were measured using the same ICP-VCV-OES device using the following protocol. At each 30-minute time point, 0.1 mL of the downstream was collected and mixed with 0.1 mL of 12.1 M HCl for acid digestion. After 20 times dilution with DI-water, the metal content was measured via ICP analysis. Afterwards, total leached Pd content was calculated using the following equation:

$$\%\text{leached Pd} = (\text{Pd conc. (ppm)} \times V_{\text{passed}}\,\text{(L)})/\text{total Pd (mg)} \times 100$$

Where the V_{passed} is the volume of passed liquid calculated based on the flow rate (0.01 L for each step). Then the average leached %Pd was calculated as the number average of each step's record. Remaining (or starting) Pd refers to the amount of retained (or starting) Pd on the catalyst.

2.1.3.Results and Discussion

Evaluation of the monolithic graphene-based nanosheets decorated with Pd catalysts consisted of material characterization, optimization of reaction temperature and microwave irradiation conditions, testing of catalytic performance, and development of a micro-CT mapping characterization technique was evaluated. The monolithic catalysts were characterized using X-Ray photoelectron spectroscopy (XPS) to determine the oxidation stateof Pd species and the catalysts were imaged using a scanning electron microscope (SEM). The effect of microwave treatment and reaction temperature on the monolith's catalytic performance were optimized to preserve the monolithic structure and enhance the catalytic performance, which was evaluated using Suzuki cross-coupling reaction as a model. This model reaction was also used to evaluate the catalytic longevity of the 3D monolithic catalysts in comparison to the 2D catalyst packed bed. Finally, the micro-CT mapping was developed to provide a method of characterizing the Pd particle distribution throughout the monolith on a clear large-scale map.

2.1.3.1. X-ray Photoelectron Spectroscopy

According to the XPS spectra (Figure 2.2), the oxygen content was significantly higher in monolithic catalysts compared to the 2D Pd@GO catalysts (Figure 2.2.). Therefore, the monolithic catalyst was more compatible with aqueous reaction media through the functional group interactions with water. Though the highly porous structure of the monolith was preserved by steric cross-linking, preventing the structural collapse while exposed to water.

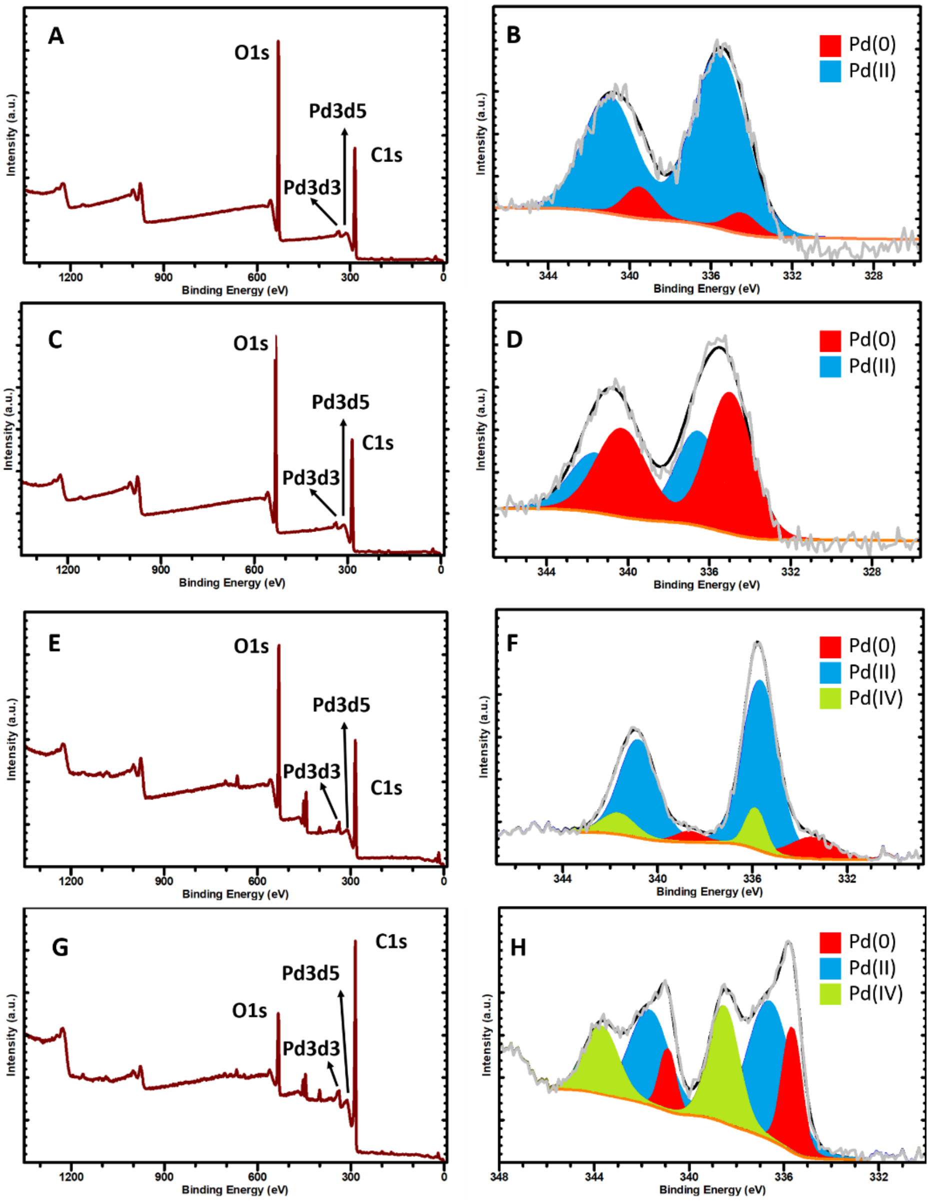

Figure 2.2. XPS analysis of A, B) Pd@M-nonMW, C, D) Pd@M-MW, E, F) Pd@GO-nonMW, G, H) Pd@GO-MW

From the XPS survey quantification analysis on catalysts (Figure 2.2-a, c, e and g) no sulfur was detected at 162-170 eV binding energies, demonstrating the preparation method prevented sulfur-poisoning [68].

Based on previous reports, metallic Pd(0) and the ionic Pd(II) palladirgies [69]. The detailed elemental analysis on Pd species revealed that the metallic species to total palladium species ratio in Pd@M (Figure 2.2-b), Pd@M- MW (Figure 2.2- D) monolithic catalysts and the 2D catalysts of Pd@GO (Figure 2.2-f), and Pd@GO-MW (Figure 2.2-h) were 34.2 ± 5.4%., 65.1 ± 7.6%, 19.4 ± 3.7% and 32 ± 3.9%, respectively.

The significant difference among the monolithic catalysts and 2D Pd@GO catalysts recorded via XPS was that a palladium (IV) (Pd(IV)) species was detected in Pd@GO and Pd@GO-MW catalysts (Figure 2.2-f and h, respectively) while such species was absent in monoliths. Due to the oxide species formation, a longer reductive pretreatment activation (initial transformation of all Pd species to Pd(0)) was needed before performing the Suzuki cross-coupling reaction. The reason for the increase in Pd(IV) fraction from 9% to 22% based on relative peak area could be attributed to the smaller particle size of the Pd(II) and Pd(0) species not masking the Pd(IV) species thus expressing the Pd(IV) peak more strongly in the microwave-treated catalyst compared to the as-prepared one [70]. .

2.1.3.2. XRD Analysis

The X-ray diffraction analysis on the 2D Pd@GO catalysts (Figure 2.3-a and b) showed that the Pd deposition was achieved in both as-prepared Pd@GO and MW-treated Pd@GO-MW entries as the 40° peak of (100) planes of palladium was detected. The Pd calculated crystallite size using the Scherrer equation were higher in Pd@GO-MW compared to its non-treated 2D catalyst counterpart (Table 2.1.). The exfoliation effect of MW treatment on the catalysts is evident as the 25° peak of sp^2 carbon emerges upon treatment, indicating the de-functionalization of GO support.

Table 2.1. Pd crystallite size of monolithic and 2D catalysts

Catalyst System	Pd Crystallite size (nm)

Pd@M	11.4 ± 1.9
Pd@M-MW	8.7 ± 1.3
Pd@M ($PdCl_2$)-MW	17.2 ± 2.6
Pd@GO	16.3 ± 3.4
Pd@GO-MW	23.2 ± 2.8

The X-ray diffraction analysis from Figure 2.3 of GO monolith, monolithic and Pd@GO 2D catalysts showed that deposition of Pd particles was achieved as the distinctive 40°, and 47° peaks attributed to (111) and (200) Pd crystallite planes were detected [71]. The average crystallite size was calculated by Scherrer method [72] (Table 2.1.).

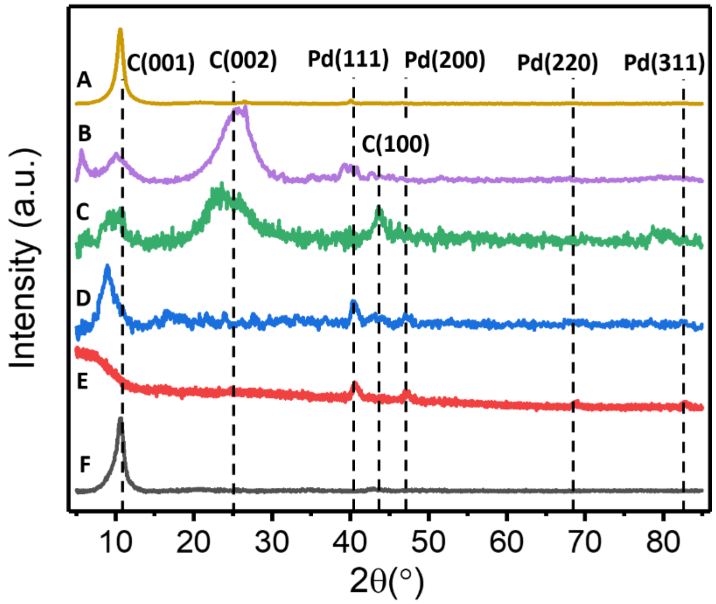

Figure 2.3. XRD spectra of various catalysts A) Pd@GO, B) Pd@GO-MW, C) Pd (PdCl2)@M, D) Pd@M, E) Pd@M-MW, F) GO Monolith, respectively

It was also shown that the Pd particle deposition while using the $PdCl_2$ precursor was achieved. However, the deposited palladium particle's crystal structure was different than the $TAPdCl_2$ specimens as the single 47° peak was detected in $PdCl_2$@M monolith indicating larger crystallites (Table 2.1.). The lower pH required for dissociation of $PdCl_2$ in aqueous media, which had a negative impact on the ascorbic acid's performance, it could be considered as one of the main reasons resulting in lower Pd uptake, which was confirmed by ICP-OES analysis (Figure 2.2) [73].

2.1.3.3. Scanning Electron Microscopy

Scanning electron microscopy revealed interesting differences in the Pd particle size and distribution as well as the microstructure of the different 2D Pd@GO and 3D Pd@M catalysts prepared using both chemical (vitamin C) and microwave irradiation reduction steps (Figure 2.4). The average Pd particle size of the 2D Pd@GO and Pd@GO-MWcatalysts (Figure 2.4-a and b) were 36.8 ± 6.2 and 28.3 ± 4.5 nm, respectively. In contrast the Pd particle size of the 3D monolithic catalysts, Pd@M and Pd@M-MW, were 27.8 ± 2.8 nm and 18.5 ± 1.2, respectively (Figure 2.4-c and d). Based on these size measurements it is thought that the potential active surface area of Pd nanoparticles for catalytic activity was higher in the monolithic catalyst samples and more so in MW entries which consist of smaller Pd particles.

Although the Pd active site measurement via hydrogen chemisorption technique was attempted multiple times, due to the natural issues of these nanoporous structures the results were inconclusive.

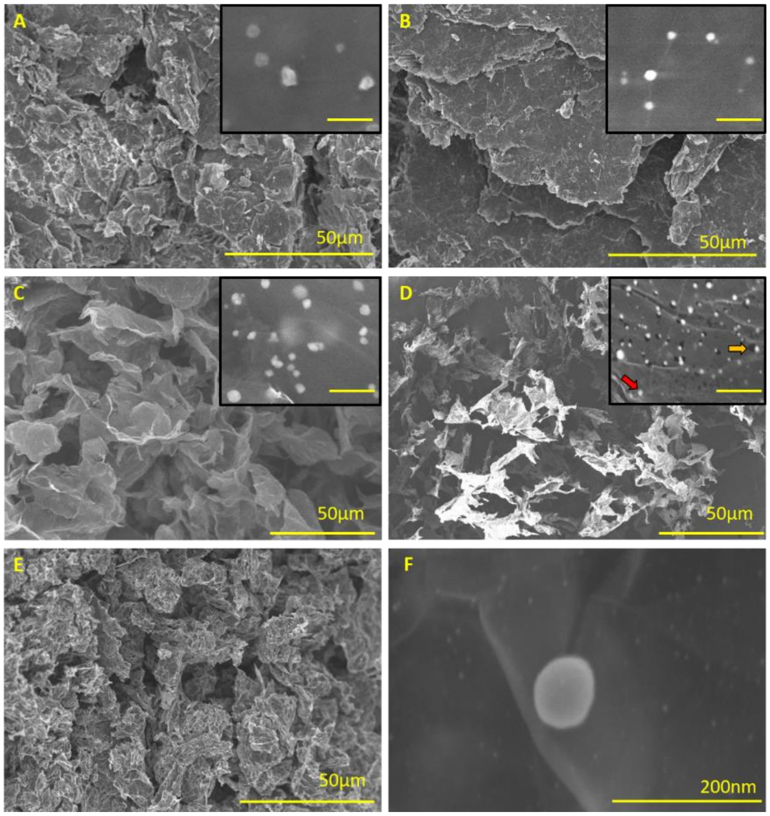

Figure 2.4. SEM images of A) Pd@GO, B) Pd@GO-MW, C) Pd@M, D) Pd@M-MW (In the inset image: the Pd particles are the bright spots, and the holes into graphene are the dark spots, indicated by the red and yellow arrows, respectively.),and E, and F) overall porous structure and particle imaging of Pd@M after the reaction, respectively. The inset image scale bars are 50 nm

Another important characteristic revealed by electron microscopy was physical evidence of defects in the support structure resulting from MW irradiation treated catalyst compared to the as-prepared one. These hole-like defects formed within the GO sheets during microwave irradiation due to extremely high and localized temperatures surrounding the forming Pd nanoparticles during reduction[74]. These graphene holes or defects supporting Pd have been demonstrated to provide enhanced catalytic activity of solid-supported catalysts [45, 49, 75-76]. However, in monolithic materials these defects could result in reduced mechanical stiffness. Therefore, the formation of these holes needs to be optimized to provide enhanced catalytic performance while also retaining the mechanical and structural properties of monolith materials required for use in continuous flow reactions.

The comparison between the Pd particle size distribution before and after reaction (Figure 2.4.-c, and f) showed that in Pd@M catalyst the average particle size after Suzuki cross-coupling flow synthesis was increased to 30.6 ± 11.7 nm. The significantly higher standard deviation value is due to the formation of larger Pd particles (>100nm). The post-reduction of Pd(II) particles to Pd(0) via electron donation from GO monolith to the Pd particles during the reaction could be the responsible phenomenon for such aggregation.

The microstructure of Pd@M monolithic catalyst before and after flow (Figure 2.4.-c, and e, respectively) also revealed that while the macroporous structure of the monolith was preserved, the micropores were filled with organic compound crystal residue, indicating that mass transfer deactivation was one of the effects playing an important role in the lifetime of the monolith. Additionally, the partially insoluble cross-coupling product residue on the monolithic catalyst structure, resulting in Pd particle-poisoning and deactivation.

2.1.3.4. Transmission Electron Microscopy

As shown in Figure 2.5., the Pd particles were successfully deposited on the monolith structure. The particle size study (based on 250 counted particles), showed that compared to the non-microwaved monolith, a narrower distribution in microwaved monoliths were observed (Figure 2.5.-a & b, respectively). This phenomenon could be the result of Ostwald Ripening effect of the treatment [77] which was also observed in SEM images of the monoliths.

The Figure 2.5.-c and d represent the crystal structure study and d-spacing measurement conducted on the Pd@M and Pd@M-MW monolithic catalysts, respectively. As shown in the figure, the Pd particles pertain Pd’s typical cubic close-packed (CCP) crystal structure [78]. The measured d-spacing were 2.06 ± 0.07 Å and 2.18 ± 0.02 Å for Pd@M and Pd@M-MW, respectively. The observation showed a slight increase in d-spacing through microwave treatment, while the distance between atomic layers were more consistent in Pd@M-MW monolith as the error value was decreased.

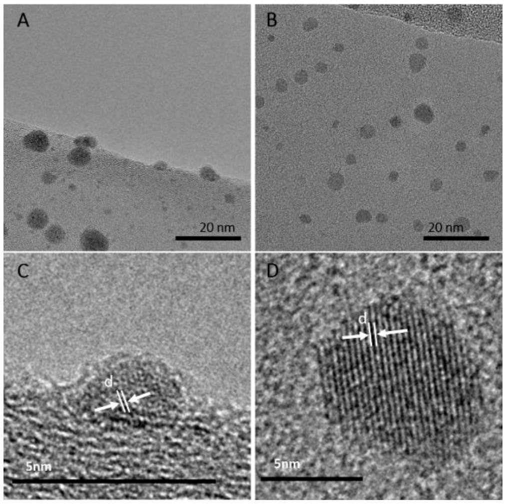

Figure 2.5. HRTEM images of A) Pd@M, and B)Pd@M-MW and the representative particles used for d-spacing measurements and crystal structre analysis of C) Pd@M, and D)Pd@M-MW, respectively

2.1.3.5. Differential Scanning Calorimetry

As shown in Figure 2.6., the endotherm starting at 80°C and ending at 120°C is attributed to glass transition of PVA followed by evaporation of water [79]. The exotherm detected at 210°C is attributed to decomposition of PVA which then leads to formation of a completely graphitic structure. This observation was confirmed by the calorimetric behavior of the monolith as it was almost identical to that of GO after 230°C. Therefore, it could be concluded that the water entrapped within the structure plays a critical role in its properties; and its removal will irreversibly alter monolith’s properties, rendering any analysis on the “dehydrated” samples unreliable.

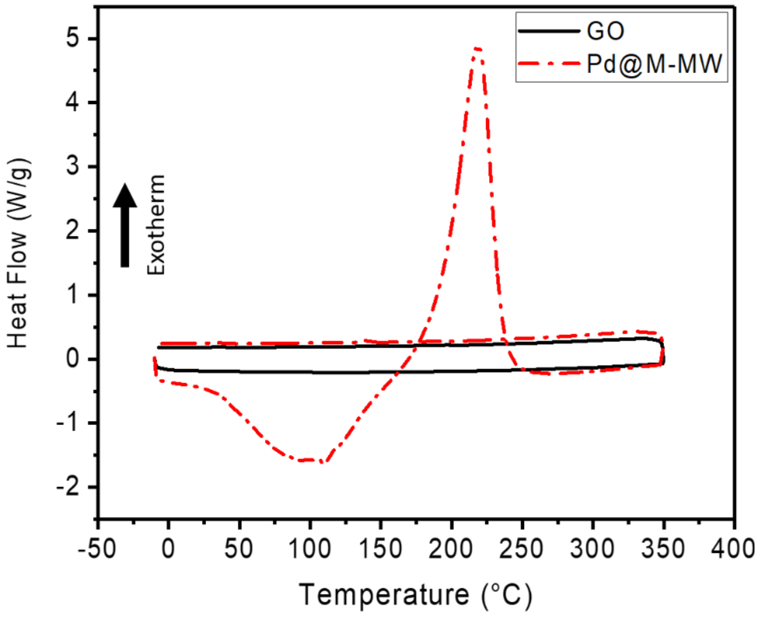

Figure 2.6. DSC analysis of the monolithic catalyst and GO

2.1.4.Insights and Findings

A state of art, all aqueous method for preparation and nondestructive analysis of palladium @ graphene monolithic catalysts was developed and systematically studied. The proposed route in this work it is the result of the optimized monolithic catalyst pursuing high catalytic activity as well as long lifetime for Suzuki cross-coupling model reaction in flow.

In addition to the higher activity obtained from $TAPdCl_2$-based monoliths compared to $PdCl_2$-based catalysts, it was shown that microwave treatment can have noticeable effects on these hybrid materials performances.

The ICP-OES results recorded slightly higher Pd uptake in MW-treated monoliths. However, by XPS analysis it was shown that the majority of Pd species in those catalysts were Pd(II), requiring initial activation prior to contributing into the Suzuki catalytic cycle.

The scanning electron microscopy of monolithic catalysts showed that the average Pd particle size distribution went through a significant change during the flow chemistry. The formation of particles with over 200nm diameter in MW-treated monoliths after flow, was thought to be the result of Pd(II) to Pd(0) post-reduction phenomena. Hence, correlating closely with elemental analysis conducted via XPS.

2.2. Palladium/Reticulated vitreous carbon monoliths as catalytic electrodes for electrochemical Wacker-type oxidation reactions.

2.2.1.Motivation and Background

Electrochemistry is a well-established method for synthesis. [24] Though, it has not been utilized to its utmost potential in complex organic molecules [24]. The scalability and low throughput are considered as traditional drawbacks of this approach. It has been proven that the use of active electrocatalysts can reduce the activation energy of certain reactions by over 30% and 35% in oxygen reduction and hydrogen oxidation reactions, respectively [48]. The conditions of such reactions are milder when performed electrocatalytically rather than via their conventional routes. For example, the metal-catalyzed Wacker chemistry is used for alkene oxidation, is typically run at over 70°C and require over 5 mol % of the homogeneous palladium catalysts [80]. Nevertheless, the regioselectivity of oxidation reaction towards ketone or aldehyde products is one of the main challenges of Wacker-type reactions. Therefore, the conventional reaction conditions make it financially unfeasible [81]. During Chapter 3 the design space for optimized catalyst synthesis as well as process conditions for high selectivity electrochemical oxidation of olefins were presented. The graphene-based monolithic catalysts as large-scale catalyst bodies have shown a significant advantage in various reactions in batch and flow chemistry. [57] In Chapter 2 it was shown that their superior activity is mainly empowered by their high porosity structure, fast charge transfer through the structure, and lower metal particle leaching. [82] Hence, they could be considered as potential electrodes for electrochemical reactions. It has been shown [83-84] that the TEMPO used in Wacker-type electrooxidation of terminal olefins is among the crucial reagents promoting a faster charge transfer between the solid-supported catalyst and the electrode in the current approach (refer to Chapter 3). Hence, significantly improving the redox cycle of the Pd catalyst yielding higher TOFs in electrochemical framework. However, since this mediator constitutes about 30% of the overall process cost, [84] it's elimination through direct deposition of Pd particles on a highly conducting monolithic electrode could significantly improve the economy and throughput of the electrochemical route. [85]

To do so, a glassy carbon monolith with high mechanical and chemical robustness as well as electrical conductivity was identified as the suitable option for such catalytic electrodes [86]. Considering the desired chemistry (Wacker) an extremely inexpensive, completely aqueous, and foam-templated method for preparation of such monoliths was developed in-house.

2.2.2.Methodology and Characterizations

The monolith preparation was based on hydrothermal polymerization of inexpensive hydrocarbons as the carbon precursor around a reticulated polyurethane foam template. Afterwards, through annealing the foam template would be removed while the polymer would be turned into a porous reticulated vitreous carbon monolith.

2.2.2.1. Materials

The sucrose, ammonium hydroxide (NH_4OH), potassium hydroxide (KOH) palladium chloride ($PdCl_2$), acetonitrile, and ethyl acetate were purchased from Caisson Labs (Smithfield, UT, USA), and Millipore-Sigma (NJ, USA), respectively. TEMPO, and 1-octene were purchased from Alfa-Aesar (USA). The template used was a commercially available polyurethane foam. Colloidal silver (resistivity $<2400\ \Omega/\square$) as well as conductive double-sided carbon tape, and adhesive epoxy resin were purchased from TED PELLA INC, USA. and Ellsworth Adhesives, USA., respectively. The 22-gauge chemical resistant silver-coated stranded wire was purchased from McMaster-Carr, USA. The materials were used without any further purification.

2.2.2.2. Catalytic Electrode Preparation

The detailed protocol for preparation of templated polymer network included incipiently wetting a commercial reticulated polyurethane foam with a 10:3 mixture of 2 g/mL sucrose in DI-water and concentrated ammonium hydroxide (NH_4OH). Prior to incipient wetness of the template foam, the pore volume of the foam was measured as 32.5 mL/g. The sucrose/ammonium hydroxide mixture amount was calculated accordingly. The mixture was stirred for 10 minutes at 25°C at 500 rpm. Finally, the foam was immersed in the solution and then was put in an autoclave enclosure and heat treated at 100°C for 24 hours.

The polymerized, and templated monoliths were then dried in room temperature vacuum chamber followed by lyophilization for 12 and 24 hours, respectively. The dried monoliths were then annealed in a horizontal tube furnace under a mixture of compressed air (Air) and argon (Ar) atmosphere (flow 0.2 mL/min) for 1 hour (Figure 2.7.).

Figure 2.7. Image of the prepared Pd-glassy carbon monolith

In order to deposit the Pd particles on the monolith, the incipient wetness impregnation (IWI) method (Section 3.3.2) was utilized (nominal 5 wt% Pd on carbon monolith) prior to annealing. The $PdCl_2$ salt was used in this process. As proven by our group's previous studies, microwave treatment was crucial for embedding the particles within the monolith structure, then minimizing the leaching of the Pd catalyst off the support. [49] This treatment was conducted using Discover S microwave reactor at 200 watts for 30 seconds. The effect of microwave treatment was studied via Hitachi SU-70 FE-SEM at 5 KV (Figure 2.8.).

2.2.2.3. Monolithic electrode Optimization

In order to optimize the monolith preparation process, 2 different property modifications were pursued. 1. Although the amount of added solution to foam was controlled in the beginning, the final product often contained extra polymeric solution which then would be entrapped within the pores of the template and result in a low porosity, bulky structure. To address this issue, the monoliths prior to drying and subsequent annealing were put under a 50 lbf/cm2 compression for 30 seconds. This process was repeated three times, pushing the extra sucrose polymer solution out of the templated structure.

2. The annealing temperature suggested in the literature [67] was 200°C and 500°C. The thermogravimetric analysis (TGA) of identical monoliths annealed under the mentioned conditions

showed heterogeneity in results in terms of residual mass (Figure 2.10.). Therefore, to optimize the annealing conditions, a two-level of screening DOE was designed based on the temperature and atmosphere of the chamber (Table 2.2).

Table 2.2. The screening DOE for annealing conditions optimization

Entry	Ar:Air ratio (%)	Temperature (°C)
Pd-GC-1	100:00	200
Pd-GC-2	80:20	200
Pd-GC-3	90:10	350
Pd-GC-4	100:00	500
Pd-GC-5	80:20	500

The structural properties of the DOE samples were probed using a Phenom ProX (SEM/EDX), a Rigaku MiniFlex II X-Ray diffraction analyzer. The most promising trial was also characterized via a PHI VersaProbe III X-Ray photoelectron spectrometer utilizing Al k-Alpha X-ray source with a 2-6 eV pass energy resolution. The Pd content calculated in EDX was used as the basis for reaction screening design.

2.2.3.Results and Discussion

2.2.3.1. Effect of Microwave Treatment

As shown in chapters 2 and 3, the microwave treatment results in physical defect formation in the carbon-based support structure which then enables metallic (Pd in our case) to be embedded within the defects. [49] This process ensures the optimized interaction between the support and metallic catalyst particles. [82] Through scanning electron microscopy, it was shown that in the case of Pd-GC monolithic electrodes this treatment had the same effect yielding a successful embedding of Pd particles within the monolith structure while leaving the monolith structure undisturbed (figure 4.3.).

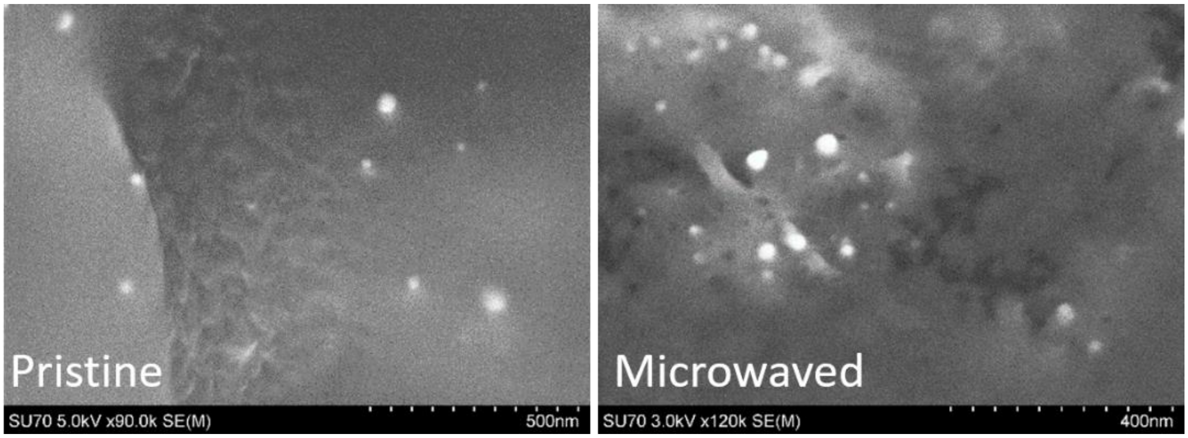

Figure 2.8. SEM images of the Pd-glassy carbon monolith (the dark spots around and near Pd particle bright circular textures are the indication of physical defect formation).

2.2.3.2. Monolithic Electrode Optimization

The micro-CT scan imaging supported the finding as the compressed monolith (Figure 2.9-top) showed a significantly higher porosity compared to the non-compressed one (Figure 2.9-bottom).

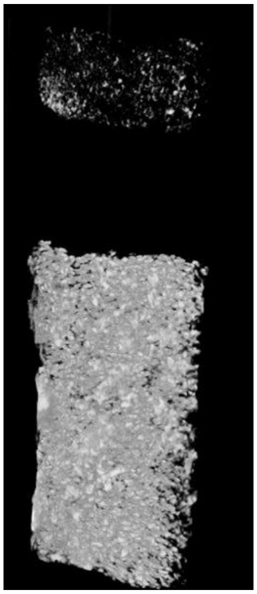

Figure 2.9. micro-CT scan imaging of top) compressed and bottom) non-compressed monoliths

The annealing temperature could affect the amount of the template foam elimination. The higher the annealing temperature, the higher the template elimination. Although the elevated temperatures are not financially favored, the TGA analysis (Figure 4.5.) showed that at the literature-suggested 200°C [67, 86] annealing temperature, there is about 50% lower mass fraction left to be eliminated from the structure. The 500°C annealing protocol depicted a steady profile signifying a successful elimination of the template. Thus, the latter temperature was chosen for further studies.

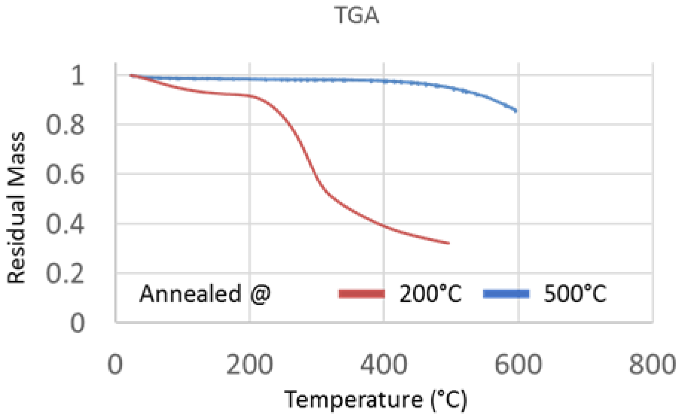

Figure 2.10. TGA analysis of monoliths annealed at various temperatures

In order to achieve the most optimal conditions for monolithic catalyst formation, the XPS and SEM/EDX analysis was conducted on the screening DOE trials. As the XRD graph (Figure 2.11.) shows, the Pd structure (specifically Pd(111) desired crystal structure) is only visible in Pd-GC-3,4, and 5. This observation indicated that the catalytic aspect of monoliths can be attained at temperatures higher than 350°C.

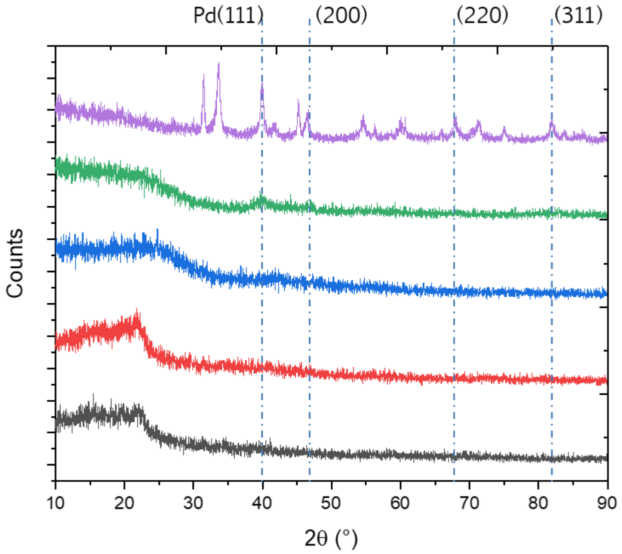

Figure 2.11. XRD analysis of prepared trials for the screening DOE. The graphs are associated with Pd-GC-1 through 5 from bottom to top.

The EDX analysis of the monoliths showed that the observed Pd structure transformation in XRD analysis, was accurate. The Pd content of the trials annealed at 200°C were significantly less than the ones with higher temperature treatments. This observation indicated that the Pd particles were potentially entrapped within the glassy carbon structure, rendering them ineffective for reaction catalysis. Although the nominal value for Pd loading was 5 wt%, the amount of Pd in the Pd-GC-5 was recorded as over 50% of the structure.

Table 2.3. EDX elemental analysis of the monolithic electrodes (3-point average)

Entry	Pd (wt%)	N (wt%)	O (wt%)
Pd-GC-1	<0.1	14.55 ± 2.39	4.09 ± 0.52
Pd-GC-2	<0.1	6.71 ± 1.82	16.38 ± 2.26
Pd-GC-3	1.43 ± 0.11	15.04 ± 1.20	32.17 ± 7.16
Pd-GC-4	3.96 ± 0.23	12.45 ± 3.72	9.20 ± 2.05
Pd-GC-5	52.67 ± 3.78	5.3 ± 1.33	29.96 ± 9.12

The SEM imaging of the Pd-GC-3,4, and 5 showed that the 10 and 20% Air content of atmosphere for Pd-GC-3 and 5 led to two undesired phenomena. In Pd-GC-3, although the temperature was lower (350°C) than Pd-GC-4, the redeposition of carbon resulted in Pd particle and the monolith porosity carbon coating (Figure 2.12-a). In Pd-GC-5, the presence of air resulted in complete decomposition of monolith structure, leaving a fragile shell mostly consisting of Pd clusters (Figure 2.12.-c). Therefore, the most optimal conditions were identified as the trial Pd-GC-4 with 100% argon flow at 500°C (Figure 2.12.-b).

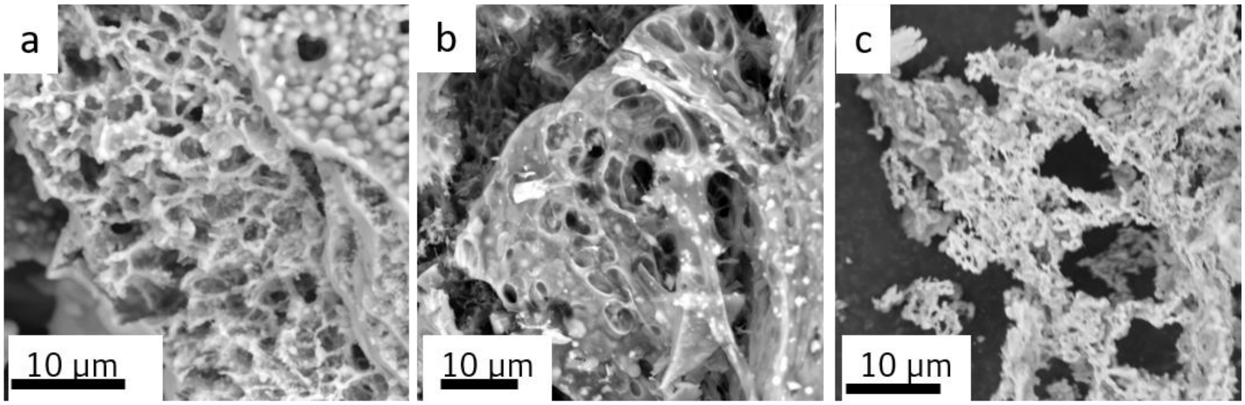

Figure 2.12. SEM images of a) Pd-GC-3, b) Pd-GC-4, and c) Pd-GC-5 monoliths

The XPS analysis of the optimal Pd-GC-4 (Figure 2.13) revealed two major points about this monolithic catalyst. Firstly, the monolithic structure was nitrogen-doped as the result of NH_4OH presence during the annealing, which then led to an improved Pd immobilization as it provides a lower binding energy site for Pd particles to be adsorbed on the support surface. [87]. Secondly, the Pd (II) fraction (desired ionic species for Wacker chemistry) was less than 40%.

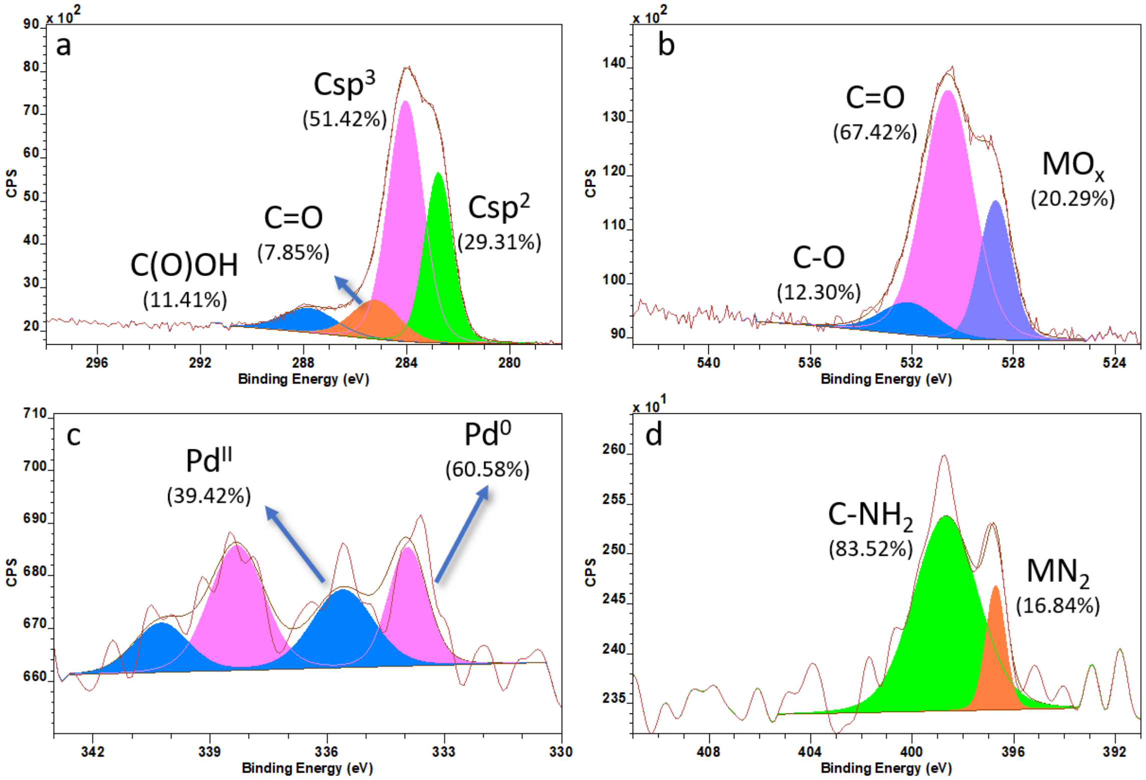

Figure 2.13. The XPS spectra of Pd-GC-4 monolith a) Carbon, b) Oxygen, c) Palladium, and d) Nitrogen scans.

3. Application of Pd-decorated GO monolithic catalysts for continuous Suzuki-Miyaura cross-coupling synthesis

3.1. Motivation

Suzuki-Miyaura cross-coupling reaction is a well-known redox process that utilizes Pd^0 as the active catalytic species. This process has been used and is actively executed in the pharmaceutical industry. The catalyst-driven improvement in continuous synthesis efficiency can have a potentially global impact in that field. Thus, a screening study of Pd-GO monoliths as packed bed cartridges was designed, and their performance and operational longevity were compared with 2D catalyst counterparts. As an innovative approach to study these materials, a CT-scan imaging approach was also utilized to have a wholistic view of the monoliths before and after the reaction. This study will provide a benchmark for application, diagnosis, and fine-tuning of monolithic catalysts in flow systems.

3.2. Materials and methods

3.2.1.Materials

Dichloromethane, and acetonitrile (Sigma-Aldrich, USA) as well as potassium carbonate, and phenyl boronic acid (Fisher Scientific, USA) were used without further purification. Both Monolithic and 2D catalysts were also used without further modifications.

3.2.2.Suzuki Cross-coupling Screening in Flow

The Suzuki cross-coupling model reaction was investigated between 4-bromotoluene, and phenyl boronic acid (3.8 mmol) (0.08 and 0.0975 M, respectively) in a 40 mL mixture of ethanol-DI water (1:1), with potassium carbonate (0.24M) to determine catalytic activity and longevity. The desired product was 4-phenyltoluene (Figure 2.1.) During this process, a H-Cube mini flow reactor by ThalesNano® was used which contains a CatCart (ID: 1.6mm, H: 7mm) packed with either the 3D monolithic catalyst or the conventional 2D Pd@GO catalyst (28.6 µg calculated Pd in each CatCart) samples to be tested.

The continuous packed bed reactions were conducted at 0.2 mL.min^{-1} flow rate and at 80-90°C. The reaction affluent mixture was collected at the reactor outlet in 30-minute time increments. An aliquot of each incremental collection vial was taken for analysis on GCMS after filtering with 0.2 µm syringe filter and 10 times volumetric dilution with dichloromethane.

To remove the reaction residue from CatCarts, after each reaction the whole system was purged with ethyl acetate, and a 1:1 ethanol:DI-water solution each for 10 minutes, respectively.

3.3. Results and Discussion

3.3.1. Suzuki Cross-Coupling Catalytic Activity and Catalyst Lifetime Analysis in Flow

The model Suzuki reaction chosen for testing of the catalyst performance was the C-C bond formation between 4-bromotoluene and phenyl boronic acid, detailed in Figure 2.1. and the methods section. In order to systematically optimize the monolithic catalyst synthesis conditions for optimal material performance in continuous catalysis, various parameters were studied. The effect of Pd precursor used in catalyst synthesis, as well as the effect of reaction temperature during the first 60 minutes of the reaction in flow was studied (Figure 3.1-a, & b, respectively).

Use of different palladium precursors, $TAPdCl_2$ and $PdCl_2$, were first investigated using the model Suzuki reaction (Figure 3.1-a). The Pd@M($PdCl_2$)-MW deactivation was recorded to be two times earlier than the Pd@M-MW entry. Hence the monolithic catalysts prepared using $TAPdCl_2$ were more catalytically active and durable than materials prepared using $PdCl_2$.

The catalytic activity drastically decreased at 90°C reaction temperature for the monolithic catalysts (Figure 2.4. B). This activity loss was related to the thermal decomposition of the ester bonds, causing the monolith to collapse and thus hinder mass transfer.

The 2D catalysts (Pd@GO and Pd@GO-MW) and 3D monolithic catalysts (Pd@M and Pd@M-MW) were next investigated for catalyst lifetime in continuous packed bed configuration (Figure 3.1-c). Most notably, the 3D monoliths, particularly Pd@M, had better catalyst performance with respect to catalyst lifetime. The rapid completion of the cross-coupling reaction by Pd@M within the first 5 minutes of reagent passage (prior to physical deactivation) signified the advantage of the proposed EtOH-assisted deposition method in preparation of highly active Pd particles. Longer reaction times at similar cross-coupling reaction conditions were reported for other Pd preparation techniques such as conventional hydrazine [88] and hydrogen gas [89] (Table 3.2.). According to XPS analysis, Pd@M-MW contained almost 2 times Pd(0) species content compared to Pd@M. The Pd(0) content as the reported effect of microwave treatment on Pd particle anchoring and activity increase [45] were attributed to the higher initial activity over the non-microwaved monolithic catalyst. However, the Pd@M outperformed the Pd@M-MW from the longevity perspective, which was attributed to the defects or holes created by microwave irradiation, decreasing the structural integrity of the monolith. The abrupt collapse of the monolith into a highly packed single piece was the reason for the observed deactivation of the MW-treated monolithic catalyst (Pd@M-MW), thus resulting in drastically reduced catalytic activity.

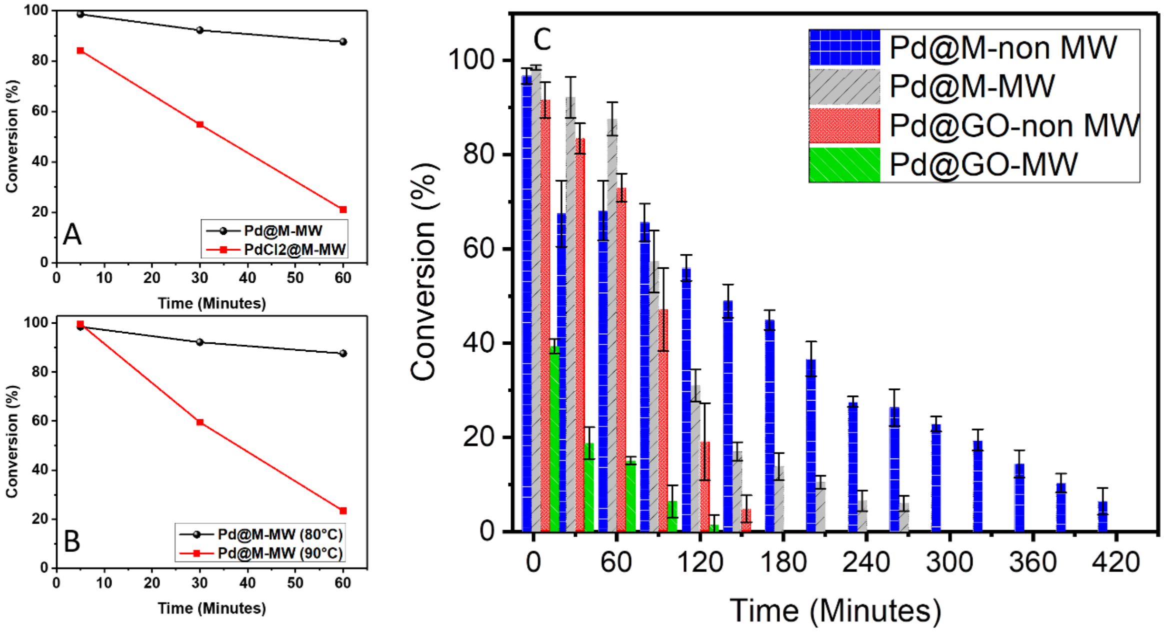

Figure 3.1. Suzuki cross-coupling screening in flow study of the effect of A) Palladium precursors ($TAPdCl_2$-black, and $PdCl_2$-red), B) reaction temperature, and C) various catalyst materials. All the reactions were conducted at 0.2 mL.min-1 and 80°C (except Figure 3.1.-B)

The backpressure of all materials was important to measure as an ideal packed bed configuration will have minimal backpressure across the packed column. No backpressure was recorded for the Pd@M monolithic catalyst during the reaction indicating this material was more suitable for flow chemistry compared to the 4-bar backpressure of the conventional 2-D catalyst. This advantage enabled a uniform flow rate through the reactor as well as higher overall throughput, potentially improving the process economy.

Table 3.1. Catalyst system oxygen and palladium contents as well as operating backpressure and lifetime in flow chemistry

Catalyst System	Oxygen content (wt%)[*]	Palladium content (wt%)[§]	Backpressure (PSI)	Lifetime (min)	TON (Average @ >20% conversion)	Average %Pd leached every 30 minutes [§]	Total %Pd leached [§]
Pristine GO Monolith	39.17	-	-	-	-	-	--

Pd@M-non MW	23.73	3.79	0	330	3591	1.11± 0.54	11.6 ± 2.3
Pd@M-MW	19.46	4.45	0	120	2340	2.64± 1.39	19.9 ± 3.4
Pd@M ($PdCl_2$)-MW	20.31	3.29	1	60	1671	9.72 ± 2.34	33.1 ± 6.6
Pd@GO-non MW	28.71	2.86	4	120	2088	13.46 ± 2.89	51.2 ± 14.7
Pd@GO-MW	14.19	3.16	4	90	76	11.97 ± 3.11	47.5 ± 9.2

[*] Measured by XPS analysis

[§] Measured by ICP-OES

The other significant advantage of the monolithic over conventional 2D Pd@GO catalysts was demonstrated by a Pd leaching study (Table 3.1.). It was determined that for every 30 minutes of operation, almost over 12% of Pd is leached off from the 2D Pd@GO catalysts into the reaction media. Compared to the 2D Pd@GO catalyst, the amount of Pd leached was significantly reduced 4-fold with the monolithic catalyst.

Table 3.2. The comparison between the previous Pd catalyzed Suzuki cross-coupling reactions in flow and the current study

Catalyst (mol% Pd)	Temperature (°C)	Reactor (minute residence time)	Flow rate (mL.min^{-1})	1st-hour average conversion (GC RPA%)	Ref.
Pd on Polyurea (--)	55	HPLC column packed bed (4)	0.2	100	90
Pd on Fibercat (--)	120	X-Cube (3)	0.155	30	38
Pd@MIL-101-NH_2 MOF (w/ glass beads) (1)	50	House-made Packed bed (35-40)	0.05	94	91
Pd on CuO [*] (1)	80	Batch (10)	--	~88	88
Pd on γ-Alumina [§] (0.5)	60	Batch (24 hrs)	--	~65	89
Pd@M-MW (0.5)	80	H-Cube mini (7)	0.2	93	This study

[*] Deposition via hydrazine

[§] Deposition via H_2 gas

Table 4.3. shows the comparison between previous reports of the same Suzuki cross-coupling reaction in flow between the Pd@M and other catalysts. Notably, the prepared Pd@M catalyst does not require a diluent, such as glass beads, due to their customizability and flexibility of shape design. The monolithic catalysts effectively outlive the conventional catalysts and maintain higher activity and physical integrity at elevated temperatures.

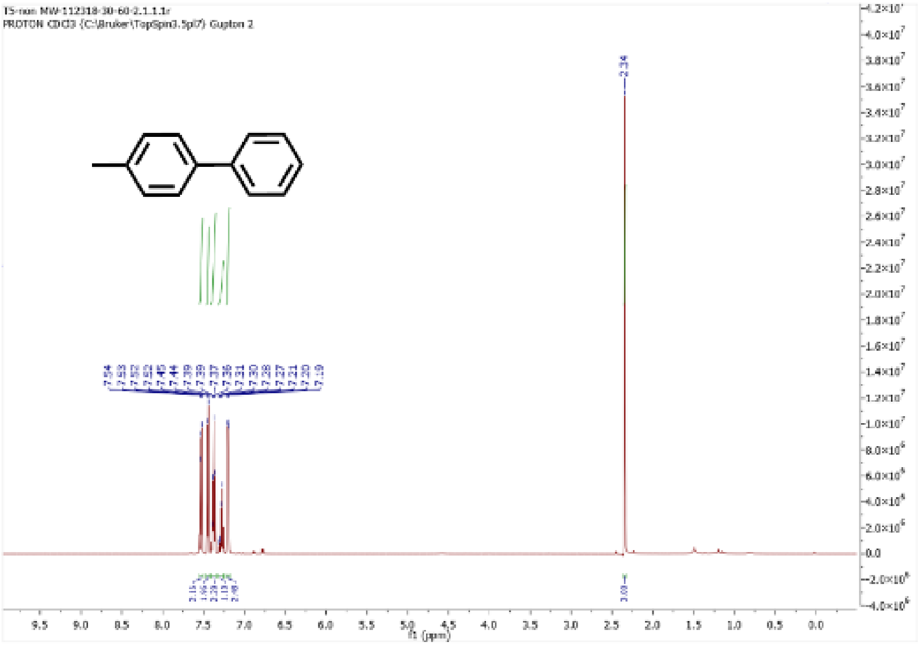

Figure 3.2. 1H-NMR spectrum of the reaction effluent collected from Pd@M-non MW in flow

As shown in Greco et al.'s work on Suzuki reactions in flow [38], packed beds of Pd(0) catalysts struggle to maintain conversion above 30% throughout the first hour of the process. However, Pd@M monolithic catalysts demonstrated over 70% average conversion during that same period (Figure 3.1-c).The superior longevity and sustainability of monolithic Pd@M catalysts over previously reported catalyst packed beds while reliably Maintain their activities for over 5 hours can be attained.

3.3.2.Computed Tomographic (CT) Scan Mapping of Monolithic Catalysts

In order to accurately characterize the Pd decorated 3D monolithic structure, a macroscopic characterization technique is needed to evaluate the distribution of Pd throughout the entire monolith material. Therefore, micro CT-mapping was investigated as a new technique to provide this characterization. Micro CT-mapping is applicable because such imaging is based on the intensity of diffracted X-rays. More specifically, two main factors provide resolution between Pd and graphene final images: the atomic number of constituent elements and the crystallinity of the materials. The heavier Pd atoms and their highly crystalline structures result in higher X-ray diffraction in comparison to the carbon of GO. This difference in X-ray diffraction provided the necessary resolution and contrast to distinguish the two materials and, therefore, the distribution of Pd throughout the GO monolith. In addition, the opacity of the 3D image can give an indirect measurement of the porosity of the structure, which was important in qualitatively evaluating the monolith for use in continuous packed bed reactors. This indirect macroscopic characterization of the structure was significant in evaluating porosity before and after reactions since complete solvent elimination was technically difficult. Consequently, surface area analysis via conventional methods (such as physisorption techniques) was not possible on ‘wet’ materials. The micro-CT scan analyses of the 3D monolithic catalysts, Pd@M and Pd@M-MW, show that a relatively uniform distribution of Pd particles were achieved throughout the entire monolith structure. (Figure 3.3-a and b). Micro-CT mapping also reveals the density of Pd detected is slightly lower in non-treated monolithic catalyst (Figure 3.3-b). This result was consistent with lower Pd uptake of Pd@M compared to Pd@M-MW (Table 4.2.) as determined by ICP-OES.

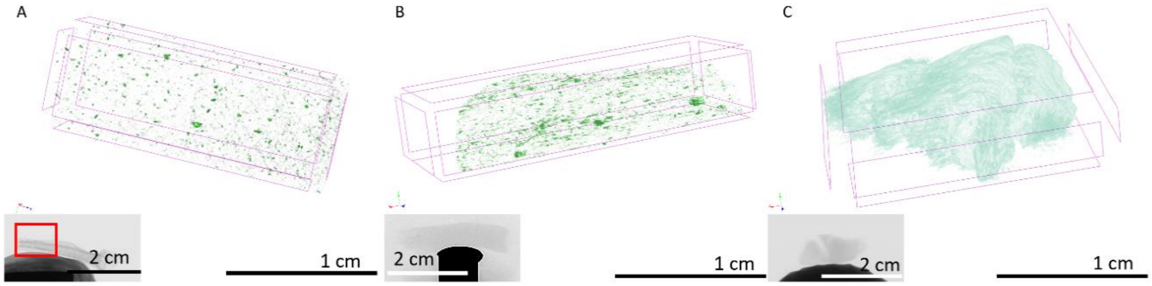

Figure 3.3. Micro-CT analysis of A) Pd@M- MW, B) Pd@M-non MW, and C) Pd@M-non MW after flow reaction

A section of reacted monolith in flow was characterized (Figure 3.3-c). The drastic change in contrast between Figure 3.3.-b and c, particularly the opacity and texture of the obtained image, indicates that a significant amount of X-ray diffraction was detected in this specimen. The two possible hypotheses for the observation are: the geometrical diffraction caused by physical deactivation and collapse of porous structure of the monolith, and/or the entrapment of crystallized 4-phenyltoluene as well as 4-bromotoluene (Figure 3.3.) inside the structure. The first hypothesis was less likely as the SEM imaging showed that the porous structure was preserved through the flow synthesis (Figure 2.4.-e). The electron microscopy technique also revealed that the texture of graphene nanosheets was altered after the reaction as they were covered with a crystalline residue. Therefore, the bulky, and opaque 3D image of monolith obtained via micro-CT technique gives a clear indication that micropores of the structure was filled with reaction product residue, which was confirmed by the SEM technique.

3.4. Insights and Findings

According to both reaction screening tests, the MW-treated monoliths collapsed at a faster pace compared to non-MW treated entries, leading to a lower catalytic lifetime. The longevity and backpressure of the monoliths in flow were compared to 2D Pd @ graphene oxide catalyst packed beds. Significant improvements in both characteristics were recorded for 3D monolithic catalysts. Specially, a 300% increase in longevity of monolithic catalysts compared to 2D catalysts was of great importance.

Finally, the proof of concept for the preparation of a model structure for large-scale elemental analysis of micro-CT was successfully demonstrated as both Pd particle distribution as well as porosity studies on monolithic catalysts were reported.

The 3D map of Pd particles size distribution throughout the monolith can provide valuable information not only from an experimental optimization perspective but also as a reference model to be used for further computational studies on solid-supported flow catalysis.

4. Application of Pd-decorated RVC monolithic catalysts for electrochemical Tsuji-Wacker cross-coupling synthesis

4.1. Background and Motivation

Electrochemical organic synthesis (EOS) has long been a significant focus of the synthetic chemistry and energy generation communities.[92] Despite the substantial progress made in electrochemical processes for energy applications, industrial electroorganic synthesis research was almost idle during the first half of the 20th century.[24] Equipment processes developed in the 1970s revitalized EOS manufacturing, showing an increase from 300 to over 1500 products by the 2000s.[93]

The EOS is critical in a variety of reactions as it provides flexibility in controlling reaction conditions and heat-sensitive reagents by utilizing electricity as the source of energy instead of heat.[94] Although the advantages of catalysis in EOS are generally widely appreciated, homogeneous catalysts that have proven successful for thermally-driven batch chemistries both on laboratory and industrial scales are often not ideally suited to electrochemistry.[95] Indeed, the direct application of homogeneous catalysts typically used in a thermally-driven reaction to EOS can be challenging and often leads to decreased reaction efficiency. Consequently, higher catalyst loading is needed due to the introduction of new decomposition pathways, presenting unique challenges in product separation, catalyst recovery, and recyclability.

In an exemplary study, Baran et al. synthesized dixiamycin B, a rare N–N linked dimeric natural product, using electrochemistry.[96] A unique electrochemical dimerization of carbazoles and carbolines made it possible to selectively “dial in” the oxidation potential at a critical oxidation step en route to the successful total synthesis. The 20 wt% homogeneous Pd catalyst required for that oxidative dimerization could limit the scalability of this synthetic approach.

In another example, Chen and co-workers developed a protocol for generating nitriles from aldehydes using 10 mol% each of various homogeneous soluble copper (Cu) salts (2,2,6,6-tetramethylpiperidin-1-yl)oxidanyl (TEMPO) as the mediator. This method proceeded under mild conditions and generated nitriles with yields of over 70% from both aromatic and aliphatic aldehydes.[94] Although the electrochemical approach showed successful results, the complexity of the reaction, notably the product isolation, was exacerbated by the incorporation of non-retrievable Cu and Pd salt catalysts.

Fluidized EOS is a novel method that is projected to revolutionize electrochemical synthesis.[97] While in traditional EOS, the catalyst is immobilized on the electrode surface, the catalyst species in the fluidized method are dispersed in the media. This approach optimally utilizes the catalyst surface area through performing the reaction at the ternary interaction surface (catalyst, reagents, and electrode) is significantly increased.

One of the most critical considerations in catalyst design for such processes is the allowed transition metal contents in pharmaceutical ingredients, implemented by regulatory agencies.[8] The large amounts of non-recyclable catalyst usage cannot satisfy that design criterion.[41] As a result, the development of catalyst systems optimally suited for synthetic electrochemistry is an area of active research and remains an unmet need.

An optimal catalyst for electrochemical organic synthesis, and particularly the fluidized approach, must possess two main qualities. First, it should be more active and selective, ideally at lower catalyst loadings, compared to its homogeneous counterpart (if one exists).[82] Second, the metallic species should be readily separated from the reaction media and reused (especially for higher throughput syntheses and processes intended for scale-up). Successful anchoring of metallic particles on solid supports ensures the satisfaction of both considerations.[41]

Such solid-supported catalysts are now readily produced and utilized both in conventional and electrochemical processes in the industry. Traditionally, the metal deposition is completed via chemical reduction (CHEM) of metallic salts (in solution) in the presence of solid supports.[48] This approach has minimal control over the properties of individual metallic particles and results in adsorption onto the support without any anchoring.[45] Therefore, despite the intrinsic scalability of CHEM, it is not a favored method, especially for industrial catalyst synthesis.

The primary method for large-scale production that can yield efficient anchoring is incipient wetness impregnation (IWI), during which the metallic salt solution incipiently covers all the support micropore volume.[98] This approach is rapid and ensures active entrapment of metallic particles within support micropores, all while maintaining their accessibility to reaction reagents. However, control over the structural properties of the deposited metallic species is limited, and consequently, (the method's) ability to tune the catalyst rationally.

Indeed, the discovery of advanced solid support materials, as well as robust, scalable methods for impregnating precious metal ions into those frameworks, continue to restrict widespread adoption of electrochemical synthesis, especially on industrially relevant scales.

Recent studies in our group have found that strong electrostatic adsorption (SEA) could yield extremely active and firmly anchored catalysts through electrostatic affinity between metal ions and the support's surface charge.[45, 49] This method has been successfully employed for anchoring metal ions onto graphene, with the effective interfacial connection between the metal and the support resulting in a faster charge transfer between them, promoting a higher rate of catalyst regeneration, and potentially leading to a significant increase in catalytic activity. Microwave treatment (MW) also results in local heating of the metal particles, which effectively lodges them within the support.[99] These generated defects act as high-activity spots improving the interaction between the particles and the support and, therefore, the catalytic activity. Consequently, our synthetic efforts have been concentrated on synergistically combining the SEA method with microwave treatment to produce the optimal solid-supported catalysts.

SEA-MW catalysts are proven to be among the most active catalysts for Suzuki cross-coupling reactions that require metallic (Pd(0)) species. Mainly because through the SEA-MW method, the ionic species are reduced to the metallic state. On the other side, the mechanism of the Pd-catalyzed oxidation reaction, e.g., Wacker oxidation (Figure 4.1.), readily uses ionic species (Pd(II)) as active catalytic species. Therefore, to make SEA-MW a viable method for Wacker oxidation reactions, a deeper understanding of the available design space to favor the production of the Pd(II) catalyst is needed. Identification of the optimal design parameters should lead to the discovery of solid-supported catalyst materials that are tailor-made for efficient electrochemical synthesis.

The Wacker oxidation is an iconic transition metal-catalyzed industrial process for the synthesis of aldehydes and ketones from olefins.[30] Adapting the reaction to an electrochemical framework has been found to noticeably improve the reaction throughput as the catalyst redox can be controlled and further promoted under electrochemical conditions.[24] However, applying the traditionally-utilized homogeneous catalyst (e.g. $PdCl_2$) to the electrochemical process suffers from the difficulties mentioned above (e.g. product contamination, additional purification steps, and economical feasibility),[42] rendering a scalable electrochemical Wacker process challenging to attain.

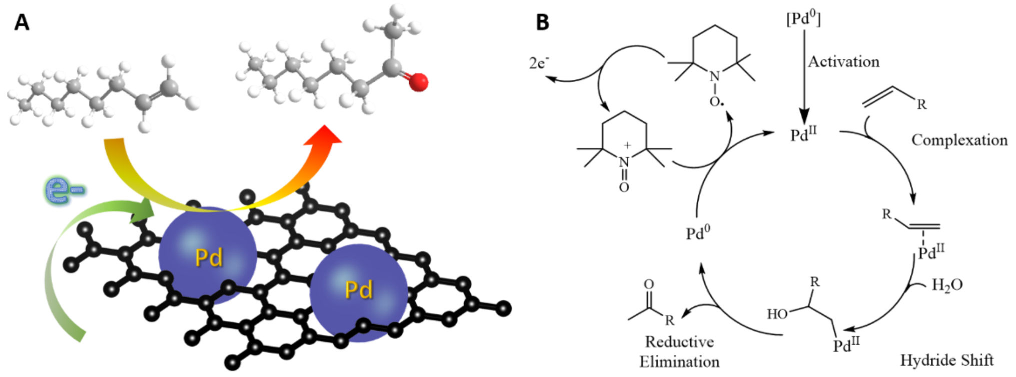

Figure 4.1. A) the schematic and B) the catalytic mechanism of the electrochemical Wacker oxidation

In order to be able to prepare a suitable monolith, a systematic study of the catalyst preparation process for this reaction and reaction setting combination is required. Herein, the electrochemical Pd-catalyzed Wacker-type oxidation of terminal olefins (Figure 4.1.) was studied. A set of Pd on graphene nanoplatelet (Pd/GNP) catalysts were rationally designed and prepared to enable Wacker oxidation of 1-octene comparing new graphene-based solid-supported catalyst materials and conventional homogeneous catalysts in both batch and electrochemical routes. In addition, the throughput obtained from the electrochemical route compared to conventional batch was evaluated as a measure of industrial suitability. Furthermore, a statistical analysis of the catalyst structure-activity relationships was conducted, leading to the identification of a catalyst design space within which catalysts could exceed industrial benchmarks. Lastly, to identify the preparation method yielding the most active catalyst for the electrochemical Wacker route, electrochemical surface area analysis was utilized as a reliable tool to compare catalyst oxidation capabilities quantitatively. Afterward, utilizing the knowledge in the catalyst preparation and considering the reaction setting requirements, a set of electrodes for Pd-RVC monolithic catalysts were prepared and as a proof of concept, the first-in-kind, monolithic electrode application for Wacker-type oxidation of terminal olefin was successfully depicted.

4.2. Materials and Methods

4.2.1. Materials

Graphene nanoplatelets (500 m^2/g), hydrochloric acid (HCl, 12.1 M in DI-water), and 1-octene were purchased from Alfa-Aesar, USA. Ascorbic acid, palladium chloride ($PdCl_2$), tetraaminepalladium chloride monohydrate ($TAPdCl_2•H_2O$), acetonitrile, hydrogen peroxide (H_2O_2, 30 vol% in DI-water), ethyl acetate, and TEMPO were purchased from Millipore-Sigma, USA. Isopropanol, potassium chloride (KCl), and potassium hydroxide (KOH, pellets) were purchased from Fisher Scientific, USA. Nafion solution (5 wt% in aliphatic alcohols) was purchased from Fuel Cell Store, USA. All the materials were of synthesis grade and used without further purification.

4.2.2. Catalyst synthesis

Catalyst preparation was performed utilizing two Pd salts ($PdCl_2$ and $TAPdCl_2•H_2O$) and three various immobilization methods (described in-depth below). Once formed, all Pd particle catalysts were further activated via a Discover S-series microwave reactor. The microwave treatment protocol was adapted from Ghobadi et al. utilizing a constant temperature approach (holding at 135 ℃ for 10 min). [100]

I. *Strong electrostatic adsorption (SEA).* The SEA catalysts were prepared by the addition of 323 mL of DI-water followed by the dissolution of Pd salt in it (5 wt% Pd/support) to 1.0 g of GNP support. [45] The pH of the mixture was then adjusted according to the point of zero surface charge (PZC) of the support, measured via gradual titration of its aqueous dispersions with varying ionic strengths (i.e., 0.0001 to 1 M aqueous solutions of KCl).[101] The PZC for our GNP support was determined as 3.56. Afterward, the mixture was shaken at 200 rpm for 1 hour. Finally, the catalysts were filtered and rinsed with DI-water and dried overnight in a vacuum oven at 80 °C.

II. *Incipient wetness impregnation (IWI).* To prepare the IWI catalysts, a GNP pore volume was determined through a method denoted as tapping-induced coagulation.[98] Specifically, 100 mg of GNPs were added to an empty centrifuge tube and titrated with DI-water. Throughout the titration, the centrifuge tube was repeatedly tapped after reaching set titration volumes. The titration was complete when tapping resulted in a single agglomerated mass of GNP. A pore volume of 0.646 mL/g was measured and was utilized to create solutions containing Pd (5 wt% with respect to GNP). The prepared solutions were added to 1.0 g GNPs and tapped, forming a single coagulated piece of wetted GNP and then allowed to dry overnight in a vacuum oven at 25 °C. The catalyst loaded supports were then washed with DI-water to remove any unbound Pd particles. The resulting catalyst was dried in an oven at 100 °C for 24 h.

III. *Chemical reduction (CHEM).* Chemically reduced Pd/GNP catalysts were conventionally made by adding 1.0 g of GNP to 40 mL aqueous solutions of Pd (150 ppm, ca. 5 wt% Pd/GNP) and L-ascorbic acid (2 molar equivalents to moles of Pd).[49, 82] The mixture was stirred for 2 h under reflux at 25 °C in a round bottom flask. The catalysts were then washed repeatedly with DI-water and ethanol:DI-water solutions (1:1, v:v). The final washing step was performed with DI-water and the catalyst was filtered via a Büchner filtration system. The chemically reduced catalysts were dried at 100 °C for 24 h.

Homogeneous $PdCl_2$, and heterogeneous Pd-carbon catalysts were used positive control trials both in batch and electrochemistry settings. For clear identification of each catalyst, the "method-treatment" nomenclature. For example, the catalyst prepared via SEA method and was treated with microwave was coded as SEA-MW.

4.2.3.Catalyst structural analysis

X-ray diffraction analysis (XRD) and X-ray photoelectron spectroscopy (XPS) were conducted on catalysts using a Bruker X'pert Pro PANanalytical XRD spectrometer with Cu Kα, λ=1.54 Å, 2ϴ = 5° to 85° and a Thermo Fisher ESCALAB 250 X-ray spectrophotometer with a 2 eV step size for the survey, respectively. Inductively Coupled Plasma-Optical Emission Spectroscopy (ICP-OES, Agilent 5110 ICP-VCV-OES) was utilized to determine Pd content of the synthesized catalysts and reaction media (leached Pd) via acid digestion (12.1 M HCl). Electron microscopy was conducted via an FEI Titan high-resolution transmission electron microscope (HR-TEM).

4.2.4.Reaction screening

Batch oxidation. Wacker-type oxidations were adapted from Jiang et al., where catalysts (ca. 5 mol% Pd/1-octene) were added to 0.05 mM 1-octene in acetonitrile (10 mL).[83] The mixtures were heated in 20 mL glass vials to 60 ℃ at 500 rpm and allowed to stabilize., 6 molar equivalents of H_2O_2 were added dropwise to the mixtures after they were stabilized. The reaction vials were held at 60 ℃ and 500 rpm for 6 hrs under airtight condition. The characterization aliquots were sampled at various time-points to monitor the conversion of reaction. The aliquots were filtered using 0.2 µm syringe filters to remove residual solids and then diluted with ethyl acetate (20-fold). The diluted aliquots were then passed through a silica column (3-cm, height) to remove dissociated Pd and then analyzed on an Agilent 5977A GC-MS system. The relative peak area percentile (RPA%) of the product(s) were utilized to calculate the percent conversion (Equation 1) of the starting material and the reaction selectivity (Equation 2).

$$\text{Conversion (\%)} = \left(\frac{\sum \text{Product (RPA\%)}}{\sum \text{Substrate \& Products (RPA\%)}}\right) \times 100 \qquad (1)$$

$$\text{Selectivity (\%)} = \left(\frac{\text{desired product (RPA\%)}}{\sum \text{All products (RPA\%)}}\right) \times 100 \tag{2}$$

Electrocatalytic oxidation. The electrochemical Wacker-type oxidation of 1-octene was studied in a divided H-Cell (24/12 PINE research), where 20 mL of 0.05 M $NaClO_4$ in CH_3CN: DI-water (7:1, v:v) was added to each half cell.[84, 94] Next, 0.5 mol% of Pd catalyst and 28 mol% TEMPO (proportional to the 314 μL starting material) were added to the anodic half-cell. Graphite rods (diameter: 0.615 cm) were used as the working and counter electrodes for both half cells and maintained at an exact immersion depth of 1.5 cm per electrode (area: 2.495 cm^2). An Ag/AgCl (solution: 4 M KCl) reference electrode was set inside the anode half-cell. The reactions were conducted in a three-electrode system operated by a Gamry Instruments Reference 600 potentiostat in galvanostatic mode. A current density of 5 mA/cm^2 was applied for 6 hr under constant stirring (320 rpm). The aliquot sampling, preparation, and analysis were identical to the batch configuration.

In order to quantitatively compare the catalyst performances in conventional batch and electrochemical frameworks, the turnover number (TON) and turnover frequency (TOF) were calculated for each catalyst as an activity indicator (Equations 3 and 4, respectively).

$$\text{TON} = \frac{m_p}{m_c} \tag{3}$$

$$\text{TOF (hr}^{-1}\text{)} = \frac{m_p}{m_c \times t} \tag{4}$$

Where m_p, m_c, and t are moles of product (2-octanone), moles of catalyst (Pd), and reaction time (hr), respectively.

Statistical analysis

The response surface of least square fits on conversion and selectivity of reactions in electrochemical and batch frameworks as a function of the Pd uptake (wt%) and Pd (II) content (%) factors were conducted using JMP 14.0 software (licensed to Virginia Commonwealth University, College of Engineering). The validities of the fits were confirmed by their P-value study (acceptance limit: 0.05) and R^2 values.

The prediction profiler tool of the JMP software was used to overlay the response surface for all conversion and selectivity fits, constrained by the industrial benchmark of Wacker oxidation of olefins (55% mass conversion of the substrate with 80% selectivity towards the desired ketone product[102]). This constrained map of fits yielded the identification of a design space for solid-supported Pd catalysts specialized in such oxidation reactions. The desirability analysis of control points, depicted in the supplementary information (Table A. 1), determined the optimum factor values.

4.2.5.Electrochemical active surface area calculation

The electrocatalytic activities of prepared catalysts were determined via cyclic voltammetry. A glassy carbon (area: 0.07065 cm^2), platinum (Pt) wire and Ag/AgCl electrodes were utilized as the working, counter and reference electrodes, respectively. Prior to electrode preparation, the glassy carbon electrode was polished with 0.1 µm diamond solution until a mirror finish was achieved. [103] Catalyst inks were prepared (2 mg/mL dispersion in isopropanol) and drop-casted onto the glassy carbon working electrode (4.5 µL). The film was then dried at room temperature inside the fume hood. Nafion solution was then drop-casted (3 µL) on top of the previous cast to create an ionomer layer. Cyclic voltammograms (CVs) were obtained for each catalyst over a potential range sweeping from -1.2 V to 1.6 V at a scan rate of 25 mV s^{-1} for three cycles in 1.0 M KOH.[104] The absolute and the normalized values electrochemical active surface area (ECSA) based on Pd content were measured based on the oxidation peak (0.75 to 1.0 V vs Ag/AgCl) integration using Equations 5 and 6, respectively.

$$\mathrm{Q(mC.\,cm^{-2})} = \frac{\mathrm{E(mA.V)}}{\mathrm{v_s(V.s^{-1})}} \times \frac{1}{\mathrm{A_e(cm^2)}} \tag{5}$$

Where Q, E, v_s, and A_e are total ECSA the integration area under the oxidation peak, scan rate, and electrode area, respectively. Subsequently, the normalized ECSAs were calculated through the equation below:

$$\mathrm{Q_n(mC.\,cm^{-2}.\,mmol^{-1})} = \frac{\mathrm{Q(mC.cm^{-2})}}{\mathrm{M_c(mmol)}} \tag{6}$$

where M_c is the millimoles of Pd in the catalysts drop-casted on the working electrode. The CV spectra can be found in supplementary information in Figure AII.1 (Appendix II).

4.2.6.Monolith electrochemical Analysis and reaction screening

The monolithic electrodes were prepared by attaching a layer of carbon tape to one face of the monolith prior to annealing. After annealing, a chemical resistant silver wire was attached to the tape surface (separating the wire from the electrolyte) via silver paste. Afterwards, the wire surface and its juncture with monoliths were covered with chemically resistant epoxy resin adhesive. (Figure 4.2-a)

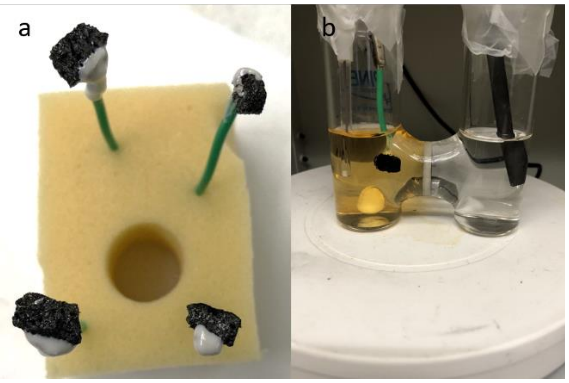

Figure 4.2. a) Image of the prepared monolithic electrodes, and b) electrochemical reaction setup

Both electrochemical analyses, as well as Wacker-type oxidation screening of 1-octene on monolithic electrodes (Pd-GC), were conducted using a Gamry Reference 600 potentiostat in a Pine Research H-cell in a 3-electrode setting with graphite rod (Princeton Applied Research), and Ag/AgCl (CH-Instruments) as counter and reference electrodes, respectively. The open circuit potential was continued for 200 seconds. The cyclic voltammetry was conducted through 3 cycles from -1.2 to 0.8 V vs. reference with scan rate of 10 mV/s.The electrolyte used for CV analysis was a 1M KOH aqueous solution.

As proof of concept, the electrochemical Wacker-type oxidation of 1-octene using the monolithic electrodes was conducted in the same H-cell and electrode settings as CV analysis for 6 hours at 25°C under 250 rpm stirring. The cathode half-cell contained the electrolyte (20 mL of 0.05M $NaClO_4$ in acetonitrile:DI-Water (7:1) mixture). The anolyte included the electrolyte solution (20 mL) with 0.05mM of 1-octene and 0.28 molar equivalent of the TEMPO with respect to 1-octene. The reaction was conducted under galvanostatic mode at 5mA/cm^2 of the electrode. The volume of the electrode immersed was adjusted to approximately contain 1 mol% Pd with respect to 1-octene (Figure 4.2.-b). The conversion and selectivity of the reaction was tested via the obtained relative peak area from GC-MS analysis of a 10 times diluted mixture (0.2 mL of anolyte diluted with ethyl acetate) following its filtration using silica column and 0.2 µm syringe filter.

4.3. Results

The catalysts prepared and analyzed herein possess specific structural properties owing to enhanced catalytic activities. Regardless of the reaction framework (batch or electrochemistry), the SEA method yielded the most active catalysts as their turnover frequency exceeded commercially available homogeneous $PdCl_2$, and heterogeneous Pd-carbon positive control catalysts by approximately 25%, and 220%. The TOF analysis of SEA and SEA-MW catalysts categorically shows that they have surpassed the performance of solid-supported catalysts (Pd/CNT-$CuCl_2$ system [30]) for Tsuji-Wacker chemistry in batch by over 100%. In addition to improved catalytic performance in batch, $PdCl_2$-based Pd/GNP catalysts were designed to best operate in electrochemical oxidation conditions. Hence, significantly improving the potential scalability and commercialization of a room-temperature, low-waste, and energy-efficient procedure for conversion of heavily electron-deficient terminal olefins into ketone reagents.

The significance of the research results extends beyond that of performance improvement as a statistically-derived catalyst design space to ensure the satisfaction of industrial catalytic activity criteria, rapid conversion of starting material while exceeding the minimum acceptable selectivity towards the desired product, is presented and the design space's ability to predict the performance of potential catalysts is demonstrated.

It is noteworthy that the catalysts prepared using $TAPdCl_2$, despite successful Pd uptake and particle formation (Figure 4.3), had negligible catalytic activities due to noticeably different Pd properties compared to $PdCl_2$-based catalysts (Section S.1. in supplementary information). In order to maintain the focus of this study, further optimization on those catalysts for a sustainable performance will be presented in future presentations.

4.3.1.Pd Uptake methods and binding GNP

Palladium (Pd)-loaded graphene nano-platelets (GNPs) were formed via three separate methods that resulted in varying Pd loading, the amount of Pd(II) species, and metal-substrate adhesion (Table 4.1.). Of the three catalysts loading methods, the chemical reduction (CHEM) method showed the highest uptake of Pd, confirmed via ICP-OES. However, the CHEM method was observed as a mild reduction process and resulted in a large amount of the nucleated particles being physically adsorbed to the surface, with limited favorable binding to the support.[82] The IWI and SEA methods yielded a stronger anchoring effect of particles to the GNP compared to the CHEM method, despite a lower recorded Pd uptake. The formation of the Pd particles and their uptake on the graphene support was confirmed by transmission electron microscopy. An analysis on the TEM images showed the average particle sizes of 8.67 ± 2.19, 17.44 ± 9.82, and 26.21 ± 18.89 nm for SEA, IWI, and CHEM catalysts, respectively (Figure 4.3.). The SEA catalyst with the smallest particles can provide the reagents with a higher accessible catalyst surface, potentially leading to superior catalytic activities.

Table 4.1. Structural properties of the prepared catalysts

Entry	Catalyst	Preparation Method	Pd Uptake (wt%)	Pd(II) Content(%)
1	Pd-Carbon	Commercial	9.93 ± 0.12	42.5 ± 11.2
2	SEA	SEA	3.20 ± 0.42	70.6 ± 12.3
3	SEA-MW	SEA-Microwave	3.63 ± 0.18	57.1 ± 8.4

4	CHEM	Chemical Reduction	4.87 ± 0.06	68.8 ± 5.2
5	CHEM-MW	Chemical Reduction-Microwave	4.31 ± 0.17	68.8 ± 16.7
6	IWI	Incipient Wetness Impregnation	2.19 ± 0.07	65.3 ± 12.3
7	IWI-MW	Incipient Wetness Impregnation-Microwave	2.30 ± 0.19	73.7 ± 7.5

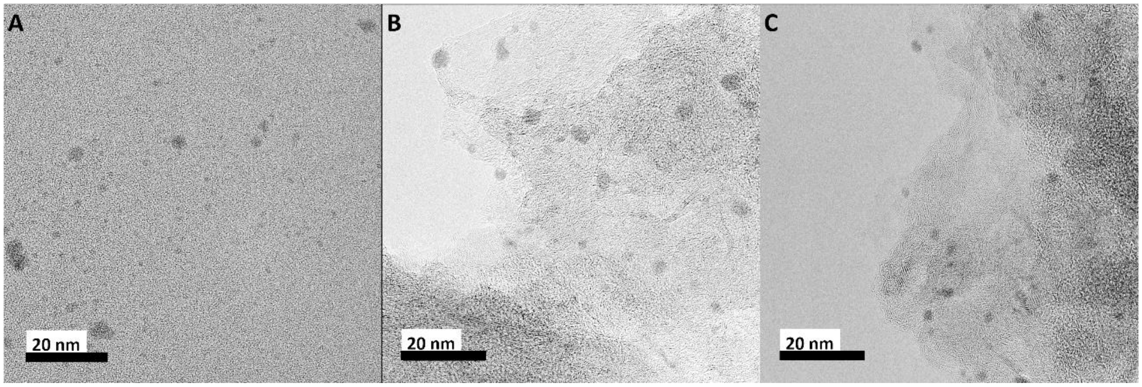

Figure 4.3. HR-TEM images of A) SEA-MW, B) IWI-MW, and C) CHEM-MW catalysts

An investigation on the effect of microwave treatment on the amount of Pd uptake (wt%) as well as Pd(II) % was found to be limited. However, this treatment was found to be crucial to obtain any catalytic activity regardless of reaction framework (Table 3.2.), as the interaction between the catalyst particles and the support were drastically improved after microwaving. The microwave-induced formation of Pd particle-bearing physical defects into the GNP support structures leads to establishing an interface between the catalyst and support, further promoting a faster charge transfer. This phenomenon is a necessity for a rapid catalyst regeneration through redox processes.[45, 82]

The X-ray diffraction analysis was done using an X'pert Pro PANanalytical XRD diffractometer (Cu Kα, λ=1.54 Å, scanned from 5° to 85°). The change in the crystalline structure of loaded palladium particles compared to their precursor was studied for each synthesis method.

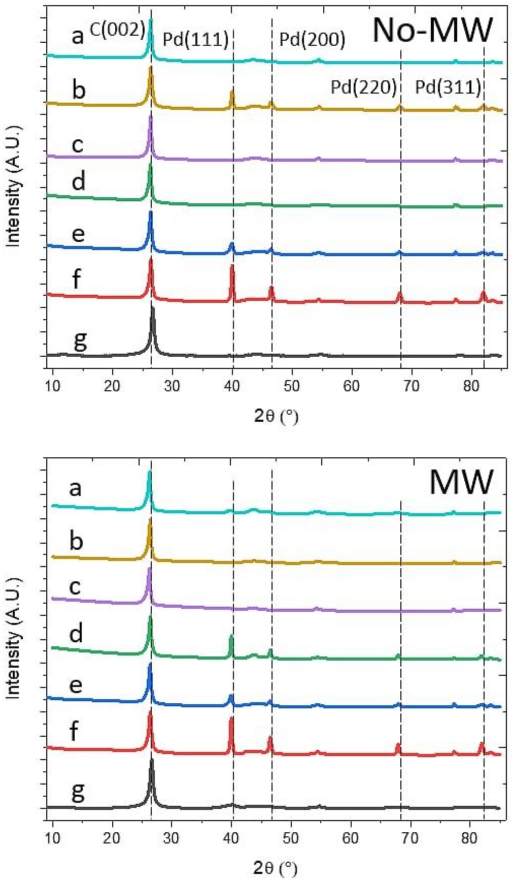

Figure 4.4. XRD spectra of No-MW (top) and MW treated (bottom) a) TAPdCl2-SEA, b) PdCl2-SEA, c) TAPdCl2-IWI, d) PdCl2-IWI, e) TAPdCl2-Chem, f) TAPdCl2-Chem, and g) Pd-Carbon (commercial)

While comparing the Pd precursors, $TAPdCl_2$ (Figure 4.4-a, c, and e) generally results in the formation of (220) and (311) crystallite structures (68° and 83° 2θ, respectively), the $PdCl_2$ (Figure 4.4- b, d, and f) leads to a dominant peak at 40° indicating the (111) plane. This noticeable change can then affect the catalytic performance of the attributed catalysts during the Wacker oxidation. However, in the commercial catalyst (Figure 4.4-g), there is no clear indication of a dominant crystalline orientation showing that the Pd-carbon does not contain a preferential crystalline orientation.

4.3.2.Investigation on Catalytic Activities

Once the formed Pd/GNP catalysts (Table 4.2., Entries 3-8) were characterized based upon composition, the catalysts were further screened for the effectiveness of traditional batch and electrochemical Wacker-type oxidations. The faster charge transfer between catalyst and support in the prepared solid-supported catalyst systems, coupled with their optimized Pd(II)%, led to significantly higher turnover frequencies (TOFs) compared to the reports in the literature (Table 4.2., Entries 9-13) as well as our control trial of homogeneous $PdCl_2$ in batch oxidation (Table 4.2., Entry 1). This observation not only showed that lower amounts of catalytic Pd were used, but also that these catalysts led to over 3 times higher selectivity towards the desired ketone product (Table 4.2.). Specifically, the SEA-MW catalyst (Table 4.2. Entry 4), with the most robust catalyst-support binding, showed the highest activity among the prepared catalysts.

In this study the amount of catalyst used in the electrochemically driven reactions was lowered by 80% compared to the batch-type experiments (Table 4.2. Entries 1-8); conversion and selectivity of the Wacker-type oxidation were also improved by at least 20% for each of the prepared catalysts (Table 4.2. Entries 3-8). The enhancement of the electrochemical configuration arose from a faster Pd(II) regeneration in solid-supported Pd/GNP catalysts.

A comparison between the activities of prepared catalysts mentioned in Table 4.2. Entries 3-8 revealed a clear superiority of the electrochemical approach over batch by efficiently converting the 1-octene substrate to 2-octanone product. Specifically, over 500% increase in turnover number (TON) and turnover frequency (TOF) values were reported simply by this reaction setup transfer. A comparative analysis among the prepared catalysts (Table 4.2. Entries 3-8) and previous reports (Table 4.2. Entries 9-13) depicted an overall 400% improvement in TOF of batch reactions. It is worthy to note that most of the reports (Table 4.2. Entries 9-12) utilize unrecyclable homogeneous catalysts at approximately one order of magnitude smaller reaction scales.[30, 105]

Table 4.2. Batch and electrochemical catalytic performance of the prepared and commercial catalysts

Entry	Reagent	Catalyst	Batch (**5 mol% Pd**, 1.8 mol equiv H_2O_2 oxidant)				Electrochemical (**1 mol% Pd**, 0.28 mol equiv TEMPO mediator)			
			Conversion (RPA%)	Selectivity (%)	TON/TOF (hr^{-1})	Metal Leached (wt%)	Conversion (RPA%)	Selectivity (%)	TON/TOF (hr^{-1})	Metal leached (wt%)
1	1-octene	$PdCl_2$	98.87 ± 0.97	24 ± 11.19	4.75/0.79	-	74.13 ± 3.27	44.91 ± 12.83	56.8/9.5	100
2	1-octene	Pd-Carbon	85.57 ± 8.83	20.36 ± 26.87	3.42/0.57	13.16 ± 3.52	17.21 ± 6.33	21.51 ± 9.18	2.3/0.4	17.86 ± 4.13
3	1-octene	SEA	67.24 ± 1.63	76.41 ± 2.85	10.3/1.7	3.28 ± 1.06	98.33 ± 0.25	84.62 ± 9.47	83.21/13.86	5.33 ± 2.25
4	1-octene	SEA-MW	74.5 ± 5.31	83.52 ± 4.66	12.45/2.07	2.91 ± 1.27	98.43 ± 0.73	98.49 ± 1.16	96.9/16.2	3.67 ± 1.23
5	1-octene	CHEM	0	0	0	14.64 ± 6.21	0	0	0	14.88 ± 3.19
6	1-octene	CHEM-MW	87.82 ± 4.18	100	17.56/2.93	11.43 ± 2.83	76.22 ± 6.87	86.19 ± 12.33	65.7/11	12.59 ± 3.88
7	1-octene	IWI	77.91 ± 6.18	93.1 ± 1.45	14.51/2.42	9.79 ± 3.33	100	81.23 ± 4.31	81.23/13.54	10.22 ± 3.86
8	1-octene	IWI-MW	91.84 ± 2.88	100	18.37/3.06	7.16 ± 4.22	91.26 ± 4.49	84.4 ± 10.56	77/12.8	8.26 ± 4.91
9	Cycloalkenes [106]	$Pd(OAc)_2$	-	-	-	-	100	59-85	17/0.9	100
10	Heterocyclic amines [107]	$Cu(OAc)_2$	-	-	-	-	100	61-80	2.7/0.11	100

11	cinnamyl alcohol [105]	$FeCl_2$	100	92	9.2/3.7	100	-	-	-	
12	Terminal olefins [84]	$Pd(OAc)_2$	-	-	-	-	100	82	8.2/0.51	100
13	Styrene[30]	Pd/CNT-$CuCl_2$	100	93	16.6/0.7	<1%	-	-	-	-

4.3.3.Pd Leaching Study

The leaching study in both batch and electrochemical frameworks showed about 40% lower leaching from IWI (Entries 7 and 8) compared to CHEM (Entries 5 and 6) catalysts. Additionally, SEA catalysts (Entries 3 and 4) showed the lowest leaching (less than 4%) due to the strong electrostatic affinity established between catalyst particles and the support. Nonetheless, the amounts of leached Pd in all the prepared (Pd/GNP) catalysts (Entries 3-8) were lower than the commercial Pd-carbon catalyst (Entry 2) depicting the superior anchoring of the Pd particles on the support via developed methods.

4.3.4.ECSA Analysis

While the advantage of electrochemical over conventional batch oxidation approaches, as well as the proposed design space for such catalysts over conventional homogeneous and commercially available counterparts have been established, the identification of the most suitable solid-supported catalyst preparation method, specifically for the electrochemical application, required further analysis. Cyclic voltammetry of the catalysts (Figure 4.5.) led to respective electrochemical surface area calculations (Figure 4.6).

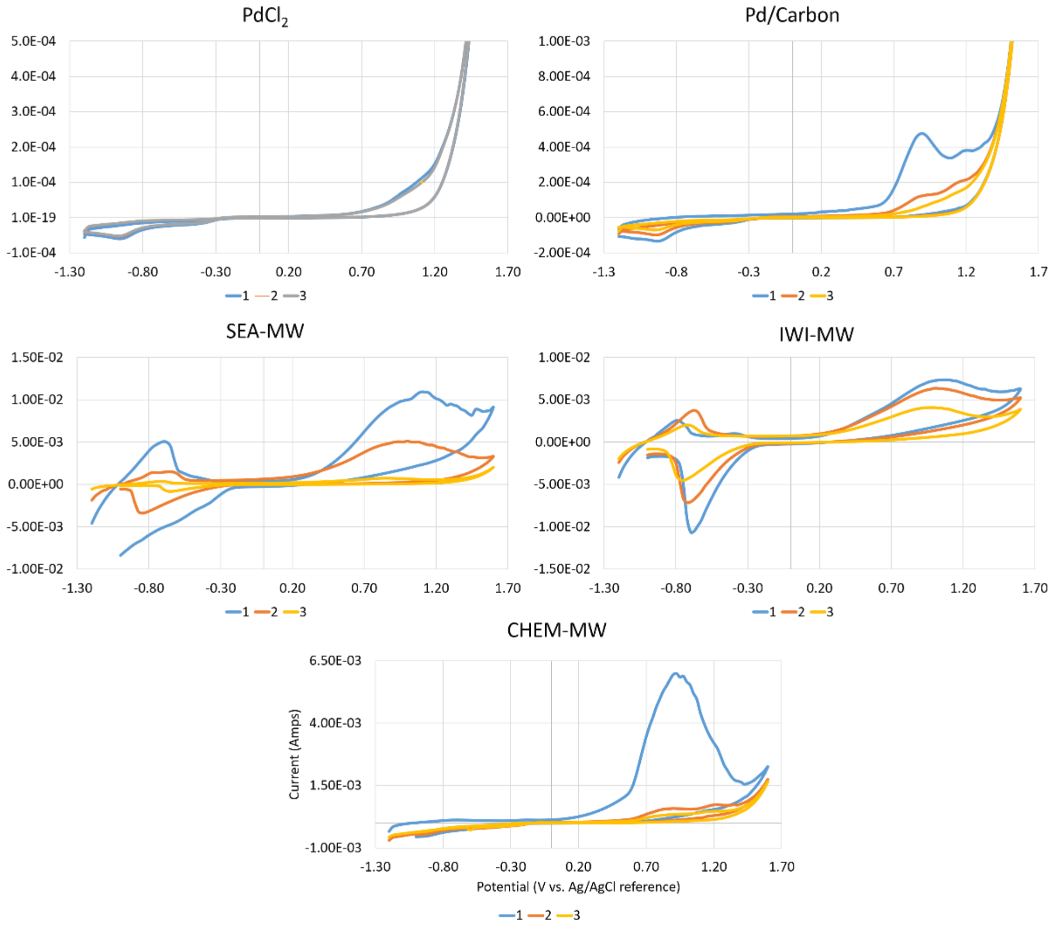

Figure 4.5. Cyclic voltammetry spectra of catalysts utilized for ECSA calculation

The ECSA analysis measures a normalized oxidation capability of each catalyst. Additionally, the deactivation of catalysts was observed through the decay in the ECSA measurement over multiple cycles. There are various reasons for catalyst deactivation. The interactions between the highly conducting GNP support and Pd particles were formed in the prepared catalysts leading to three orders of magnitude higher ECSA than both the commercial Pd-carbon and the homogeneous $PdCl_2$ catalysts. Particle anchoring in those catalysts was more effective as the Pd leaching was 50% lower than the commercial Pd-carbon catalyst throughout all the tested reaction frameworks.

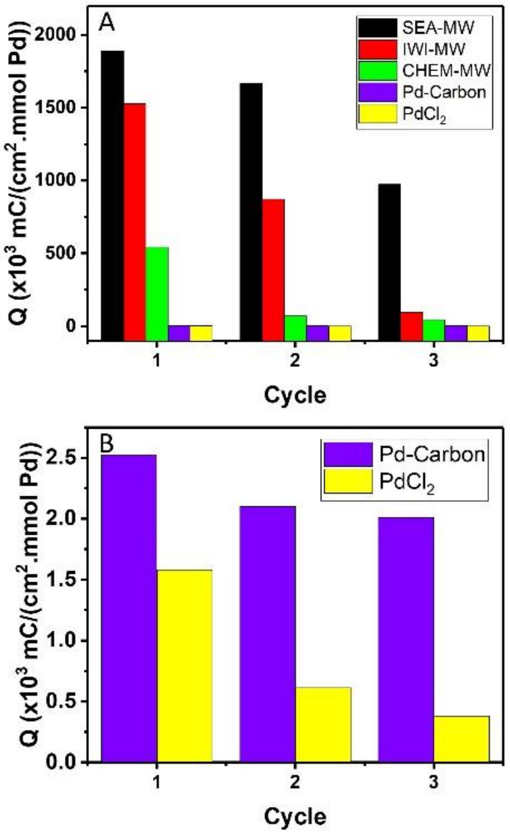

Figure 4.6. Specific ECSA of A) prepared catalysts and B) commercial and homogeneous catalysts

In an overall look, it is evident that the prepared catalysts except for the CHEM trial, prior to microwave treatment, were catalytically more active compared to the homogeneous and heterogeneous positive controls both in batch and electrochemical settings. The effect of microwave treatment showed an overall positive influence in catalytic activity and reaction selectivity induced by the catalysts.

While comparing the prepared catalysts in the batch setting, the SEA catalysts showed slightly lower activity compared to IWI and CHEM working catalysts. The possible reason for this observation could be the higher Pd leaching in the latter trials, promoting a potential secondary homogeneous catalysis. Nonetheless, SEA-MW catalyst with optimized Pd particle immobilization showed the highest catalytic activity with the least Pd leaching in electrochemical activity, projecting the discovery of high-performance, true solid-supported catalysts for fluidized electrochemical organic synthesis. Therefore, the design space for rational preparation of these catalysts, presented in the discussion section, can pave the way for further studies on catalysts for more complex reactions in fluidized electrochemistry configuration.

4.4. Discussion

4.4.1. Analysis of 2-dimensional Pd/GNP catalyst preparation and design space generation for Wacker-type oxidations

Due to the nature of the chemical reduction process (CHEM), which utilizes a weak reducing agent (vitamin C), there is limited control over nucleation, growth, and adsorption of Pd particles on the surface of the GNPs.[108] The procedural design of IWI and SEA catalysts (e.g., accurate pore volume measurement, and pH adjustment to PZC of the support, respectively) ensure the physical wetting of the surface support by the Pd solution, then promoting the electrostatic adsorption of the Pd ions on the support.[109]

As previously reported, [45, 76] microwave treatment induces abrupt vibrations of the Pd particles, sintering them through the support and embedding the metal clusters within the graphene structure. According to electromagnetic relative permittivity ($\mathcal{E}\mathrm{r}$) equation of elements (Equation 7), the real ($\mathcal{E}_{\mathrm{r}}'$) and arbitrary ($\mathcal{E}_{\mathrm{r}}''$) components account for the electromagnetic energy transmitted and absorbed through the material, respectively. These values are functions of the wave frequency and unique to each element.[110] This absorbed energy is lost through atomic vibrations. The loss component for Pd and the support (C) for the microwave used are 13.70[111] and 0.0[112], respectively. Thus, during microwave treatment, the Pd particles were embedded within the physical defects of graphene sheets via extreme heating.

$$\mathcal{E}\mathrm{r}(\omega) = \mathcal{E}_{\mathrm{r}}'(\omega) - \mathrm{i}\mathcal{E}_{\mathrm{r}}'' \tag{7}$$

The particle size analysis of the prepared catalysts (Figure 4.3.) depicts that the SEA method was highly controlled and yielded ca. 50% and 72% smaller mean particle sizes compared to IWI and CHEM methods. Nevertheless, the narrower distribution of SEA-prepared particles signified improved consistency of this method both in nucleation and growth of Pd particles. Reducing the catalyst particle size provides reagents with a higher accessible surface area leading to significant increases in reaction conversion and selectivities.[113]

The driving force for reaction activation in the electrochemical setup and catalyst turnover was the electrical charge instead of the traditionally utilized thermal heating. Therefore, potential heat-sensitive reactions can be carried out effectively. Nevertheless, the optimized tri-component interactions among the electrodes, reagents, and catalysts were established by using high conductivity and surface area GNP supports, leading to a faster redox cycle necessary for catalyst regeneration in the electrochemical framework. This phenomenon led to obtaining industrially acceptable conversion and selectivity values at room temperature, with 80% less Pd catalyst used in comparison with batch setups.

A previous report for Wacker-type batch oxidations using solid-supported catalysts (Pd on carbon nanotubes) utilized lower content of Pd than the syntheses reported in this study.[30] However, utilizing low Pd loadings only facilitated conversion when the vessel was pressurized with oxygen at 101 KPa for 24 hrs. In addition to the four times longer reaction time, consequently five times lower TON and TOF, and the associated risks of pressurized pure O_2, the required 5 mol% $CuCl_2$ co-catalyst added to the cost and complexity of the Wacker oxidation. Hence, the catalysts synthesized herein are more efficient and viable, even with lower metal loadings. The significance of the observation on prepared catalyst activities is also shown by comparing to literature where the GNP supported catalysts described in this study significantly exceeded the reaction throughput (both in TON and TOF) compared to batch [30, 105], and electrochemical[84, 106] Wacker-type oxidations (Table 4.2.).

A comparison of the performance between the prepared catalysts and literature for an electrochemical framework showed that all of the prepared catalysts yielded higher reaction selectivity with an order of magnitude lower Pd content.[84] The SEA, CHEM, and IWI catalysts possess meticulously-controlled properties, such as less than 10% particle size distribution, strongly adsorbed to the graphene support leading to improved catalytic performance consistency observed in Wacker oxidation screening. The activity of prepared catalysts was in corroboration with the observed structural features. Mainly a higher catalytic performance was observed when the catalysts constituted increased Pd (II) % and reduced average particle sizes.

A Pd metal leaching investigation via ICP-OES analysis of the analyte post-reaction was carried out, showing that all prepared catalysts incurred at least 14% lower loss of catalyst particles compared to the commercial Pd-carbon catalyst. The microwave treatment embedded the Pd particles within the graphene nanosheets was a significant factor in lowering the amount of Pd leached into the reaction media (Table 4.2.). The electrochemical oxidation for all the prepared catalysts had a decrease in Pd leaching by ca. 10% compared to both literature and the commercial catalyst, attributed to the microwave treatment. The merit of the SEA catalysts over other catalysts was expected based on a higher TOF and lower Pd leaching. A specific ECSA analysis confirmed that the SEA preparation method yielded catalysts with 33, 300, and 10,000 % higher ECSA compared to the IWI, CHEM, and commercial Pd-carbon catalysts, respectively.

The response plots (Figure 4.7-a–d) for the prepared catalysts fit by a least square method correlated the catalytic activity parameters with respect to the catalyst particles' properties (Pd uptake (wt%) and Pd(II) %) in batch and electrochemical setups provided an opportunity to compare the expected results with industrial benchmarks. The validity of the approach for this statistical study was confirmed by eigenvalue analysis (Figure AII.1) depicted as scree plot of variables. As the scree plot showed, only 2 exploratory factors could explain, over 99% of the observed phenomena.

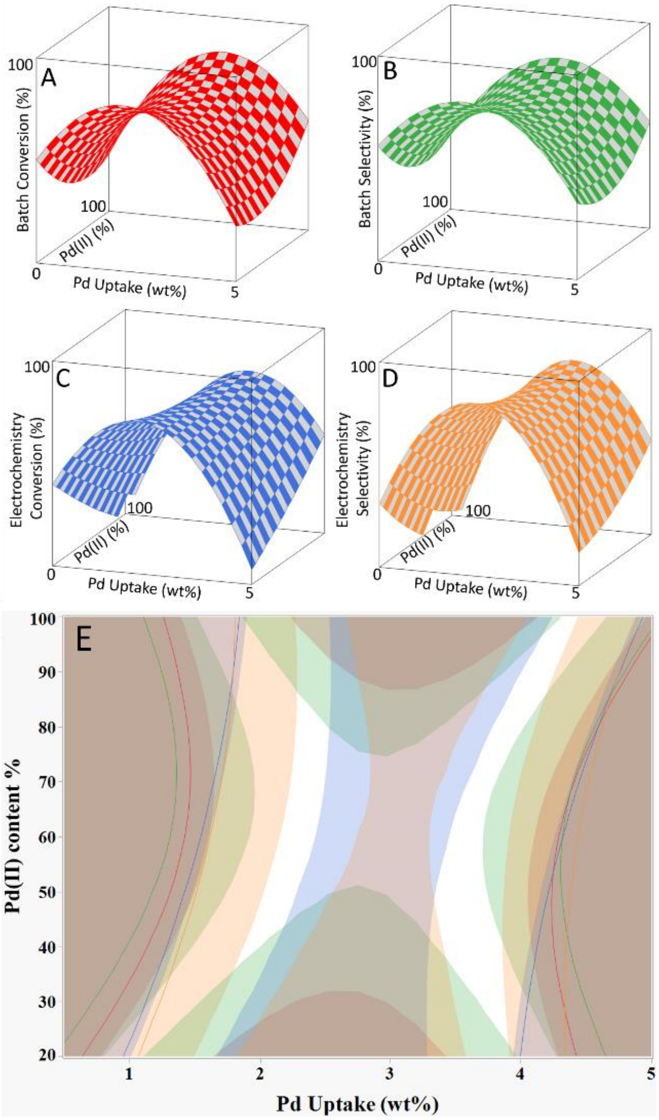

Figure 4.7. Response surface of the least square fit for A) batch conversion, B) batch selectivity, C) electrochemistry conversion, D) electrochemical selectivity, and E) design space for catalyst preparation for Wacker-type oxidation

The overlay plot of response surfaces while constrained with the industrial benchmark for the oxidation of terminal olefins revealed the design space of Pd catalyst preparation for such reactions (depicted in white, Figure 4.7-e). This design space depicts of two acceptable regionsat both low and high Pd uptake sections. In order to study the efficacy of the design space a desirability analysis was conducted. The desirability analysis of various points within these regions (Table 4.3, Figure AII.2) revealed the most desirable conditions within the design space with the maximum theoretical desirability value as 86.23% according to the JMP software.

Table 4.3. The predicted activities and the related desirability of control-points

Point	Pd Uptake (wt%)	Pd (II) Content (%)	Batch Conversion (%)	Batch Selectivity (%)	Electrochemical Conversion (%)	Electrochemical Selectivity (%)	Desirability (%)
A	2.48	73.0	84.59	95.49	99.08	90.48	84.71
B	4.28	94.9	84.75	91.36	92.08	84.10	81.38
C	3.69	44.5	71.64	84.88	83.26	88.44	76.56
D	3.63	58.0	73.21	82.83	92.46	91.63	78.81

The desirability analysis of control-points shows that the highest desirability (depicted as activity) was achieved in point A, with less than 2% deviation from maximum desirability. The reduction in desirability for points in the high-Pd uptake (wt%) (Points C and D) signifies the importance of Pd(II) content over the total amount of Pd present. Hence, we have provided experimental evidence with statistical proof that with meticulous control of the Pd particle ionic properties during their synthesis, the most active catalysts can be achieved with uptakes as low as 2.3 wt%.

4.4.2.Electrochemical analysis and proof of concept reaction screening of Pd-GC monolithic electrodes

The open circuit potential (OCP) graph of the Pd-GC-4 monolithic electrode (Figure 4.8-a) shows a stable current passage indicating that the contact between the monolith and attached wire is successfully made with minimal fluctuation over time. The CV analysis of the prepared monolithic electrode (Figure 4.8-b) depicted a noticeable Pd redox set of peaks where the oxidation peak was located at 0.68 and reduction at 0.43 V vs. Ag/AgCl reference electrode. [114] The asymmetric redox process is proportional to the ionic species present in the Pd particles (Pd(0) and

Pd(II)) where over multiple cycles, the Pd(0) species are oxidized which then improves the oxidative abilities of the monolithic electrode. This phenomenon is evident as from cycle 1 to 3 there was an approximately 10% increase in power consumption and generation in Pd oxidation and reduction steps, respectively. These ratios were obtained via integration of area under the redox peaks.

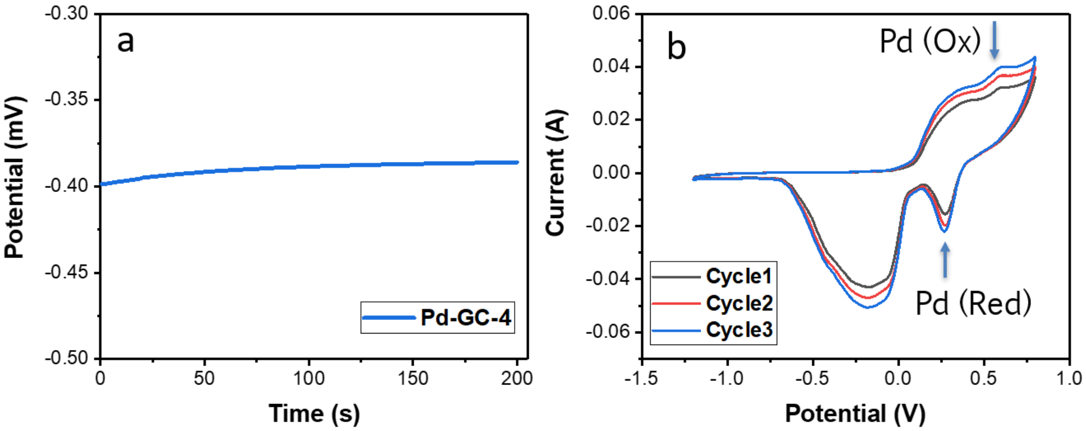

Figure 4.8. A) OCP graph and C) CV diagram of Pd-GC-4 monolithic electrodes

The proof of concept Wacker reaction conducted using the Pd-GC-4 monolithic electrode (Figure 4.9.) yielded 36.19 % conversion and 82.44% selectivity towards the 2-octanone product. The byproducts were mainly 2- and 3-octene, which are the results of isomerization of the starting material. It is noteworthy that only 1 of 11 electrodes prepared was able to complete the reaction time. Hence, further emphasizing the design and preparation details require to consider for such electrodes.

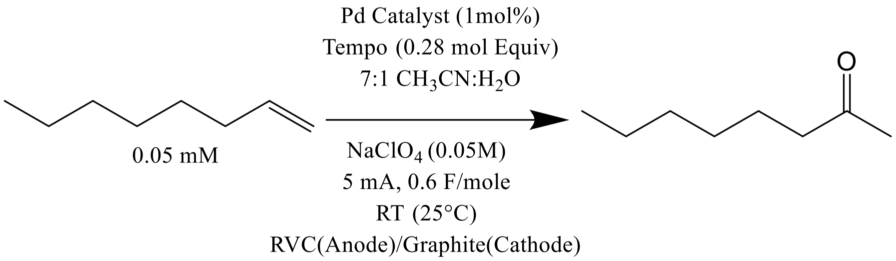

Figure 4.9. The Proof of concept Wacker-electrooxidation of 1-octene using Pd-Glassy carbon monolithic electrode.

4.5. Insights and Findings

Graphene nanoplatelets–supported palladium catalysts (Pd/GNP) with enhanced structural properties were prepared via three different methods, among which the optimal catalyst with significantly higher throughput in Tsuji-Wacker oxidations of electron-deficient substrates was discovered. Of the various preparation methods, the strong electrostatic adsorption (SEA) method provided added control over catalyst synthesis conditions when compared with the conventional chemical reduction (CHEM) and incipient wetness impregnation (IWI) methods. Furthermore, SEA, in combination with microwave treatment, led to improved Pd particles embedding within graphene structures as well as narrower particle size distributions. Microwave treatment aided in Pd particle-substrate bonding for all catalysts and preparation methods. Two Tsuji-Wacker oxidation reaction configurations were developed, a conventional batch and an electrochemical configuration, to evaluate the efficiency and selectivity of the prepared catalysts as well as an enhancement of traditional chemistries enabled via electrochemistry. The prepared catalysts yielded faster and more efficient Tsuji-Wacker oxidations in both configurations. In addition, it was confirmed that the Pd (II) content was found to directly correlate to catalyst performance, whereas the overall Pd content (wt%) did not directly relate to high throughput. Furthermore, the turnover numbers (TONs) and frequencies (TOFs), as reaction throughput indicators, reported superior conversion for the electrochemical oxidation process over the conventional batch process. The highest TON values were achieved using SEA-MW catalyst at 12.45 and 96.9 for batch, and electrochemical oxidation, respectively. The electrochemical configuration allowed for an electrochemical surface area (ECSA) analysis, which justified the high activity of the SEA catalysts. The ECSA for the SEA catalysts was higher than the other prepared-catalysts, and the homogeneous catalyst by 2 and 4 orders of magnitude, respectively. The average throughput of the electrochemical trials was at least 350% higher than the batch reactions (using the same catalysts), significantly surpassing the turnover characteristics of homogeneous, as well as commercial Pd-carbon trials by 25%, and 220%, respectively. Nonetheless, the SEA-MW catalyst surpassed electrochemical solid-supported catalyzed (Pd/CNT) reports in the literature by 100%. A least-square fitting method was utilized to correlate the catalysts to industrially relevant design space and show that by satisfying the minimum Pd(II) content of 60.5%, only a 2.3 wt% Pd loading on GNP support was required to obtain excellent structural properties for both batch and electrochemical frameworks.

Through chapter 4, the need for elimination of TEMPO mediator via deposition of Pd particles on a highly conducting monolithic structure as the route for further process intensification was identified. A protocol for the preparation of glassy carbon monoliths decorated with Pd particles as the desired structure for catalytic electrodes was developed. The rational optimization of the manufacturing protocol as well as Pd particle deposition (including microwave-assisted immobilization) was achieved. Further analyses determined the optimized conditions for annealing the monoliths (including atmosphere composition and temperature) were identified through a screening DOE. As a proof of concept, the catalytic activity of the monolithic Pd-GC electrodes as the replacement for conventional graphite electrodes used for electrochemical oxidation of 1-

octene was demonstrated. Further manufacturing and reaction condition optimizations can potentially lead to higher reaction efficacy using the prepared electrodes.

5. Conclusions and Future Work

This multi-disciplinary systematic research on solid-supported palladium catalysts focuses on three major aspects related to this family of catalysts. Firstly, fundamental analysis on the properties of the supports (all carbon-based) as well as catalyst synthesis parameters and their effects on catalyst properties, including catalytic activity and metallic particle leaching, was pursued. Secondly, the application-driven comparison between the optimally prepared catalyst and the homogeneous as well as commercially available solid-supported Pd catalysts, as positive controls, were investigated. During this objective, the superiority of prepared catalysts in maximizing the catalytic activity and minimizing the Pd particle leaching was pursued. Lastly, the improvement upon conventional 2D solid-supported catalysts was made through the preparation of 3D macroscopic monolithic structures as supports for Pd particles. During this process, the advantage of monolithic catalysts over conventional 2D solid-supported catalyst packed beds for Suzuki cross-coupling of aryl halides and boronic acids in flow was analyzed via a preparation method developed by the author utilizing techniques from chemistry, ceramics engineering, and process chemistry. It was shown that Pd-graphene oxide (GO) monolithic catalyst packed beds had 300% higher catalytic longevity, with over 60% reduction in Pd leaching into the reaction stream. In order to comprehensively analyze the interior structure of the monolithic catalysts, a creative approach was taken during that analysis the microCT-Scan was utilized to study the effect of reaction mixture precipitation into the porous monolith structure as well as the desirable distribution of Pd particles within the structure was successfully studied.

The secondary reaction setting chosen as the engineering challenge was electrochemical Wacker oxidation of terminal olefins. In order to assist revitalizing this synthetic approach for commercialization purposes, Pd on graphene nanoplatelets (Pd-GNP) catalysts were prepared via 3 different methods, and their efficacy in catalyzing fluidized electrochemical oxidation of electron-deficient olefins towards ketone products was pursued. The superiority of catalyst prepared via strong electrostatic adsorption (SEA) method in this application with respect to catalytic activity and minimized Pd particle leaching over positive controls, reports in the literature, and the other two prepared catalysts signified the advantage of this method over the others as it yields smaller particles with stronger binding to the support. In order to provide a catalyst synthesis roadmap, a design space based on least square fitting of conversion and selectivity of catalysts in batch and electrochemistry was prepared. The dependent variables were the Pd uptake and Pd (II) species content. The acceptable criteria for this design space were selected based on the industrial benchmark for the electrochemical Wacker-type reaction that was used. Lastly, a monolithic catalyst-oriented approach was taken to prepare catalytic monoliths as anodes used for electrochemical Wacker oxidation of 1-octene as the model olefin substrate. The optimized synthesis process included the deposition of Pd particles on glassy carbon monoliths, which then showed reliable electrical stability and catalyst redox activity tested via open circuit potential and cyclic voltammetry analyses. The proof of concept reaction screening using the Pd-GC monolithic electrodes yielded 36% conversion of starting material with over 80% selectivity towards the interested ketone product.

The main takeaway of this work is that a monolithic catalyst is a viable option for process intensification in unconventional synthetic processes such as synthesis in flow and in electrochemical frameworks. Since these methodologies have strong potential for process intensification in industrial scales, the future work is suggested as follows.

The preparation scope of such monolithic metal-GO catalysts can be expanded through the utilization of other 2D support structures such as boron nitride, which have been proven to be useful for various reactions. Nonetheless, utilization of other metal particles as catalytic species such as platinum and ruthenium for hydrogenation and other cross-coupling reactions could be explored.

In case of electrochemical reaction, the 2D catalyst preparation design space can be expanded to other reactions. Specifically, the utilization of such an approach for bimetallic catalysts for both organic and energy electrochemistry can be significantly interesting for industrial applications. Further optimization of the Pd-GC monolithic electrode is required to make sure they are desired for the reaction of interest. The parameters to focus on are the electrode preparation process as well as metallic particle properties (e.g. ionic species content). The latter parameter can be predicted using a design space, in which its generation process was detailed in the previous section.

6. References

1. Cooper, M. M.; Stowe, R. L.; Crandell, O. M.; Klymkowsky, M. W., Organic Chemistry, Life, the Universe and Everything (OCLUE): A Transformed Organic Chemistry Curriculum. *Journal of Chemical Education* **2019,** *96* (9), 1858-1872.
2. Llanos, E. J.; Leal, W.; Luu, D. H.; Jost, J.; Stadler, P. F.; Restrepo, G., Exploration of the chemical space and its three historical regimes. *Proceedings of the National Academy of Sciences* **2019,** *116* (26), 12660.
3. Wisniak, J., The History of Catalysis. From the Beginning to Nobel Prizes. *Educación Química* **2010,** *21* (1), 60-69.
4. Jagtap, R. A.; Punji, B., C–H Functionalization of Indoles by 3d Transition-Metal Catalysis. *Asian Journal of Organic Chemistry* **2020,** *9* (3), 326-342.
5. Cao, Z.-z., Metal-Free-Catalyzed Synthesis of Allyl Nitriles via $\mathrm{C_{sp2}}$–$\mathrm{C_{sp3}}$ Coupling between Olefins and Azobis (Alkyl-carbonitrile). *Journal of organic chemistry* **2020,** *v. 85* (no. 5), pp. 3287-3296-2020 v.85 no.5.
6. Livingston, A.; Trout, B. L.; Horvath, I. T.; Johnson, M. D.; Vaccaro, L.; Coronas, J.; Babbitt, C. W.; Zhang, X.; Pradeep, T.; Drioli, E.; Hayler, J. D.; Tam, K. C.; Kappe, C. O.; Fane, A. G.; Szekely, G., Chapter 1 - Challenges and Directions for Green Chemical Engineering—Role of Nanoscale Materials. In *Sustainable Nanoscale Engineering*, Szekely, G.; Livingston, A., Eds. Elsevier: 2020; pp 1-18.
7. Zou, F.; Yao, F.; Liu, L.; Cai, M., Recyclable heterogeneous palladium-catalyzed carbon–carbon coupling polycondensations toward highly purified conjugated polymers. *Journal of Polymer Research* **2019,** *27* (1), 1.
8. Administration, U. F. a. D., Q3D elemental impurities guidance for industry. 2015.
9. Shende, V. S.; Saptal, V. B.; Bhanage, B. M., Recent Advances Utilized in the Recycling of Homogeneous Catalysis. *The Chemical Record* **2019,** *19* (9), 2022-2043.
10. Alonso, D. A.; Baeza, A.; Chinchilla, R.; Gómez, C.; Guillena, G.; Pastor, I. M.; Ramón, D. J., Solid-Supported Palladium Catalysts in Sonogashira Reactions: Recent Developments. *Catalysts* **2018,** *8* (5), 202.
11. Lanari, D.; Piermatti, O.; Morozzi, C.; Santoro, S.; Vaccaro, L., Recent Applications of Solid-Supported Ammonium Fluorides in Organic Synthesis. *Synthesis* **2017,** *49* (05), 973-980.
12. Larionov, V. A.; Cruchter, T.; Mietke, T.; Meggers, E., Polymer-Supported Chiral-at-Metal Lewis Acid Catalysts. *Organometallics* **2017,** *36* (8), 1457-1460.
13. Julkapli, N. M.; Bagheri, S., Graphene supported heterogeneous catalysts: An overview. *International Journal of Hydrogen Energy* **2015,** *40* (2), 948-979.
14. Liang, H.; Chen, G.; Desinan, S.; Rosei, R.; Rosei, F.; Ma, D., In situ facile synthesis of ruthenium nanocluster catalyst supported on carbon black for hydrogen generation from the hydrolysis of ammonia-borane. *International Journal of Hydrogen Energy* **2012,** *37* (23), 17921-17927.
15. Xiao, L.-P.; Wang, S.; Li, H.; Li, Z.; Shi, Z.-J.; Xiao, L.; Sun, R.-C.; Fang, Y.; Song, G., Catalytic Hydrogenolysis of Lignins into Phenolic Compounds over Carbon Nanotube Supported Molybdenum Oxide. *ACS Catalysis* **2017,** *7* (11), 7535-7542.
16. Rodríguez-Escrich, C.; Pericàs, M. A., Catalytic Enantioselective Flow Processes with Solid-Supported Chiral Catalysts. *The Chemical Record* **2019,** *19* (9), 1872-1890.
17. Amara, Z.; Poliakoff, M.; Duque, R.; Geier, D.; Franciò, G.; Gordon, C. M.; Meadows, R. E.; Woodward, R.; Leitner, W., Enabling the Scale-Up of a Key Asymmetric Hydrogenation Step in the Synthesis of an API Using Continuous Flow Solid-Supported Catalysis. *Organic Process Research & Development* **2016,** *20* (7), 1321-1327.
18. Gupton, B. F.; McQuade, D. T., A Holistic Approach to Streamlining Pharmaceutical Processes: A Conversation. *Organic Process Research & Development* **2019,** *23* (5), 711-715.

19. Tosso, N. P.; Desai, B. K.; De Oliveira, E.; Wen, J.; Tomlin, J.; Gupton, B. F., A Consolidated and Continuous Synthesis of Ciprofloxacin from a Vinylogous Cyclopropyl Amide. *The Journal of Organic Chemistry* **2019,** *84* (6), 3370-3376.

20. Kong, C. J.; Fisher, D.; Desai, B. K.; Yang, Y.; Ahmad, S.; Belecki, K.; Gupton, B. F., High throughput photo-oxidations in a packed bed reactor system. *Bioorganic & Medicinal Chemistry* **2017,** *25* (23), 6203-6208.

21. Elazab, H. A.; Siamaki, A. R.; Gupton, B. F.; El-Shall, M. S., Pd-Fe3O4/RGO: a Highly Active and Magnetically Recyclable Catalyst for Suzuki Cross Coupling Reaction using a Microfluidic Flow Reactor. *Bulletin of Chemical Reaction Engineering & Catalysis* **2019,** *14* (3), 478-489.

22. Naber, J. R.; Buchwald, S. L., Packed-Bed Reactors for Continuous-Flow C⍰N Cross-Coupling. *Angewandte Chemie International Edition* **2010,** *49* (49), 9469-9474.

23. Punniyamurthy, T.; Velusamy, S.; Iqbal, J., Recent Advances in Transition Metal Catalyzed Oxidation of Organic Substrates with Molecular Oxygen. *Chemical Reviews* **2005,** *105* (6), 2329-2364.

24. Ren, G.; Gao, L.; Teng, C.; Li, Y.; Yang, H.; Shui, J.; Lu, X.; Zhu, Y.; Dai, L., Ancient Chemistry "Pharaoh's Snakes" for Efficient Fe-/N-Doped Carbon Electrocatalysts. *ACS Applied Materials & Interfaces* **2018,** *10* (13), 10778-10785.

25. Sequeira, C. A. C.; Santos, D. M. F., Electrochemical routes for industrial synthesis. *Journal of the Brazilian Chemical Society* **2009,** *20*, 387-406.

26. Chai, D.; Genders, D.; Weinberg, N.; Zappi, G.; Bernasconi, E.; Lee, J.; Roletto, J.; Sogli, L.; Walker, D.; Martin, C. R.; Menon, V.; Zelenay, P.; Zhang, H., Ceftibuten: Development of a Commercial Process Based on Cephalosporin C. Part IV. Pilot-Plant Scale Electrochemical Reduction of 3-Acetoxymethyl-7(R)-glutaroylaminoceph-3-em-4-carboxylic Acid 1(S)-Oxide. *Organic Process Research & Development* **2002,** *6* (2), 178-183.

27. Zeybek, B.; Özçiçek Pekmez, N.; Kılıç, E., Electrochemical synthesis of bilayer coatings of poly(N-methylaniline) and polypyrrole on mild steel and their corrosion protection performances. *Electrochimica Acta* **2011,** *56* (25), 9277-9286.

28. Horn, E. J.; Rosen, B. R.; Baran, P. S., Synthetic Organic Electrochemistry: An Enabling and Innately Sustainable Method. *ACS Central Science* **2016,** *2* (5), 302-308.

29. ElMekawy, A.; Hegab, H. M.; Mohanakrishna, G.; Elbaz, A. F.; Bulut, M.; Pant, D., Technological advances in CO2 conversion electro-biorefinery: A step toward commercialization. *Bioresource Technology* **2016,** *215*, 357-370.

30. Donck, S.; Gravel, E.; Shah, N.; Jawale, D. V.; Doris, E.; Namboothiri, I. N. N., Tsuji–Wacker Oxidation of Terminal Olefins using a Palladium–Carbon Nanotube Nanohybrid. *ChemCatChem* **2015,** *7* (15), 2318-2322.

31. Ghobadi, S.; Roper, T. D.; Gupton, B. F.; Castano, C. E., Optimal Regioselectivity Control in Electrocatalytic Oxidation of Terminal Olefins. **2019**.

32. Zhou, M.; Wu, Z.; Ma, X.; Cong, Y.; Ye, Q.; Wang, D., A novel fluidized electrochemical reactor for organic pollutant abatement. *Separation and Purification Technology* **2004,** *34* (1), 81-88.

33. Zhu, E.; Yan, X.; Wang, S.; Xu, M.; Wang, C.; Liu, H.; Huang, J.; Xue, W.; Cai, J.; Heinz, H.; Li, Y.; Huang, Y., Peptide-Assisted 2-D Assembly toward Free-Floating Ultrathin Platinum Nanoplates as Effective Electrocatalysts. *Nano Letters* **2019,** *19* (6), 3730-3736.

34. Tschöpe, A.; Wyrwoll, M.; Schneider, M.; Mandel, K.; Franzreb, M., A magnetically induced fluidized-bed reactor for intensification of electrochemical reactions. *Chemical Engineering Journal* **2020,** *385*, 123845.

35. Olaya, A. J.; Hidalgo-Acosta, J. C.; Omatsu, T.; Girault, H. H., Photosensitized Hydrogen Evolution on a Floating Electrocatalyst Coupled to Electrochemical Recycling. *Journal of the American Chemical Society* **2018,** *140* (32), 10149-10152.

36. Jerdan, W., *Practical and Experimental Chemistry: adapted to Arts and Manufactures*. H. Colburn [etc.]: London, 1838; p 392-392.

37. Chapter 1 History of catalysis. In *Studies in Surface Science and Catalysis*, Moulijn, J. A.; van Leeuwen, P. W. N. M.; van Santen, R. A., Eds. Elsevier: 1993; Vol. 79, pp 3-21.

38. Greco, R.; Goessler, W.; Cantillo, D.; Kappe, C. O., Benchmarking Immobilized Di- and Triarylphosphine Palladium Catalysts for Continuous-Flow Cross-Coupling Reactions: Efficiency, Durability, and Metal Leaching Studies. *ACS Catalysis* **2015,** *5* (2), 1303-1312.

39. Noël, T.; Naber, J. R.; Hartman, R. L.; McMullen, J. P.; Jensen, K. F.; Buchwald, S. L., Palladium-catalyzed amination reactions in flow: overcoming the challenges of clogging via acoustic irradiation. *Chemical Science* **2011,** *2* (2), 287-290.

40. Wisniak, J., The History of Catalysis: From the Beginning to Nobel Prizes. *Educación química [online]* **2010,** *21* (1), 10.

41. Pritchard, J.; Filonenko, G. A.; van Putten, R.; Hensen, E. J. M.; Pidko, E. A., Heterogeneous and homogeneous catalysis for the hydrogenation of carboxylic acid derivatives: history, advances and future directions. *Chemical Society Reviews* **2015,** *44* (11), 3808-3833.

42. Glasnov, T. N.; Findenig, S.; Kappe, C. O., Heterogeneous Versus Homogeneous Palladium Catalysts for Ligandless Mizoroki–Heck Reactions: A Comparison of Batch/Microwave and Continuous-Flow Processing. *Chemistry – A European Journal* **2009,** *15* (4), 1001-1010.

43. Eaton, R. E. Y., *Synthesis gas conversion with ZSM-5 supported ruthenium catalysts*. Virginia Commonwealth University, Dept. of Chemistry: 1983.

44. Chen, S.; Chen, X.; Zhang, H., Nanoscale size effect of octahedral nickel catalyst towards ammonia decomposition reaction. *International Journal of Hydrogen Energy* **2017,** *42* (27), 17122-17128.

45. Gilliland, S. E.; Tengco, J. M. M.; Yang, Y.; Regalbuto, J. R.; Castano, C. E.; Gupton, B. F., Electrostatic adsorption-microwave synthesis of palladium nanoparticles on graphene for improved cross-coupling activity. *Applied Catalysis A: General* **2018,** *550*, 168-175.

46. Song, X.; Guan, Q.; Cheng, Z.; Li, W., Eco-friendly controllable synthesis of highly dispersed ZIF-8 embedded in porous Al2O3 and its hydrogenation properties after encapsulating Pt nanoparticles. *Applied Catalysis B: Environmental* **2018,** *227*, 13-23.

47. Işıkel Şanlı, L.; Bayram, V.; Ghobadi, S.; Düzen, N.; Alkan Gürsel, S., Engineered catalyst layer design with graphene-carbon black hybrid supports for enhanced platinum utilization in PEM fuel cell. *International Journal of Hydrogen Energy* **2017,** *42* (2), 1085-1092.

48. Şanlı, L. I.; Bayram, V.; Yarar, B.; Ghobadi, S.; Gürsel, S. A., Development of graphene supported platinum nanoparticles for polymer electrolyte membrane fuel cells: Effect of support type and impregnation–reduction methods. *International Journal of Hydrogen Energy* **2016,** *41* (5), 3414-3427.

49. Yang, Y.; Gilliland, S. E.; Ghobadi, S.; Burkholder, M.; Smith, S. E.; Gupton, B. F.; Castano, C. E., Three dimensional composites of graphene as supports in Pd-catalyzed synthetic applications. *Reaction Chemistry & Engineering* **2018**.

50. Ahmed, M. J.; Kadhum, A. A. H., Hydrogenation of d-fructose over activated charcoal supported platinum catalyst. *Journal of the Taiwan Institute of Chemical Engineers* **2011,** *42* (1), 114-119.

51. Palanisamy, S.; Thirumalraj, B.; Chen, S.-M.; Ali, M. A.; Al-Hemaid, F. M. A., Palladium nanoparticles decorated on activated fullerene modified screen printed carbon electrode for enhanced electrochemical sensing of dopamine. *Journal of Colloid And Interface Science* **2015,** *448*, 251-256.

52. Potukuchi, H. K.; Spork, A. P.; Donohoe, T. J., Palladium-catalyzed -arylation of carbonyls in the de novo synthesis of aromatic heterocycles. *Org. Biomol. Chem.* **2015,** *13* (15), 4367-4373.

53. Li, M.; González-Esguevillas, M.; Berritt, S.; Yang, X.; Bellomo, A.; Walsh, P. J., Palladium-Catalyzed C−H Arylation of α,β-Unsaturated Imines: Catalyst-Controlled Synthesis of Enamine and Allylic Amine Derivatives. *Angewandte Chemie International Edition* **2016,** *55* (8), 2825-2829.

54. Graf von der Schulenburg, D. A.; Johns, M. L., Catalyst effectiveness factor distributions in isothermal packed bed reactors. *Chemical Engineering Science* **2011,** *66* (13), 3003-3011.

55. Rahimpour, M. R.; Pourazadi, E.; Iranshahi, D.; Bahmanpour, A. M., Methanol synthesis in a novel axial-flow, spherical packed bed reactor in the presence of catalyst deactivation. *Chemical Engineering Research and Design* **2011,** *89* (11), 2457-2469.

56. He, P.; Haswell, S. J.; Fletcher, P. D. I.; Kelly, S. M.; Mansfield, A., Scaling up of continuous-flow, microwave-assisted, organic reactions by varying the size of Pd-functionalized catalytic monoliths. *Beilstein Journal of Organic Chemistry* **2011,** *7*, 1150-1157.

57. Liguori, F.; Barbaro, P.; Said, B.; Galarneau, A.; Santo, V. D.; Passaglia, E.; Feis, A., Unconventional Pd@Sulfonated Silica Monoliths Catalysts for Selective Partial Hydrogenation Reactions under Continuous Flow. *ChemCatChem* **2017,** *9* (16), 3245-3258.

58. Modak, A.; Bhaumik, A., Surface-exposed Pd nanoparticles supported over nanoporous carbon hollow tubes as an efficient heterogeneous catalyst for the CC bond formation and hydrogenation reactions. *Journal of Molecular Catalysis A: Chemical* **2016,** *425*, 147-156.

59. Cai, S.; Zhang, D.; Shi, L.; Xu, J.; Zhang, L.; Huang, L.; Li, H.; Zhang, J., Porous Ni–Mn oxide nanosheets in situ formed on nickel foam as 3D hierarchical monolith de-NOx catalysts. *Nanoscale* **2014,** *6* (13), 7346-7353.

60. Mukdasai, S.; Crowley, U.; Pravda, M.; He, X.; Nesterenko, E. P.; Nesterenko, P. N.; Paull, B.; Srijaranai, S.; Glennon, J. D.; Moore, E., Electrodeposition of palladium nanoparticles on porous graphitized carbon monolith modified carbon paste electrode for simultaneous enhanced determination of ascorbic acid and uric acid. *Sensors & Actuators: B. Chemical* **2015,** *218* (C), 280-288.

61. Nakhate, A. V.; Yadav, G. D., Palladium Nanoparticles Supported Carbon Based Graphene Oxide Monolith as Catalyst for Sonogashira Coupling and Hydrogenation of Nitrobenzene and Alkenes. *ChemistrySelect* **2016,** *1* (13), 3954-3965.

62. Fam, Y.; Sheppard, T. L.; Diaz, A.; Scherer, T.; Holler, M.; Wang, W.; Wang, D.; Brenner, P.; Wittstock, A.; Grunwaldt, J.-D., Correlative Multiscale 3D Imaging of a Hierarchical Nanoporous Gold Catalyst by Electron, Ion and X-ray Nanotomography. *ChemCatChem* **2018,** *10* (13), 2858-2867.

63. Kreutzer, M. T.; Kapteijn, F.; Moulijn, J. A.; Ebrahimi, S.; Kleerebezem, R.; van Loosdrecht, M. C. M., Monoliths as Biocatalytic Reactors: Smart Gas−Liquid Contacting for Process Intensification. *Industrial & Engineering Chemistry Research* **2005,** *44* (25), 9646-9652.

64. Garcea, S. C.; Wang, Y.; Withers, P. J., X-ray computed tomography of polymer composites. *Composites Science and Technology* **2018,** *156*, 305-319.

65. Li, L., Modeling of fatigue hysteresis behavior in carbon fiber-reinforced ceramic–matrix composites under multiple loading stress levels. *Journal of Composite Materials* **2017,** *51* (7), 971-983.

66. Ghobadi, S.; Sadighikia, S.; Papila, M.; Cebeci, F. A.; Grsel, S. A., Graphene-reinforced poly(vinyl alcohol) electrospun fibers as building blocks for high performance nanocomposites. *RSC Adv.* **2015,** *5* (103), 85009-85018.

67. Picot, O. T.; Rocha, V. G.; Ferraro, C.; Ni, N.; D'Elia, E.; Meille, S.; Chevalier, J.; Saunders, T.; Peijs, T.; Reece, M. J.; Saiz, E., Using graphene networks to build bioinspired self-monitoring ceramics. *Nature Communications* **2017,** *8*, 14425.

68. Quan, B.; Yu, S.-H.; Chung, D. Y.; Jin, A.; Park, J. H.; Sung, Y.-E.; Piao, Y., Single Source Precursor-based Solvothermal Synthesis of Heteroatom-doped Graphene and Its Energy Storage and Conversion Applications. *Scientific Reports* **2014,** *4*, 5639.

69. Ghosh, T.; Chandra, P.; Mohammad, A.; Mobin, S. M., Benign approach for methyl-esterification of oxygenated organic compounds using TBHP as methylating and oxidizing agent. *Applied Catalysis B: Environmental* **2018,** *226*, 278-288.

70. Militello, M. C.; Simko, S. J., Palladium Oxide (PdO) by XPS. *Surface Science Spectra* **1994,** *3* (4), 395-401.

71. Poulston, S.; Hyde, T. I.; Hamilton, H.; Mathon, O.; Prestipino, C.; Sankar, G.; Smith, A. W. J., EXAFS and XRD characterization of palladium sorbents for high temperature mercury capture from fuel gas. *Physical Chemistry Chemical Physics* **2009,** *12* (2), 484-491.

72. Patterson, A. L., The Scherrer Formula for X-Ray Particle Size Determination. *Physical Review* **1939,** *56* (10), 978-982.

73. Cookson, J., The Preparation of Palladium Nanoparticles. *Platinum Metals Review* **2012,** *56* (2), 83-98.

74. Savaram, K.; Li, M.; Tajima, K.; Takai, K.; Hayashi, T.; Hall, G.; Garfunkel, E.; Osipov, V.; He, H., Dry microwave heating enables scalable fabrication of pristine holey graphene nanoplatelets and their catalysis in reductive hydrogen atom transfer reactions. *Carbon* **2018,** *139*, 861-871.

75. Siamaki, A. R.; Khder, A. E. R. S.; Abdelsayed, V.; El-Shall, M. S.; Gupton, B. F., Microwave-assisted synthesis of palladium nanoparticles supported on graphene: A highly active and recyclable catalyst for carbon–carbon cross-coupling reactions. *Journal of Catalysis* **2011,** *279* (1), 1-11.

76. Yang, Y.; Reber, A. C.; Gilliland, S. E.; Castano, C. E.; Gupton, B. F.; Khanna, S. N., More than just a support: Graphene as a solid-state ligand for palladium-catalyzed cross-coupling reactions. *Journal of Catalysis* **2018,** *360*, 20-26.

77. Zhang, Z.; Wang, Z.; He, S.; Wang, C.; Jin, M.; Yin, Y., Redox reaction induced Ostwald ripening for size- and shape-focusing of palladium nanocrystals. *Chemical Science* **2015,** *6* (9), 5197-5203.

78. Arblaster, J. W., Crystallographic Properties of Palladium. *Platinum Metals Review* **2012,** *56* (3), 181-189.

79. Sudhamani, S. R.; Prasad, M. S.; Udaya Sankar, K., DSC and FTIR studies on Gellan and Polyvinyl alcohol (PVA) blend films. *Food Hydrocolloids* **2003,** *17* (3), 245-250.

80. DeLuca, R. J.; Edwards, J. L.; Steffens, L. D.; Michel, B. W.; Qiao, X.; Zhu, C.; Cook, S. P.; Sigman, M. S., Wacker-Type Oxidation of Internal Alkenes using Pd(Quinox) and TBHP. *The Journal of Organic Chemistry* **2013,** *78* (4), 1682-1686.

81. Jira, R., Acetaldehyde from Ethylene—A Retrospective on the Discovery of the Wacker Process. *Angewandte Chemie International Edition* **2009,** *48* (48), 9034-9037.

82. Ghobadi, S.; Burkholder, M. B.; Smith, S. E.; Gupton, B. F.; Castano, C. E., Catalytically sustainable, palladium-decorated graphene oxide monoliths for synthesis in flow. *Chemical Engineering Journal* **2020,** *381*, 122598.

83. Jiang, Y.-Y.; Zhang, Q.; Yu, H.-Z.; Fu, Y., Mechanism of Aldehyde-Selective Wacker-Type Oxidation of Unbiased Alkenes with a Nitrite Co-Catalyst. *ACS Catalysis* **2015,** *5* (3), 1414-1423.

84. Mitsudo, K.; Kaide, T.; Nakamoto, E.; Yoshida, K.; Tanaka, H., Electrochemical Generation of Cationic Pd Catalysts and Application to Pd/TEMPO Double-Mediatory Electrooxidative Wacker-Type Reactions. *Journal of the American Chemical Society* **2007,** *129* (8), 2246-2247.

85. Jiang, X.-F.; Li, R.; Hu, M.; Hu, Z.; Golberg, D.; Bando, Y.; Wang, X.-B., Zinc-Tiered Synthesis of 3D Graphene for Monolithic Electrodes. *Advanced Materials* **2019,** *31* (25), 1901186.

86. Witold Sarna, J. K., Jarosław Przybylski, Krystyna Sylwestrzak, RVC — reticulated vitreous carbon. Structure, precursor polymer materials, process of manufacturing and applications. *Inżynieria Materiałowa* **2016,** *2* (210), 15.

87. Perini, L.; Durante, C.; Favaro, M.; Agnoli, S.; Granozzi, G.; Gennaro, A., Electrocatalysis at palladium nanoparticles: Effect of the support nitrogen doping on the catalytic activation of carbonhalogen bond. *Applied Catalysis B: Environmental* **2014,** *144*, 300-307.

88. Elazab, H. A.; Sadek, M. A.; El-Idreesy, T. T., Microwave-assisted synthesis of palladium nanoparticles supported on copper oxide in aqueous medium as an efficient catalyst for Suzuki cross-coupling reaction. *Adsorption Science & Technology* **2018,** *36* (5-6), 1352-1365.

89. Ulusal, F.; Darendeli, B.; Erünal, E.; Egitmen, A.; Guzel, B., Supercritical carbondioxide deposition of γ-Alumina supported Pd nanocatalysts with new precursors and using on Suzuki-Miyaura coupling reactions. *The Journal of Supercritical Fluids* **2017,** *127*, 111-120.

90. Lee, C. K. Y.; Holmes, A. B.; Ley, S. V.; McConvey, I. F.; Al-Duri, B.; Leeke, G. A.; Santos, R. C. D.; Seville, J. P. K., Efficient batch and continuous flow Suzuki cross-coupling reactions under mild conditions, catalysed by polyurea-encapsulated palladium (ii) acetate and tetra-n-butylammonium salts. *Chemical Communications* **2005,** (16), 2175-2177.

91. Pascanu, V.; Hansen, P. R.; Bermejo Gómez, A.; Ayats, C.; Platero-Prats, A. E.; Johansson, M. J.; Pericàs, M. À.; Martín-Matute, B., Highly Functionalized Biaryls via Suzuki–Miyaura Cross-Coupling Catalyzed by Pd@MOF under Batch and Continuous Flow Regimes. *ChemSusChem* **2015,** *8* (1), 123-130.

92. Harnisch, F.; Schröder, U., Tapping Renewables: A New Dawn for Organic Electrosynthesis in Aqueous Reaction Media. *ChemElectroChem* **2019,** *6* (16), 4126-4133.

93. Verschueren, R. H.; De Borggraeve, W. M., Electrochemistry and Photoredox Catalysis: A Comparative Evaluation in Organic Synthesis. *Molecules* **2019,** *24* (11), 2122.

94. Chen, Q.; Fang, C.; Shen, Z.; Li, M., Electrochemical synthesis of nitriles from aldehydes using TEMPO as a mediator. *Electrochemistry Communications* **2016,** *64*, 51-55.

95. Costentin, C.; Robert, M.; Savéant, J.-M., Current Issues in Molecular Catalysis Illustrated by Iron Porphyrins as Catalysts of the CO2-to-CO Electrochemical Conversion. *Accounts of Chemical Research* **2015,** *48* (12), 2996-3006.

96. Rosen, B. R.; Werner, E. W.; O'Brien, A. G.; Baran, P. S., Total Synthesis of Dixiamycin B by Electrochemical Oxidation. *Journal of the American Chemical Society* **2014,** *136* (15), 5571-5574.

97. Zhou, Y.-G.; Kang, Y.; Huang, J., Fluidized Electrocatalysis. *CCS Chemistry* **2020,** *2* (1), 31-41.

98. Hao, X.; Barnes, S.; Regalbuto, J. R., A fundamental study of Pt impregnation of carbon: Adsorption equilibrium and particle synthesis. *Journal of Catalysis* **2011,** *279* (1), 48-65.

99. Yang, Y.; Reber, A. C.; Gilliland, S. E.; Castano, C. E.; Gupton, B. F.; Khanna, S. N., Donor/Acceptor Concepts for Developing Efficient Suzuki Cross-Coupling Catalysts Using Graphene-Supported Ni, Cu, Fe, Pd, and Bimetallic Pd/Ni Clusters. *The Journal of Physical Chemistry C* **2018,** *122* (44), 25396-25403.

100. Ghobadi, S., Thomas D. Roper, B. F. Gupton, and Carlos E. Castano, Optimal Regioselectivity Control in Electrocatalytic Oxidation of Terminal Olefins. *ECSrXiv* **2019**.

101. Kosmulski, M., pH-dependent surface charging and points of zero charge. IV. Update and new approach. *Journal of Colloid and Interface Science* **2009,** *337* (2), 439-448.

102. James, M. T.; Xun-tian, J., The Wacker Reaction and Related Alkene Oxidation Reactions. *Current Organic Chemistry* **2003,** *7* (4), 369-396.

103. Ghobadi, S.; Işıkel Şanlı, L.; Bakhtiari, R.; Alkan Gürsel, S., Green Composite Papers via Use of Natural Binders and Graphene for PEM Fuel Cell Electrodes. *ACS Sustainable Chemistry & Engineering* **2017,** *5* (9), 8407-8415.

104. Hubkowska, K.; Soszko, M.; Symonowicz, M.; Łukaszewski, M.; Czerwiński, A., Electrochemical Behavior of a Pd Thin Film Electrode in Concentrated Alkaline Media. *Electrocatalysis* **2017,** *8* (4), 295-300.

105. Liu, B.; Han, W., Iron-Catalyzed Wacker-Type Oxidation. *Synlett* **2018,** *29* (04), 383-387.

106. Horn, E. J.; Rosen, B. R.; Chen, Y.; Tang, J.; Chen, K.; Eastgate, M. D.; Baran, P. S., Scalable and sustainable electrochemical allylic C–H oxidation. *Nature* **2016,** *533* (7601), 77-81.

107. Yi, X.; Hu, X., Formal Aza-Wacker Cyclization by Tandem Electrochemical Oxidation and Copper Catalysis. *Angewandte Chemie International Edition* **2019,** *58* (14), 4700-4704.

108. Yarar Kaplan, B.; Haghmoradi, N.; Biçer, E.; Merino, C.; Alkan Gürsel, S., High performance electrocatalysts supported on graphene based hybrids for polymer electrolyte membrane fuel cells. *International Journal of Hydrogen Energy* **2018,** *43* (52), 23221-23230.

109. Regalbuto, J., *Catalyst preparation: science and engineering*. CRC press: 2016.

110. Jackson, J. D., *Classical electrodynamics*. Wiley: New York, 1962.

111. Johnson, P. B.; Christy, R. W., Optical constants of transition metals: Ti, V, Cr, Mn, Fe, Co, Ni, and Pd. *Physical Review B* **1974,** *9* (12), 5056-5070.
112. Phillip, H. R.; Taft, E. A., Kramers-Kronig Analysis of Reflectance Data for Diamond. *Physical Review* **1964,** *136* (5A), A1445-A1448.
113. Goulas, K. A.; Song, Y.; Johnson, G. R.; Chen, J. P.; Gokhale, A. A.; Grabow, L. C.; Toste, F. D., Selectivity tuning over monometallic and bimetallic dehydrogenation catalysts: effects of support and particle size. *Catalysis Science & Technology* **2018,** *8* (1), 314-327.
114. Amin, R. S.; Hameed, R. M. A.; El–Khatib, K. M., Microwave heated synthesis of carbon supported Pd, Ni and Pd–Ni nanoparticles for methanol oxidation in KOH solution. *Applied Catalysis B: Environmental* **2014,** *148-149*, 557-567.

Appendix

Appendix I. X-ray induced preparation of metal-decorated GO monoliths and their catalytic applications

The study presented below is an example of application for GO monoliths as substrate for X-ray induced deposition of metallic particles. The prepare hybrid materials can be used for a variety of applications including catalysis. During this study the catalytic activity of the structure as well as confirmation on formation of particles within the bulk of monoliths is described.

AI.1. Abstract

Gold (Au), palladium (Pd), and Ruthenium (Ru) nanoparticles were synthesized onto 2D and 3D graphene oxide using X-ray induced synthesis. Absorbed doses of ~ 20 kGy produced Pd and Au nanoparticles of ~ 5 nm and ~17 nm in size, respectively. Higher absorbed doses such as 60 kGy, generated Ru nanoparticles with an average size of ~ 3 nm. CT-scan imaging confirmed metal particle formation inside the 3D graphene oxide supports, an advantage of X-ray induced synthesis over conventional approaches. The catalytic activity of Ru/GO monoliths, the smallest nanoparticles produced on monoliths, was tested through the olefination of alkyl acrylates. Results showed the high catalytic activity of the heterogeneous Ru catalysts structures similar to the homogeneous catalysis reported in the literature. Overall, this work demonstrates that X-ray assisted synthesis is a method that allows for nanoparticle formation at mild conditions of room temperature and pressure, in the absence of harsh chemicals in aqueous media suitable to fabricate catalysts in 2D and 3D carbon supports.

AI.2. Introduction

Noble metal nanoparticles are of great importance for diverse fields such as electronics, sensing, catalysis, medicine, and energy storage, among others, due to their non-conventional physical and chemical properties [1–6]. Nowadays, metal nanoparticles are commonly synthesized using wet chemistry methods, whereby features such as size, shape, composition, and crystalline structure can be tuned by the reagents used and other synthesis parameters [7]. One of the challenges faced in the synthesis of nanoparticles in suspension is their tendency to aggregate, and this phenomenon causes a decrease in the surface area of the nanomaterial, which would ultimately lead to a reduced material performance for various applications [8]. The deposition of nanoparticles onto multifunctional supports is an alternative approach to avoid aggregation. Metal nanoparticles have been successfully supported on oxides such as TiO_2, Al_2O_3, ZnO, CeO_2 [9–15], and carbon-based supports that include carbon nanotubes, graphene oxide (GO), graphite, and mesoporous carbon [16–21]. In particular, carbon-based supports deserve special attention because of their chemical and structural versatility, since they can be designed with different functional groups that facilitate a strong particle/support interaction [22]. Moreover, carbon supports offer various features such as tunability of the water permeability and charge surface properties, which allow them to respond to different physicochemical reactions with little effect on their stability [23–25]. Overall, the deposition of noble metal onto carbon supports allows for synergistic effects, where the physical and chemical properties of both support and particles are combined, leading to a nanomaterial with a superior performance [25,26]. Catalysis, for instance, is one of the fields that have benefited from the use of composites made of metal nanoparticles supported on carbon-based structures [17, 27–33]. Nanomaterials have a high surface area that favors the interaction of reactants onto their surfaces [7, 29–34]. Furthermore, nanomaterials have a high number of active sites, which leads to high catalytic activity and improved selectivity, and they can be easily cleaned and reused in several cycles [28]. The final characteristics of the nanomaterials intended for catalysis can be controlled and optimized through the synthesis process. Both computational and experimental results have demonstrated that graphene-based materials may enhance catalytic activities by serving as charge reservoirs for cross-coupling reactions [29–33]. Despite the significant advantages of transition metals on graphene-based supports for the catalysis field, these systems still tend to agglomerate, leading to an abrupt decrease in performance [33,35]. The engineering of 3D graphene structures, such as graphene monoliths, is an alternative to avoid agglomeration of these systems mainly because the restacking of the graphene layers is completely impeded. Nevertheless, other challenges like the formation of stable and active catalysts in the interior of the monoliths must be addressed. Therefore, fabrication methods that depart from conventional wet chemistry approaches are sought to explore new methodologies with improved efficiencies, minimal waste generation, low energy consumption, and able to form active catalysts inside of complex supports [35–37].

Alternative fabrication methods to synthesize metal nanoparticles include sonochemical synthesis, hydrothermal synthesis, UV- and, ionizing radiation-assisted synthesis [38–42]. Among these different fabrication methods, ionizing radiation synthesis has shown to be an efficient and reliable method for nanomaterial production [39,43–45]. Even more, this method has the advantage of being carried out at ambient temperature and pressure, in the absence of harsh chemicals and reducing agents while exploiting the ability of ionizing radiation to penetrate deep in the materials [43,46]. In radiation synthesis, high energy photon beams such as X-rays and gamma rays interact with aqueous solutions containing a metallic salt [46–48]. The interaction of ionizing radiation with water leads to the creation of species such as e^-_{aq}, $H^\bullet$, H+, $OH^\bullet$, $O_2^{\bullet-}$, H_3O^+, H_2, and H_2O_2 [11,45,46]. The species formed during the radiolysis of water are classified as reducing and oxidizing species. Species such as e^-_{aq} and $H^\bullet$ reduce the metal ions in solution into metal atoms [43]. These atoms can either dimerize or interact with the remaining metal precursor ions in a multi-step process that leads these species to coalesce progressively and eventually form nanoparticles [45]. On the other hand, radicals such as $OH^\bullet$ are oxidizing species that may interact with the ions or atoms present in the solution, bringing them to a higher valence state [43]. To prevent these oxidation processes, scavengers such as isopropanol are added to the reaction mixture. Oxidizing species such as $OH^\bullet$ and reducing species such as $H^\bullet$ interact with isopropanol creating secondary reducing radicals such as $(CH_3)_2COH$ and $COO^{\bullet-}$ [43]. X-rays synthesis of nanoparticles is a highly controllable process since the nucleation and growth are regulated by the dose and dose rate used during synthesis. Nonetheless, despite the advantages of gamma and X-rays radiolytic synthesis, there are few reports of supported particles using X-rays. Literature about X-rays radiolytic synthesis refers to gold-platinum, copper, silver and gold nanoparticles deposited onto different supports such as titanium dioxide (TiO_2), polymethyl methacrylate (PMMA), Polymeric acid-polyethyleneimine (PAA-PEI) films, polytetrafluoroethylene (PTFE) and polyimide (PI) films [49–53]. Although the penetration of ionizing radiation is materials is a well-known fact, to date, there are no systematic studies on the use of X-rays to synthesize metal nanoparticles in the interior of these 2D and complex 3D graphene-based supports.

Ma et al., prepared gold film on polyimide substrates using synchrotron radiation X-rays. During that photoinduced selective deposition, technique it was shown the gold particles from salt solution were successfully deposited on flange-patterned polyimide substrates. The thickness of the prepared film was directly controlled by irradiation dosages.

In the early stages of investigating the irradiation-induced metal particle formation, Rosenberg et al. showed that a variety of particles can be precisely formed due to the unique absorption energies at certain lengths It was shown the substrate modification could also be accomplished through this process via irradiation-driven etching, which led to specific interactions between formed particles and the substrate. This process led to formation of metallic particles with strictly controlled dimensional, crystallographic, chemical properties. A study by Karadas et al. showed that via a similar methodology gold (Au) particles can be formed on poly(methyl methacrylate) (PMMA) patterned substrates (*F. Karadas et al., Langmuir 21 (2005) 437)*. The XPS spectra of particles formed via variating irradiation times showed that by increasing that period, formation of ionic gold (Au^{3+}) species were favored over metallic (Au^0) species, depicting the effective control over the formed species achieved via irradiation-driven particle synthesis.

Yamaguchi and co-workers have done extensive research on formation of metallic particles on patterned substrates via photochemical synthesis utilizing synchrotron irradiation. In their study on preparation of gold nanoparticles (*Yamaguchi et al., Material Chemistry and Physics 160 (2015) 205),* it was shown that by controlling the substrate functionality (through patterning) and irradiation dosage gold nanoparticles assemble into higher order particles with fractal-like properties. These Au clusters (~ 500 nm) possessed the same structural features as the individual particles of less than 10 nm as their Raman spectra didn't shows any significant shift. They utilized the same process and equipment to produce highly crystalline copper (Cu) particles (*Japanese Journal of Applied Physics, 55 (2016) 055502)* with tunable geometries that can be readily used for micromanufacturing and electroplating purposes. The fine-tuned spike-like cupric (CuO) particles was also prepared on a silica substrate by dipping the substrate into the metal aqueous solution and exposing to irradiation for only 5 minutes (*Journal of Synchrotron Radiation 24 (2017) 653)*. These particle properties (average diameter, geometry, and elemental composition) were controlled by changing the ratio of a co-solvent (ethanol). The geometries obtained were ranged from multi-crystalline spike shapes to cubical formations. The team's most recent study (*Journal of Synchrotron Radiation 26 (2019) 1986)* also showed the chain length of the alcohol co-solvent used can control, diversify and fine-tune the cupric particle size.

Bharti and co-workers have recently revealed an effective method of preparing silver (Ag) particles using gamma rays in aqueous media and polymeric species (*A. Bharti et al. Scientific Report 6 (2016) 22394)*. This method compared to traditional solution-based reduction approach was shown to yield particles with smaller average diameters with narrower polydispersity. Additionally, the Mie theory analysis on the TEM micrographs showed a significantly higher stability in particle size distribution when the presented method was used. Hence, rendering the gamma-induced particle formation a more effective and consistent method than the conventional counterparts.

Given the potential of radiation synthesis to fabricate well-dispersed metal nanoparticles onto organic and inorganic supports, this work presents X-ray synthesis of Gold (Au), Palladium (Pd), and Ruthenium (Ru) onto 2D and 3D GO nanostructures. Furthermore, as a proof of concept, the catalytic activity of Ru supported on 3D GO structures, the smallest particles obtained in the study, was tested through olefination reactions. These reactions are crucial to the fine chemical industry. GO is a 2D nanomaterial that has high adsorption capacity, high thermal conductivity, and mechanical strength. For these reasons, it has been studied in the fields of sensing, drug delivery, energy storage, fuel cells, and catalysis. In catalysis, GO has been successfully used in chemical reactions such as selective oxidation of carbon monoxide and alcohols, reduction of nitroarenes, hydrogenation, cross-coupling reactions, fuel production, and pollutant removal [17,28–33]. Seeking for more robust carbon catalysts, 3D networks of GO also known as carbon monoliths, have been successfully used as supports [35,54]. The type of metals deposited on 2D and 3D GO are current catalysts used in several chemical industries. For instance, Ru is a stable metal at low temperatures, while at high temperatures, it forms compounds such as Ruthenium oxide (RuO_2), hydrous ruthenium oxide (RuO_2xH_2O), and other Ru-based oxides (RuOx) [39,55]. Overall, deposition of Ru and Ru oxides on carbon supports such as carbon nanotubes, GO, and mesoporous carbon has improved electrical conductivity and catalytic activity on these systems[55–57]. Similarly, supported Au nanoparticles onto carbon supports have also been studied as a catalyst due to the strong absorption, stability, and conductivity of Au [58]. However, due to its high-cost Au nanoparticles have been anchored to inexpensive inorganic and organic supports, to modify surface functionalities and improve the catalytic activity. Results indicated that Au supported GO catalysts have high stability, and they are good candidates for gas-solid oxidation reactions [18]. Finally, Pd-based catalysts have shown an enhanced oxidation activity for hydrazine, alcohols, and hydrogenation of unsaturated hydrocarbons in Suzuki reactions. Among the noble metals used as catalysts, Pd has gathered the most attention due to its activity, abundance, and stability [18,59,60]. Herein, the ability of X-ray synthesis to produce well-dispersed nanoparticles of the aforementioned metals onto supports with intricate 3D geometries is shown, a feature that is not always achievable with conventional chemical methods. This feature could potentially push forward the fabrication of active catalysts for different industrial applications.

AI.3. Experimental Procedure

AI.3.1. Materials and Reagents

Chloroauric acid ($HAuCl_4$•$3H_2O$, ≥ 99.9%), Sodium tetrachloropalladate (Na_2PdCl_4 ≥ 98%), Sodium Dodecyl Sulfate (SDS≥ 99.0%) , sulfuric acid, nitric acid, dichloromethane, hydrogen peroxide, ethanol, polyvinyl alcohol (PVA) (99% hydrolyzed, MW. 89000-98000 g/mol), acetonitrile, (2-bromovinyl)benzene, acetyl acrylate, dimethylformamide, sodium acetate, and isopropanol (IPA) (C_3H_8O, $\geq 99.7\%$) were obtained from Sigma-Aldrich. Ruthenium chloride hydrate ($RuCl_3 \cdot xH_2O \geq 99.9\%$), graphite flakes (> 325 mesh size), Sucrose, phenylboronic acid, and 4-bromotoluene were purchased from Alfa Aesar.

AI.3.2. Synthesis of Carbon Monolith

The detailed preparation procedure for the carbon monoliths was presented in our previous study [35]. Briefly, after oxidation of graphite flakes into GO through Hummers modified method, the covalent bonding between GO layers was conducted in the aqueous phase. The aqueous esterification of GO sheets was catalyzed by PVA/sucrose (5 wt% each with respect to GO) system for 2 hours under stirring at 500 rpm at room temperature (25°C).

Afterward, the monolith solution was poured into molds of the desired shape and went through the freeze-casting process. This process is made by generating a temperature gradient from bottom to top of the mold by exposing the base to liquid nitrogen. Lyophilization is then ensued, providing the 3D monolith structure. The monoliths were exposed to ethanol vapor (1 hour at 74°C) followed by overnight autoclave partial reduction (24 hours at 100°C).

AI.3.3. X-ray induced synthesis of noble metals onto carbon supports

The synthesis of solid-supported metal composites were conducted through the following process. In case of GO-supported structures, the GO was first dispersed in DI-water:IPA mixture. Then a solution of metal salt in the same solvent mixture was prepared and added to the GO dispersion, followed by irradiation. The irradiation of the solution was carried out in an X-RAD

225 XL, an X-ray irradiator from PXI with a tungsten (W) source, operating at a voltage and current conditions of 225 kV and 13.3 mA and irradiation rate of 127 Gy/min. Afterwards the mixture was washed by centrifuging and re-dispersing in DI-water: IPA mixture multiple times to ensure removal of unreacted and oxidizing species.

In case of metal@monolith samples, first the solution of metal precursor was prepared in DI-water:IPA mixtures, followed by immersion of the monolith into those solutions. Afterwards the monoliths were extracted, and immersed in another DI-water:IPA solution, followed by irradiation and washing steps identical to that of the GO samples. The details of preparation conditions for each sample are presented in Table 1.

Table 4. The preparation process details of metal@support composite structures

Sample	Support (concentration mg/mL)	Metal Salt (Concentration mM)	Metal Uptake (wt%)	DI-water:IPA Solution ratio	Irradiation	
					Period (hrs)	Dose (kGy)
Au@GO	GO (5.3)	$HAuCl_4$ (2)	10	9:1	3	22.8
Au@Monolith	Monolith (9.7)	$HAuCl_4$ (2)	5	9:1	3	22.8
Ru@GO	GO (1)	$RuCl_3$ (1.15)	10	9:1	8	60

Ru@Monolith	Monolith (9)	$RuCl_3$ (1.15)	10	2:1	8	60
Pd@GO-10	GO (1)	Na_2PdCl_4 (2)	10	1:4	2	15.2
Pd@GO-1	GO (1)	Na_2PdCl_4 (2)	1	1:2	2	15.2

AI.3.4. Catalysis assessment of noble metal onto carbon supports

The catalytic activity screening of metal-decorated carbon monoliths was conducted through reactions best known for being able to catalyze. Smaller particle sizes are easily related to high catalytic activity, and therefore, the Ru decorated monoliths were the system selected for the assessment. An olefination of alkyl acrylates, particularly (2-bromovinyl) benzene, and acetyl acrylate was the test reaction. The conversion and selectivity of reactions towards the product were analyzed via an Agilent gas chromatography-mass spectroscopy (GC-MS) analysis of the reaction effluent after 10 times volumetric dilution by dichloromethane, and ethyl acetate, respectively.

AI.3.5. Material's characterization of noble metal deposited on carbon-based supports

Morphology and particle size analysis were performed with scanning electron microscopy (SEM), transmission electron microscopy (TEM), and computed tomography (CT-scan). SEM characterization used a Phenom ProX microscope at an operating voltage of 10 kV. For this purpose, dry samples of the metal-loaded carbon supports were dispersed in acetone using an ultrasonic probe to ensure a homogeneous solution. Then, a drop of the solution was pipetted onto a silicon wafer. For TEM analysis, a drop of the suspension was deposited onto formvar/carbon coated grid and analyzed with a Zeiss Libra 120 Plus operating at 120 kV. High-resolution TEM was performed in an FEI Titan 30, operated at 300 keV. Moreover, scanning transmission electron microscopy (STEM) was carried out in a Hitachi FE-SEM Su-70, at an operating voltage of 30 kV. Micro CT-scan of the Au@Monolith was conducted, as a proof of concept for large scale 3D mapping of particle distribution within such structures, using a Bruker Skyscan 1173 Micro-CT scanner at 130 kV with 4000ms exposure time. The CT image reconstruction was completed using CTVOX free software. The crystalline structure of the nanomaterials was evaluated using an X-ray diffractometer PANalytical Empyrean with a copper anode at a voltage and current of 45 kV and 40 mA respectively. For this purpose, the samples were dried in an oven at a mild temperature of 50°C and powders of the nanomaterials were place onto low background silicon. The wafer was placed onto a spinning stage with an angular velocity of 120 rpm, and the XRD patterns were analyzed using HighScore Xpert. Finally, X-ray photoelectron spectroscopy (XPS) in PHI Versaprobe III Scanning XPS microprobe was used for chemical analysis. The samples were prepared by dispersing the nanomaterial in acetone and depositing the suspension onto a silicon wafer; then samples were allowed to dry at room temperature.

AI.4. Results and Discussion

AI.4.1. Crystalline structure Analysis of supported nanoparticles

The XRD patterns of metal nanoparticles supported onto GO and carbon monoliths are shown in Figures 1a and 1b respectively. The 2D and 3D GO supports revealed a hexagonal closed pack

(HCP) crystalline structure (pdf 01-075-1621), typical of these graphitic structures. Ruthenium nanoparticles showed HCP crystal structure (pdf 00-006-0663). Palladium and gold nanoparticles showed face cubic centered crystal structures (pdf 01-088-2325 and pdf 01-071-4614, respectively). Furthermore, the crystallite size of the particles was calculated using the Scherrer equation. The crystallite size of the Pd nanoparticles in Pd@GO, was ~ 9.7 nm, whereas the Au in the Au@GO and Au@monolith systems showed crystallite sizes of 32.9 nm, and 15.9 nm. Finally, Ru on the Ru@GO and Ru@Monolith systems showed a particle size of 3.1 nm and 4.2 nm, respectively. The sharp peak observed at $2\theta = 40°$ in Figure 1b corresponds to PVA residues on the monolith.

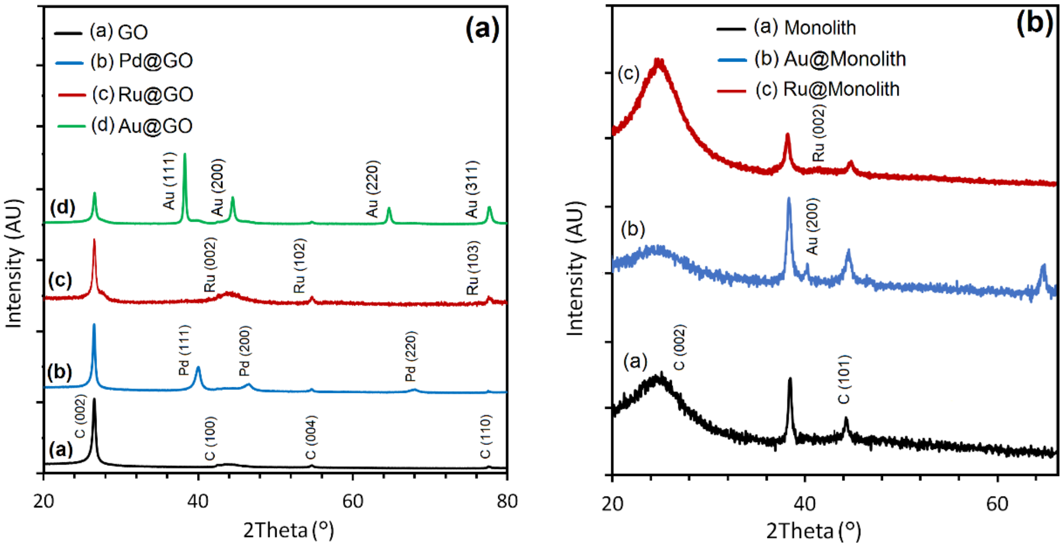

Figure 1. XRD patterns of **a)** Metals@GO **b)** Metals@Monolith

AI.4.2. Morphology analysis of supported nanoparticles

The SEM images of GO and the carbon monolith prior to noble metal particle deposition are shown in Figures 2a and 2c, respectively. The Figures 2b, 2d, 2e, and f are representative SEM images at low magnification of the different noble metals deposited on both GO and GO monoliths. These images evidence the formation of metal particles on the surface of the various supports, and since most of the experiments attempt a nominal loading of about 10 wt%, it is expected to form aggregates after small nanoparticles are created. For instance, the Au@GO micrograph (Figure 2b) evidenced the presence of Au aggregates with a mean particle size of 0.71 ± 0.22 µm. Similarly, while Au@Monolith showed Au particles in the micron size with a mean of 0.12 ± 0.04 µm (Figure 2e), a more significant fraction of smaller nanoparticles were identified under STEM, having an average size of 16.3 ± 4.2 nm as shown in Figure 2f. Ru nanoparticles with a mean particle size of 13.2 ± 3.4 nm (Figure 2e) were observed on the monolith, though some scattered aggregates were present. In X-ray radiolytic synthesis, the interaction of photons with water molecules induces radiolysis of water, a process that generates reducing species such as e^-_{aq} and $H^\bullet$ with a high reducing potential of $E°$ (H_2O/e^-_{aq}) = -2.87 V_{NHE} and E^0 ($H^+/H\bullet$) = -2.3 V_{NHE} [61]. These species will reduce metal ions in solution, avoiding the need for chemical reducing agents typically used in traditional synthesis methods [45,49]. Once metal ions are reduced, they interact with other species in solution, to dimerize and form nucleation centers, that will coalesce and grow into nanoparticles [43,62]. This process is controlled by the dose rate; high absorbed dose rates produce an abundance of reducing species that will form a high number of nucleation centers leading to well-dispersed nanoparticles with a narrow particle size distribution [11,44]. The metal concentration is also an essential factor to be controlled, particularly in the synthesis of nanoparticles on supports which adds the restriction of available surface area. Once the surface of the support has been saturated with nanoparticles, the presence of metal species in solution will rather lead to aggregates or nanoparticles free from the support. Therefore, managing the quality of the final product requires the adjustment of various parameters. Another critical variable is the addition of stabilizers during synthesis; they may also allow for better control of nanoparticle growth [44]. Nanoparticles in suspension are easily attracted to each other by Van der Waals forces. Nanoparticle stability is attained when there is an equilibrium between the repulsive and attractive forces through electrostatic or steric interactions. The stabilization of particles can be attained with polymers with functional groups such as NH_2, -COOH, and -OH, which have high affinity for metal atoms. Some of the stabilizers agents used in synthesis of nanoparticles include Polyvinyl alcohol (PVA), Polyvinylpyrrolidone (PVP) and Sodium Dodecyl Sulfate (SDS) [39,43,63–65]. Furthermore, the addition of surfactants or stabilizers to the reaction volume prior to irradiation may also play a role as may contribute to better control over the particle size and, preventing aggregation [44]. In Figures 2b and 2e, aggregation of Au and Ru nanoparticles is observed. In this case, stabilizing agents were not added to the solution's prior irradiation. Nonetheless, these images also display very small particles at other areas where less aggregates are present.

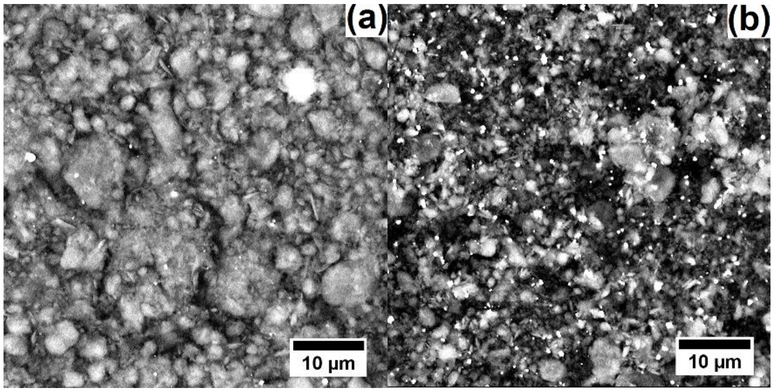

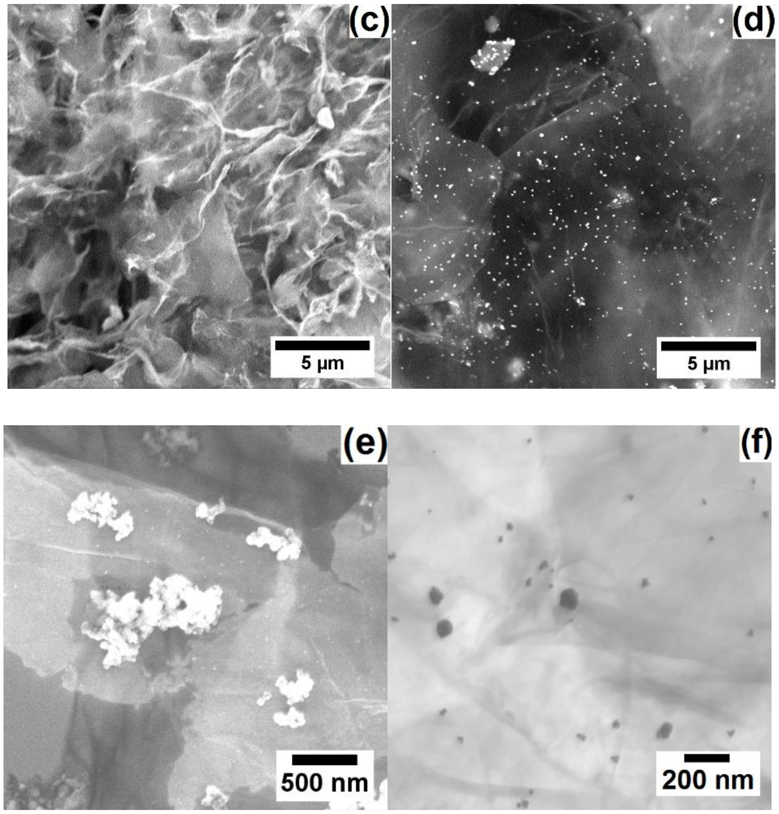

Figure 2. SEM images of **a)** Pristine GO **b)** Au@GO **c)** Pristine carbon monolith **d)** Au@Monolith **e)** Ru@Monolith. **f)** STEM of Au@Monolith

TEM images of pristine GO and Pd particles and Ru particles onto GO are presented in Figures 3 a-d. In radiolytic synthesis, as in conventional aqueous routes, the final nanoparticle size is also dependent upon the initial ion concentration in solution. Then, since aggregates are expected at high metal loadings, this hypothesis was evaluated using different Pd metal loadings on GO. When the Pd loading was set to 10 wt%, the obtained particle size was ~8.4 ± 2.6 nm. A reduction in the mean particle size down to ~4.9 ± 2.5 nm was reached by reducing the metal loading to 1 wt%. Also, it is possible to see through close inspection under electron microscopy that samples loaded with 10 times more nominal Pd metal present more clusters. Small Ru nanoparticles formed when using 60 kGy with a mean size of 2.9 ± 1.0 nm, evidencing a narrow size distribution even at a high metal loading of 10 wt%. A larger absorbed dose was set for the synthesis of Ru nanoparticles as our preliminary work evidenced a partial reduction of metal ions in solution at lower doses.

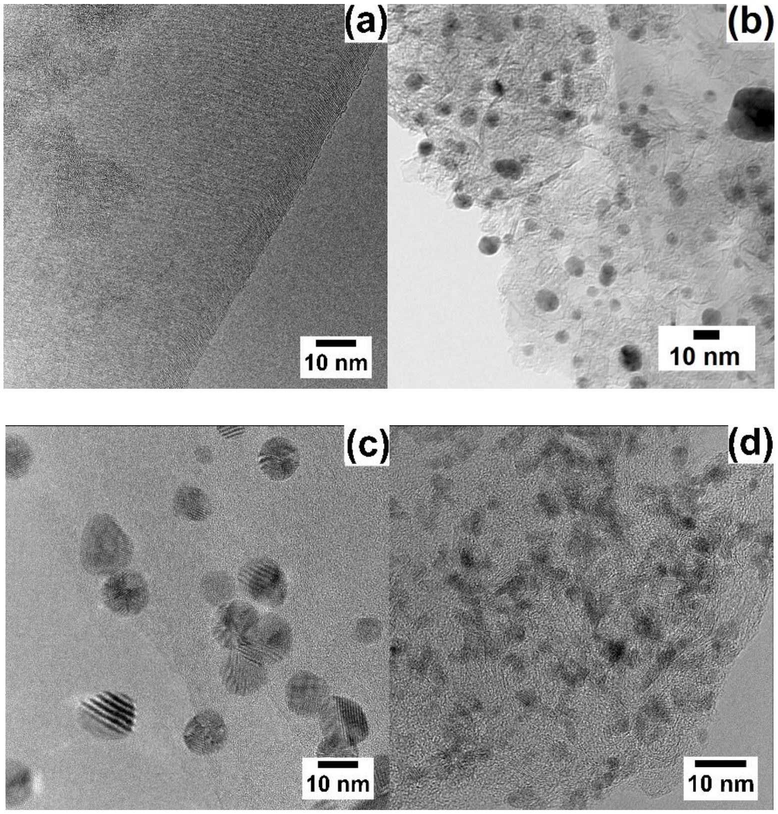

Figure 3. TEM micrographs of a) Pristine GO b)) Pd@GO-1% loading c) Pd@GO-10% loading d) Ru@GO.

The micro CT-scan imaging of Au@monolith (Figures 4a and b) and Ru@Monolith (Figures 4c, and b) structures proved that the metal particles successfully reduced and immobilized within the 3D structure. It was established that the bright spots within the slice of the structure (Figure 4b) to be attributed to metal particles, which then confirms the incorporation of Au particles not only on the surface but also inside of the monolithic structure [35]. As the two extremes cases in particle size both largest for Au and smallest for Ru nanoparticles on monolith, these specimens were analyzed using CT-scan. High contrast is evidenced for the Au-containing sample and the aggregates are easily identified since their size, in the micrometer range, is close the resolution of the CT-scan. In the case of Ru on monolith, the contrast differences are less evident because particles are much smaller overall, and fewer aggregates were produced in the sample. However, this imaging tool still allows to see particles forming on large volumes of the monoliths.

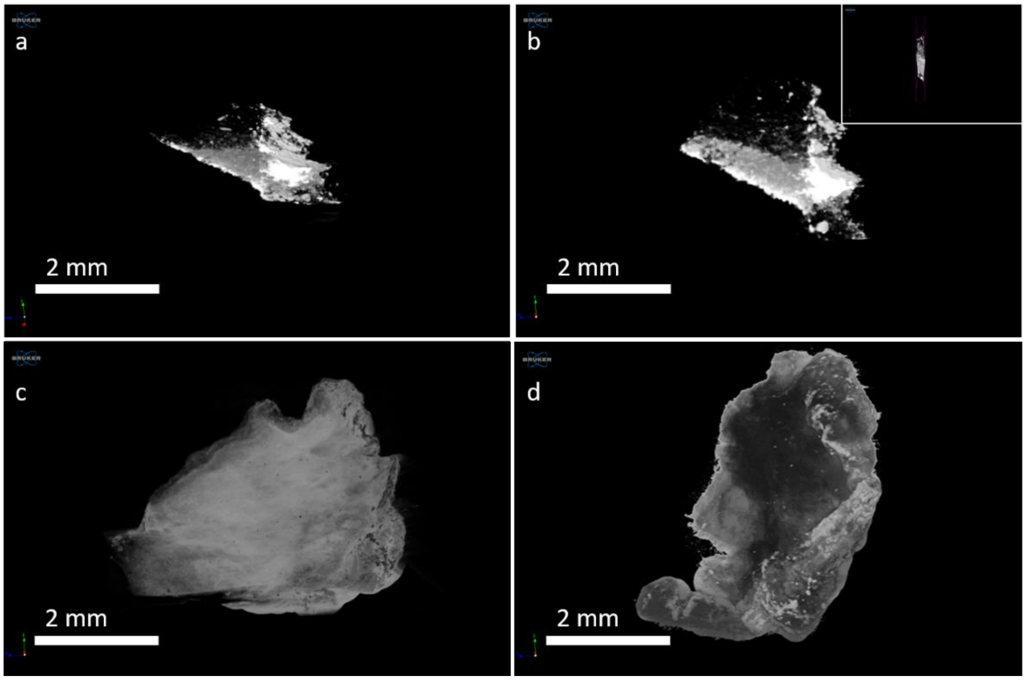

Figure 4. Micro CT-scan images of a) the Au@monolith, and b) Image taken from middle of the structure, (The inset shows the cross-section of the slice), c and d) the Ru@monolith

AI.4.3. Surface Chemistry Analysis of supported metal nanoparticles.

Catalysis is one significant field where transition metal nanoparticles deposited on GO and GO monoliths can provide the most benefit. It is also relevant to have the particles evenly distributed, and small particle size would generally increase the activity due to the higher number of active sites present at the surface. However, other important aspects such as the chemistry and electronic state must be understood. To further investigate the catalytic activity of these systems, the Ru on GO monolith was selected for the analysis largely due to the small particle size obtained while using 60 kGy. The high-resolution XPS results of Ru@Monolith are displayed in Figure 5. The analysis of Ru3p state (Figure 5a) revealed both Ru(0) and Ru(IV) chemical states. It was observed that even both chemical states are present, Ru(0) prevailed over the Ru(IV) species, showing the power of reduction of the chosen process. The XPS analysis of the Ru may be performed by using either Ru3d or Ru3p peaks. However, the spectral lines of Ru3d overlap with the peaks that correspond to the carbon peak C1s. Therefore, the Ru3p was chosen for analysis [66]. Peaks at binding energies of 463.4 and 485.8 eV were identified as stable Ru(0) and peaks located at binding energies of 466.8 and 492.1 eV referred to Ru (IV) [39,66,67]. Moreover, peaks at energies of 463.4 and 466.8 eV have been linked to RuO_2 and RuO_x signals [68]. The evaluation of the C1s peak (Figure 5b) showed peaks at binding energies of 284.8, 285.7, 287.1, 288.8, and 289.9 eV; these peaks were associated with C sp^2, C sp^3, C-O-C, O=C-OH and -COOH respectively [39,69]. In Figure 5b, a peak at 282.3 eV is also observed, which peak corresponds to Ru3d [70]. Analysis of the oxygen O1s (figure 5c) showed three different peaks located at binding energies of 531.5, 532.9, and 534.9 eV. The peak at 531.5 eV is associated with Ru-O bonds; this could indicate that Ru NPs bond with the monolith support through oxygen found within the functional groups on the surface of the support [39,66]. The peaks located at 532.9 and 534.9 eV are associated with C-O and H_2O chemical bonds respectively [39].

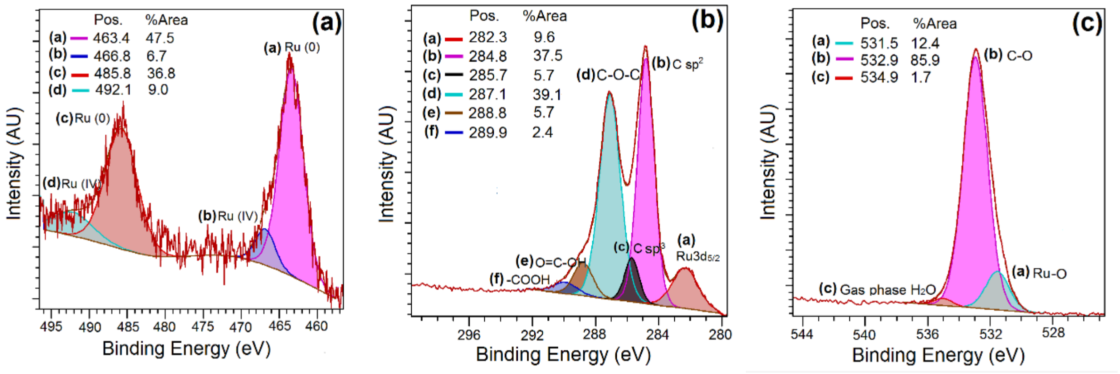

Figure 5. High-resolution XPS spectra of **a)** Ru3p **b)** C1s and **c)** O1s

AI.4.4. Catalytic performance of supported nanoparticles

The proof of concept as an application of the prepared metal@Monolith structures was conducted through various reactions. The catalytic activity of Ru@Monolith was tested through the olefination of alkylates (Figure 6). The olefination reaction catalyzed by Ru@Monolith yielded to 86.4% and 58% conversion and selectivity ratios towards the (E)-acetic (E)-4-phenylbut-3-enoic anhydride product, respectively. Both of the results were reliable for further optimizations, making the metal-decorated monoliths as potentially viable catalysts for a variety of reactions. While these reactions were tested in batch, it is possible, based on the robustness of the monolithic supports, to implement the reactions in-flow. The ability to cast the monoliths into any desired shape and further on deposit virtually any nanoparticle made of active catalysts allow for numerous setups in-flow. In particular, using modular instrumentation where the catalysts can be inserted as a plug-and-play cartridge while forcing reagents to pass through the channels, which ultimately will form the desired product as long as resident time and flow are properly optimized.

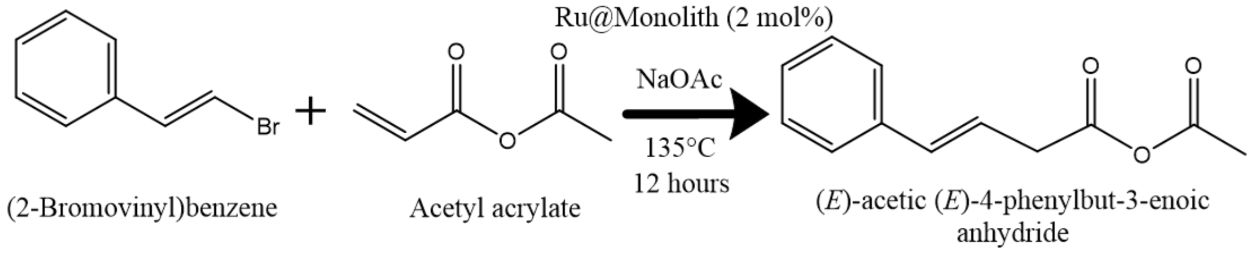

Figure 6. Olefination reactions used for catalytic screening of metal decorated monoliths

In this work, several important hypotheses have been tested in order to demonstrate the potential applications of X-ray induced synthesis of metal nanoparticles on 2D and 3D GO supports. It is also implicit that any metal can be produced by this method on complex supports as long as the parameters are optimized to be able to reduce the starting metal ions into their metallic state. Even more, controlling processing and design parameters, particle size and uniformity are likely to be narrowed to the desired values. The penetration depth of X-rays is by far more powerful than similar methods of UV irradiation. CT-scans are powerful methods to assess particles inside 3D supports, but higher resolution nano-CT-scan systems will likely provide more insights. The proof of concept in catalysis is a very straightforward test to evidence the applicability of the concept of X-ray synthesis as a whole. Particularly, olefination reactions performed in these newly designed Ru@GO monolith systems were compared to the homogeneous phase standards available in the literature. A similar conversion was obtained but the fact of using heterogeneous systems makes this approach a powerful alternative since the separation of the catalyst out of the reagents and products can be easily made by physical means. While the homogenous counterpart has intrinsically a tedious workup of separating the catalyst made in the same liquid phase. All in all, the presented results are an attempt to open new areas of applications of radiation-induced synthesis where other techniques may underperform due to the lack of control or ability to form nanoparticles in hidden and inaccessible places.

AI.5. Conclusions

Au, Ru, and Pd nanoparticles were successfully deposited on the surface on 2D, and 3D GO supports. SEM, TEM and CT-scan analysis proved the potential of X-rays to produce homogeneously distributed nanoparticles throughout the whole volume of a 3D support due to their high penetration in matter. Moreover, noble metal nanoparticles were synthesized onto multifunctional supports using clean solvents such as water and isopropanol, in a method that does not require harsh chemical reducing agents or extensive nanoparticle purification processes. Ru nanoparticles showed a small particle size of ~ 3 nm obtained at high absorbed doses of ~ 60 kGy during the irradiation process. Additionally, Pd nanoparticles were synthesized in the presence of stabilizing agents at two conditions of metal loadings of 1 and 10 wt%, the former one resulting in smaller and better-dispersed nanoparticles than the latter one. Finally, Au nanoparticles of ~17 nm were obtained on both 2D and 3D carbon structures. The nanoparticle synthesis on the supports was carried out in the absence of surfactants, resulting in sub-micron sized aggregates. The micro CT-scan imaging of the metal-decorated carbon monoliths proved that the particles were formed and deposited within the monolith structure. These results showed that parameters such as the chemistry and concentration of the precursors, and absorbed dose influence the characteristics of the final product, e.g. particle size and size distribution. Furthermore, our results indicated high catalytic activity of the Ru@monolith versus the homogeneous control values from literature, showing that X-ray synthesis of nanomaterials has the potential to be implemented as a reliable method to fabricate catalysts for pharmaceutical and fine chemical reactions.

AI.6. References

[1] J. Li, T. Zhao, T. Chen, Y. Liu, C.N. Ong, J. Xie, Engineering noble metal nanomaterials for environmental applications, Nanoscale. 7 (2015) 7502–7519. doi:10.1039/C5NR00857C.

[2] R.R. Arvizo, S. Bhattacharyya, R. Kudgus, K. Giri, R. Bhattacharya, P. Mukherjee, Intrinsic Therapeutic Applications of Noble Metal Nanoparticles: Past, Present and Future, Chem Soc Rev. 41 (2012) 2943–2970. doi:10.1039/c2cs15355f.

[3] D. Kohl, The role of noble metals in the chemistry of solid-state gas sensors, Sensors and Actuators B: Chemical. 1 (1990) 158–165. doi:10.1016/0925-4005(90)80193-4.

[4] Y. Yan, T. Wang, X. Li, H. Pang, H. Xue, Noble metal-based materials in high-performance supercapacitors, Inorg. Chem. Front. 4 (2017) 33–51. doi:10.1039/C6QI00199H.

[5] E.E. Elemike, D.C. Onwudiwe, L. Wei, L. Chaogang, Z. Zhiwei, Noble metal –semiconductor nanocomposites for optical, energy and electronics applications, Solar Energy Materials and Solar Cells. 201 (2019) 110106. doi:10.1016/j.solmat.2019.110106.

[6] C.M. Aikens, Electronic and Geometric Structure, Optical Properties, and Excited State Behavior in Atomically Precise Thiolate-Stabilized Noble Metal Nanoclusters, Acc. Chem. Res. 51 (2018) 3065–3073. doi:10.1021/acs.accounts.8b00364.

[7] T.S. Rodrigues, A.G.M. da Silva, P.H.C. Camargo, Nanocatalysis by noble metal nanoparticles: controlled synthesis for the optimization and understanding of activities, J. Mater. Chem. A. 7 (2019) 5857–5874. doi:10.1039/C9TA00074G.

[8] F. Maillard, S. Schreier, M. Hanzlik, E.R. Savinova, S. Weinkauf, U. Stimming, Influence of particle agglomeration on the catalytic activity of carbon-supported Pt nanoparticles in CO monolayer oxidation, Phys. Chem. Chem. Phys. 7 (2005) 385–393. doi:10.1039/B411377B.

[9] S.J. Tauster, S.C. Fung, R.L. Garten, Strong metal-support interactions. Group 8 noble metals supported on titanium dioxide, J. Am. Chem. Soc. 100 (1978) 170–175. doi:10.1021/ja00469a029.

[10] J.F. Gomes, K. Bednarczyk, M. Gmurek, M. Stelmachowski, A. Zaleska-Medynska, F.C. Bastos, M.E. Quinta-Ferreira, R. Costa, R.M. Quinta-Ferreira, R.C. Martins, Noble metal–TiO2 supported catalysts for the catalytic ozonation of parabens mixtures, Process Safety and Environmental Protection. 111 (2017) 148–159. doi:10.1016/j.psep.2017.07.001.

[11] M.C. Molina Higgins, D.M. Clifford, J.V. Rojas, Au@TiO2 nanocomposites synthesized by X-ray radiolysis as potential radiosensitizers, Applied Surface Science. 427 (2018) 702–710. doi:10.1016/j.apsusc.2017.08.094.

[12] Q. Zhang, K.T. Chuang, Alumina-Supported Noble Metal Catalysts for Destructive Oxidation of Organic Pollutants in Effluent from a Softwood Kraft Pulp Mill, Ind. Eng. Chem. Res. 37 (1998) 3343–3349. doi:10.1021/ie980111v.

[13] B. Miranda, E. Díaz, S. Ordóñez, A. Vega, F.V. Díez, Performance of alumina-supported noble metal catalysts for the combustion of trichloroethene at dry and wet conditions, Applied Catalysis B: Environmental. 64 (2006) 262–271. doi:10.1016/j.apcatb.2005.12.008.

[14] Z. Bao, Y. Yuan, C. Leng, L. Li, K. Zhao, Z. Sun, One-Pot Synthesis of Noble Metal/Zinc Oxide Composites with Controllable Morphology and High Catalytic Performance, ACS Appl. Mater. Interfaces. 9 (2017) 16417–16425. doi:10.1021/acsami.7b02667.

[15] N. Acerbi, S. Golunski, S.C. Tsang, H. Daly, C. Hardacre, R. Smith, P. Collier, Promotion of Ceria Catalysts by Precious Metals: Changes in Nature of the Interaction under Reducing and Oxidizing Conditions, J. Phys. Chem. C. 116 (2012) 13569–13583. doi:10.1021/jp212233u.

[16] B. Wu, Y. Kuang, X. Zhang, J. Chen, Noble metal nanoparticles/carbon nanotubes nanohybrids: Synthesis and applications, Nano Today. 6 (2011) 75–90. doi:10.1016/j.nantod.2010.12.008.

[17] Y. Cheng, Y. Fan, Y. Pei, M. Qiao, Graphene-supported metal/metal oxide nanohybrids: synthesis and applications in heterogeneous catalysis, Catal. Sci. Technol. 5 (2015) 3903–3916. doi:10.1039/C5CY00630A.

[18] N.M. Julkapli, S. Bagheri, Graphene supported heterogeneous catalysts: An overview, International Journal of Hydrogen Energy. 40 (2015) 948–979. doi:10.1016/j.ijhydene.2014.10.129.

[19] A. Mishra, A. Mehta, S. Basu, N.P. Shetti, K.R. Reddy, T.M. Aminabhavi, Graphitic carbon nitride (g–C3N4)–based metal-free photocatalysts for water splitting: A review, Carbon. 149 (2019) 693–721. doi:10.1016/j.carbon.2019.04.104.

[20] M. Miola, X.-M. Hu, R. Brandiele, E.T. Bjerglund, D.K. Grønseth, C. Durante, S.U. Pedersen, N. Lock, T. Skrydstrup, K. Daasbjerg, Ligand-free gold nanoparticles supported on mesoporous carbon as electrocatalysts for CO2 reduction, Journal of CO2 Utilization. 28 (2018) 50–58. doi:10.1016/j.jcou.2018.09.009.

[21] P. Veerakumar, N. Dhenadhayalan, K.-C. Lin, S.-B. Liu, Highly stable ruthenium nanoparticles on 3D mesoporous carbon: an excellent opportunity for reduction reactions, J. Mater. Chem. A. 3 (2015) 23448–23457. doi:10.1039/C5TA06875D.

[22] E. Pérez-Mayoral, V. Calvino-Casilda, E. Soriano, Metal-supported carbon-based materials: opportunities and challenges in the synthesis of valuable products, Catal. Sci. Technol. 6 (2016) 1265–1291. doi:10.1039/C5CY01437A.

[23] J. Sun, C. Hu, Z. Liu, H. Liu, J. Qu, Surface charge and hydrophilicity improvement of graphene membranes via modification of pore surface oxygen-containing groups to enhance permeability and selectivity, Carbon. 145 (2019) 140–148. doi:10.1016/j.carbon.2018.12.098.

[24] Z. Xu, Z. Ao, D. Chu, A. Younis, C.M. Li, S. Li, Reversible Hydrophobic to Hydrophilic Transition in Graphene via Water Splitting Induced by UV Irradiation, Sci Rep. 4 (2014). doi:10.1038/srep06450.

[25] G. Modugno, C. Ménard-Moyon, M. Prato, A. Bianco, Carbon nanomaterials combined with metal nanoparticles for theranostic applications, Br J Pharmacol. 172 (2015) 975–991. doi:10.1111/bph.12984.

[26] A.B. Yousaf, M. Imran, A. Zeb, X. Xie, K. Liang, X. Zhou, C.-Z. Yuan, A.-W. Xu, Synergistic effect of graphene and multi-walled carbon nanotubes composite supported Pd nanocubes on enhancing catalytic activity for electro-oxidation of formic acid, Catal. Sci. Technol. 6 (2016) 4794–4801. doi:10.1039/C5CY02217G.

[27] Y.S. Jeong, J.-B. Park, H.-G. Jung, J. Kim, X. Luo, J. Lu, L. Curtiss, K. Amine, Y.-K. Sun, B. Scrosati, Y.J. Lee, Study on the Catalytic Activity of Noble Metal Nanoparticles on Reduced Graphene Oxide for Oxygen Evolution Reactions in Lithium–Air Batteries, Nano Lett. 15 (2015) 4261–4268. doi:10.1021/nl504425h.

[28] C. Tan, X. Huang, H. Zhang, Synthesis and applications of graphene-based noble metal nanostructures, Materials Today. 16 (2013) 29–36. doi:10.1016/j.mattod.2013.01.021.

[29] Y. Yang, C.E. Castano, B.F. Gupton, A.C. Reber, S.N. Khanna, A fundamental analysis of enhanced cross-coupling catalytic activity for palladium clusters on graphene supports, Nanoscale. 8 (2016) 19564–19572. doi:10.1039/C6NR06793J.

[30] Y. Yang, A.C. Reber, S.E. Gilliland, C.E. Castano, B.F. Gupton, S.N. Khanna, Donor/Acceptor Concepts for Developing Efficient Suzuki Cross-Coupling Catalysts Using Graphene-Supported Ni, Cu, Fe, Pd, and Bimetallic Pd/Ni Clusters, J. Phys. Chem. C. 122 (2018) 25396–25403. doi:10.1021/acs.jpcc.8b07538.

[31] S.E. Gilliland, J.M.M. Tengco, Y. Yang, J.R. Regalbuto, C.E. Castano, Electrostatic adsorption-microwave synthesis of palladium nanoparticles on graphene for improved cross-coupling activity | Elsevier Enhanced Reader, Applied Catalysis A: General. 550 (2018) 168–175.

[32] Y. Yang, A.C. Reber, S.E. Gilliland, C.E. Castano, B.F. Gupton, S.N. Khanna, More than just a support: Graphene as a solid-state ligand for palladium-catalyzed cross-coupling reactions, Journal of Catalysis. 360 (2018) 20–26. doi:10.1016/j.jcat.2018.01.027.

[33] Y. Yang, S.E. Gilliland, S. Ghobadi, M. Burkholder, S.E. Smith, B.F. Gupton, C.E. Castano, Three dimensional composites of graphene as supports in Pd-catalyzed synthetic applications, React. Chem. Eng. 4 (2018) 90–99. doi:10.1039/C8RE00185E.

[34] Q.-L. Zhu, Q. Xu, Immobilization of Ultrafine Metal Nanoparticles to High-Surface-Area Materials and Their Catalytic Applications, Chem. 1 (2016) 220–245. doi:10.1016/j.chempr.2016.07.005.

[35] S. Ghobadi, M.B. Burkholder, S.E. Smith, B.F. Gupton, C.E. Castano, Catalytically sustainable, palladium-decorated graphene oxide monoliths for synthesis in flow, Chemical Engineering Journal. 381 (2020) 122598. doi:10.1016/j.cej.2019.122598.

[36] S. Falsini, U. Bardi, A. Abou-Hassan, S. Ristori, Sustainable strategies for large-scale nanotechnology manufacturing in the biomedical field, Green Chem. 20 (2018) 3897–3907. doi:10.1039/C8GC01248B.

[37] N. Kosinov, C. Liu, E.J.M. Hensen, E.A. Pidko, Engineering of Transition Metal Catalysts Confined in Zeolites, Chem. Mater. 30 (2018) 3177–3198. doi:10.1021/acs.chemmater.8b01311.

[38] S. Anandan, M. Ashokkumar, Sonochemical synthesis of Au–TiO2 nanoparticles for the sonophotocatalytic degradation of organic pollutants in aqueous environment, Ultrasonics Sonochemistry. 16 (2009) 316–320. doi:10.1016/j.ultsonch.2008.10.010.

[39] J.V. Rojas, M. Toro-Gonzalez, M.C. Molina-Higgins, C.E. Castano, Facile radiolytic synthesis of ruthenium nanoparticles on graphene oxide and carbon nanotubes, Materials Science and Engineering: B. 205 (2016) 28–35. doi:10.1016/j.mseb.2015.12.005.

[40] J.V. Rojas, M.C. Molina Higgins, M. Toro Gonzalez, C.E. Castano, Single step radiolytic synthesis of iridium nanoparticles onto graphene oxide, Applied Surface Science. 357 (2015) 2087–2093. doi:10.1016/j.apsusc.2015.09.190.

[41] D. Rajesh, C. Mahendiran, C. Suresh, A. Pandurangan, T. Maiyalagan, Hydrothermal synthesis of three dimensional reduced graphene oxide-multiwalled carbon nanotube hybrids anchored with palladium-cerium oxide nanoparticles for alcohol oxidation reaction, International Journal of Hydrogen Energy. 44 (2019) 4962–4973. doi:10.1016/j.ijhydene.2019.01.025.

[42] P. Wang, Z.-G. Liu, X. Chen, F.-L. Meng, J.-H. Liu, X.-J. Huang, UV irradiation synthesis of an Au–graphene nanocomposite with enhanced electrochemical sensing properties, J. Mater. Chem. A. 1 (2013) 9189–9195. doi:10.1039/C3TA11155E.

[43] J. Belloni, M. Mostafavi, H. Remita, J.-L. Marignier, and M.-O. Delcourt, Radiation-induced synthesis of mono- and multi-metallic clusters and nanocolloids, New J. Chem. 22 (1998) 1239–1255. doi:10.1039/A801445K.

[44] A. Abedini, A.R. Daud, M.A. Abdul Hamid, N. Kamil Othman, E. Saion, A review on radiation-induced nucleation and growth of colloidal metallic nanoparticles, Nanoscale Research Letters. 8 (2013) 474. doi:10.1186/1556-276X-8-474.

[45] D.M. Clifford, C.E. Castano, J.V. Rojas, Supported transition metal nanomaterials: Nanocomposites synthesized by ionizing radiation, Radiation Physics and Chemistry. 132 (2017) 52–64. doi:10.1016/j.radphyschem.2016.12.001.

[46] J. Belloni, Nucleation, growth and properties of nanoclusters studied by radiation chemistry: Application to catalysis, Catalysis Today. 113 (2006) 141–156. doi:10.1016/j.cattod.2005.11.082.

[47] O.V. Kharissova, B.I. Kharisov, U.O. Mndez, Radiation-Assisted Synthesis of Composites, Materials, Compounds, and Nanostructures, in: Wiley Encyclopedia of Composites, American Cancer Society, 2012: pp. 1–26. doi:10.1002/9781118097298.weoc212.

[48] J. Grand, S.R. Ferreira, V. de Waele, S. Mintova, T.M. Nenoff, Nanoparticle Alloy Formation by Radiolysis, J. Phys. Chem. C. 122 (2018) 12573–12588. doi:10.1021/acs.jpcc.8b01878.

[49] M.C. Molina Higgins, J.V. Rojas, X-ray radiation enhancement of gold- TiO2 nanocomposites, Applied Surface Science. 480 (2019) 1147–1155. doi:10.1016/j.apsusc.2019.02.234.

[50] A.A. Zezin, V.I. Feldman, A.V. Dudnikov, S.B. Zezin, S.S. Abramchuk, S.I. Belopushkin, Reduction of copper(II) ions in polyacrylic acid-polyethyleneimine complexes using X-ray radiation, High Energy Chemistry. 43 (2009) 100–104. doi:10.1134/S0018143909020064.

[51] F. Muller, P. Fontaine, S. Remita, M.-C. Fauré, E. Lacaze, M. Goldmann, Synthesis of Nanostructured Metal−Organic Films: Surface X-ray Radiolysis of Silver Ions Using a Langmuir Monolayer as a Template, Langmuir. 20 (2004) 4791–4794. doi:10.1021/la049534u.

[52] Y. Ohkubo, T. Nakagawa, S. Seino, J. Kugai, T.A. Yamamoto, H. Nitani, Y. Niwa, X-ray-induced reduction of Au ions in an aqueous solution in the presence of support materials and *in situ* time-resolved XANES measurements, Journal of Synchrotron Radiation. 21 (2014) 1148–1152. doi:10.1107/S1600577514012703.

[53] S. Remita, P. Fontaine, E. Lacaze, Y. Borensztein, H. Sellame, R. Farha, C. Rochas, M. Goldmann, X-ray radiolysis induced formation of silver nano-particles: A SAXS and UV–visible absorption

spectroscopy study, Nuclear Instruments and Methods in Physics Research Section B: Beam Interactions with Materials and Atoms. 263 (2007) 436–440. doi:10.1016/j.nimb.2007.06.032.

[54] J. Du, W.-C. Li, Z.-X. Ren, L.-P. Guo, A.-H. Lu, Synthesis of mechanically robust porous carbon monoliths for CO2 adsorption and separation, Journal of Energy Chemistry. 42 (2020) 56–61. doi:10.1016/j.jechem.2019.06.006.

[55] Q. Li, S. Zheng, Y. Xu, H. Xue, H. Pang, Ruthenium based materials as electrode materials for supercapacitors, Chemical Engineering Journal. 333 (2018) 505–518. doi:10.1016/j.cej.2017.09.170.

[56] J.-Y. Kim, K.-H. Kim, S.-B. Yoon, H.-K. Kim, S.-H. Park, K.-B. Kim, In situ chemical synthesis of ruthenium oxide/reduced graphene oxide nanocomposites for electrochemical capacitor applications, Nanoscale. 5 (2013) 6804–6811. doi:10.1039/C3NR01233F.

[57] H. K. Hassan, N. F. Atta, M. M. Hamed, A. Galal, T. Jacob, Ruthenium nanoparticles-modified reduced graphene prepared by a green method for high-performance supercapacitor application in neutral electrolyte, RSC Advances. 7 (2017) 11286–11296. doi:10.1039/C6RA27415C.

[58] G. Darabdhara, M.R. Das, S.P. Singh, A.K. Rengan, S. Szunerits, R. Boukherroub, Ag and Au nanoparticles/reduced graphene oxide composite materials: Synthesis and application in diagnostics and therapeutics, Advances in Colloid and Interface Science. 271 (2019) 101991. doi:10.1016/j.cis.2019.101991.

[59] M. Gómez-Martínez, E. Buxaderas, I.M. Pastor, D.A. Alonso, Palladium nanoparticles supported on graphene and reduced graphene oxide as efficient recyclable catalyst for the Suzuki–Miyaura reaction of potassium aryltrifluoroborates, Journal of Molecular Catalysis A: Chemical. 404–405 (2015) 1–7. doi:10.1016/j.molcata.2015.03.022.

[60] S. Yamamoto, H. Kinoshita, H. Hashimoto, Y. Nishina, Facile preparation of Pd nanoparticles supported on single-layer graphene oxide and application for the Suzuki–Miyaura cross-coupling reaction, Nanoscale. 6 (2014) 6501–6505. doi:10.1039/C4NR00715H.

[61] G.G. Flores-Rojas, F. López-Saucedo, E. Bucio, Gamma-irradiation applied in the synthesis of metallic and organic nanoparticles: A short review, Radiation Physics and Chemistry. (2018). doi:10.1016/j.radphyschem.2018.08.011.

[62] J. Khatouri, M. Mostafavi, J. Belloni, Kinetics of Electron Transfer in Solution Catalyzed by Metal Clusters, in: Photochemistry and Radiation Chemistry, American Chemical Society, 1998: pp. 293–314. doi:10.1021/ba-1998-0254.ch018.

[63] K.M. Koczkur, S. Mourdikoudis, L. Polavarapu, S.E. Skrabalak, Polyvinylpyrrolidone (PVP) in nanoparticle synthesis, Dalton Trans. 44 (2015) 17883–17905. doi:10.1039/C5DT02964C.

[64] P.S. Roy, S.K. Bhattacharya, Size-controlled synthesis and characterization of polyvinyl alcohol-coated platinum nanoparticles: role of particle size and capping polymer on the electrocatalytic activity, Catal. Sci. Technol. 3 (2013) 1314–1323. doi:10.1039/C3CY20686F.

[65] J.V. Rojas, C.H. Castano, Radiolytic synthesis of iridium nanoparticles onto carbon nanotubes, J Nanopart Res. 16 (2014) 2567. doi:10.1007/s11051-014-2567-z.

[66] S. Iqbal, S.A. Kondrat, D.R. Jones, D.C. Schoenmakers, J.K. Edwards, L. Lu, B.R. Yeo, P.P. Wells, E.K. Gibson, D.J. Morgan, C.J. Kiely, G.J. Hutchings, Ruthenium Nanoparticles Supported on Carbon: An Active Catalyst for the Hydrogenation of Lactic Acid to 1,2-Propanediol, ACS Catal. 5 (2015) 5047–5059. doi:10.1021/acscatal.5b00625.

[67] J.C. Calderón, G. García, L. Calvillo, J.L. Rodríguez, M.J. Lázaro, E. Pastor, Electrochemical oxidation of CO and methanol on Pt–Ru catalysts supported on carbon nanofibers: the influence of synthesis method, Applied Catalysis B: Environmental. 165 (2015) 676–686. doi:10.1016/j.apcatb.2014.10.077.

[68] A. Maximov, A. Zolotukhina, V. Murzin, E. Karakhanov, E. Rosenberg, Ruthenium Nanoparticles Stabilized in Cross-Linked Dendrimer Matrices: Hydrogenation of Phenols in Aqueous Media, ChemCatChem. 7 (2015) 1197–1210. doi:10.1002/cctc.201403054.

[69] R. Al-Gaashani, A. Najjar, Y. Zakaria, S. Mansour, M.A. Atieh, XPS and structural studies of high quality graphene oxide and reduced graphene oxide prepared by different chemical oxidation methods, Ceramics International. 45 (2019) 14439–14448. doi:10.1016/j.ceramint.2019.04.165.

[70] C. Elmasides, D.I. Kondarides, W. Grünert, X.E. Verykios, XPS and FTIR Study of Ru/Al2O3 and Ru/TiO2 Catalysts: Reduction Characteristics and Interaction with a Methane−Oxygen Mixture, J. Phys. Chem. B. 103 (1999) 5227–5239. doi:10.1021/jp9842291.

Appendix II. Statistical analysis information for Pd/GNP catalyst design space

Herein, the detailed results of statistical operations conducted during the preparation of the design space for solid-supported catalysts for batch and electrochemical Tsuji-Wacker oxidation reactions is presented. During this process the JMP 14.0 software (licensed to the College of Engineering at Virginia Commonwealth University) was used.

AII.1. Statistical study

Table AII. 1. The P-value and R^2 parameters of least square fits

Fit	P-Value	R^2
Batch Conversion	0.0047	0.72
Batch Selectivity	0.005	0.71
Electrochemical Conversion	<0.0001	0.92
Electrochemical Selectivity	0.0006	0.80

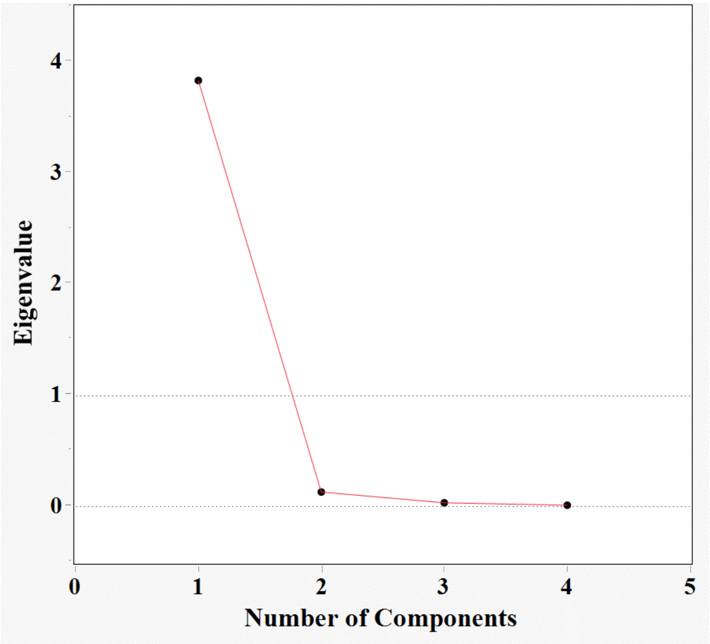

Figure AII. 1. Scree Plot of eigenvalue analysis

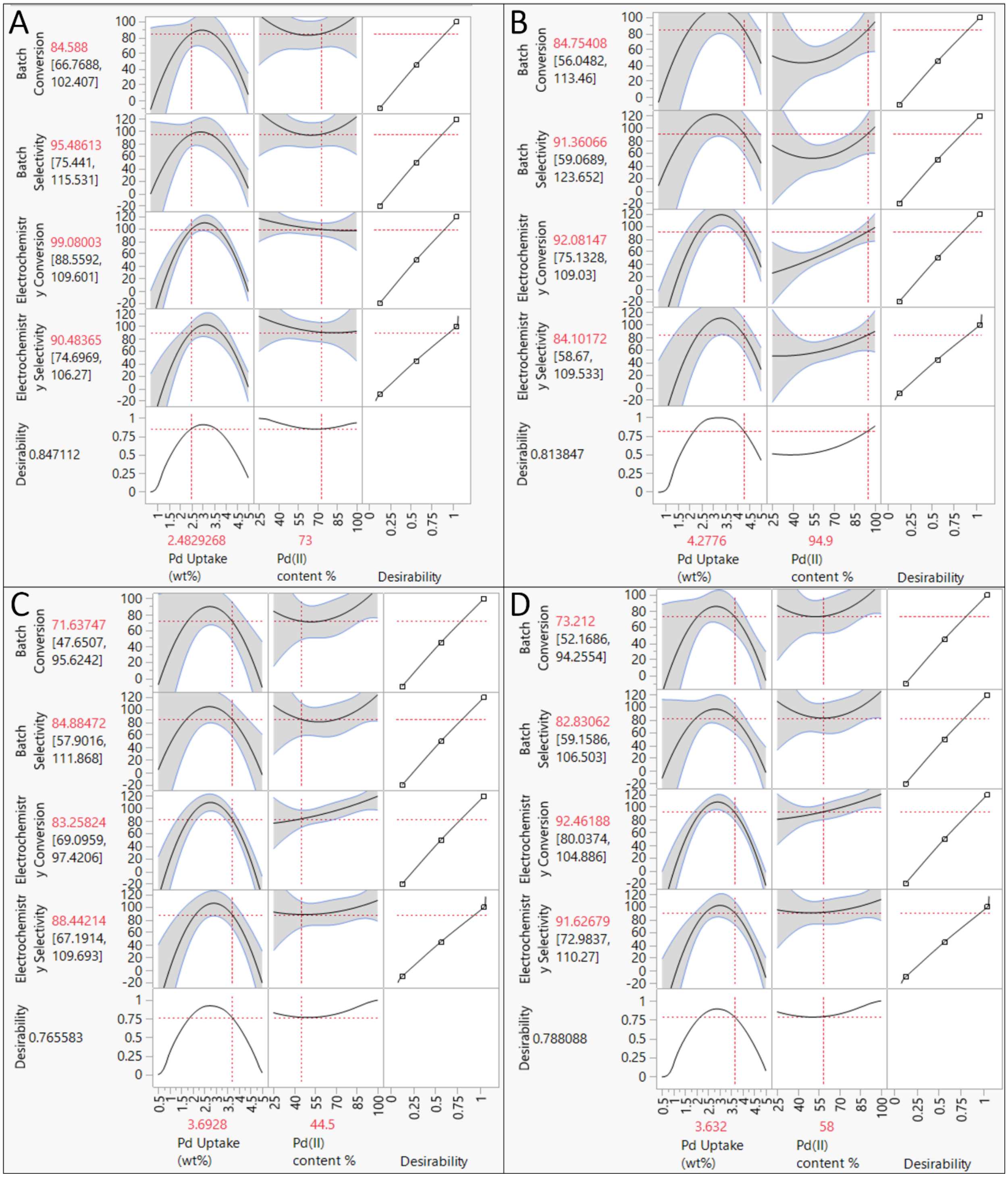

Figure AII. 2. Desirability analysis of control points in the design space